# Geodynamic and Palaeobathymetric Reconstruction between Canada and Greenland



Dissertation zur Erlangung des Grades Dr. rer. nat.

vorgelegt dem Fachbereich Geowissenschaften

der Universität Bremen im Januar 2013

von Sonja Katharina Suckro

Universität Bremen  AWI  Alfred-Wegener-Institut für Polar- und Meeresforschung in der Helmholtz-Gemeinschaft  HELMHOLTZ | GEMEINSCHAFT

# Erklärung

Hiermit versichere ich,

Sonja Katharina Suckro,
wohnhaft in der Friesenstraße 15, 27568 Bremerhaven,

dass ich

- die vorliegende Arbeit ohne fremde Hilfe angefertigt habe,

- keine anderen als die von mir angegebenen Quellen und Hilfsmittel verwendet habe,

- die den benutzten Werken wörtlich oder inhaltlich entnommenen Stellen als solche kenntlich gemacht habe.

Bremerhaven, 25. April 2013          _____

# Zusammenfassung

Die Baffin Bucht und die Labrador See befinden sich zwischen Grönland und Kanada. Beide Meeresbecken sind in der Kreide bis zum Eozän entstanden. Sie werden verbunden durch die Davis Straße, eine bathymetrische Erhebung, die den Wasseraustausch zwischen beiden Meeren limitiert.

Die Labrador See ist ein inaktives Riftsystem des frühen Nordatlantiks. Ozeanische Kruste wurde anhand magnetischer Spreizungsanomalien identifiziert. Es wird vermutet, dass auch die Kruste der Baffin Bucht ozeanisch ist, jedoch konnten Spreizungsmuster bisher nicht eindeutig identifiziert werden. Somit ist auch die Existenz gedehnter kontinentaler Kruste denkbar. Eine ähnliche Kontroverse liegt in der Davis Straße vor: dicke ozeanische Kruste und kontinentale Fragmente werden diskutiert. Die tektonische Entwicklung dieser Region birgt wichtige Informationen für die Davis Straße als polaren Durchfluss in Paläo-Ozeanmodellen.

2008 und 2010 wurden auf Forschungsreisen zur Davis Straße und in die Baffin Bucht geophysikalische Daten erhoben, um die tektonische Entwicklung zu beleuchten. Ich präsentiere hier P-Wellen Geschwindigkeits- und Dichtemodelle entlang eines 710 km langen Transekts in der südlichen Baffin Bucht und entlang eines 315 km langen Querprofils in der Davis Straße. Diese Modelle werden von Reflexionsseismik und Magnetikdaten unterstützt und erweitert.

Die Modelle bestätigen Ergebnisse vorheriger Studien: die Kruste der südliche Baffin Bucht ist ozeanisch mit einer mittleren Mächtigkeit von 7,5 km. Sie ist überlagert von bis zu 6 km mächtigen Sedimenten. Konjugierend zu den Aufbruchsvulkaniten vor der Baffin Insel, finden wir seewärts geneigte Reflektorsequenzen in der Reflexionsseismik vor Grönland. Wir schließen somit auf eine magmatisch geprägte Öffnung der südlichen Baffin Bucht. Auch die Davis Straße ist von Vulkanismus geprägt - entlang des gesamten Querprofils sind Basaltflüsse zu erkennen. Die Modelle zeigen, dass die Davis Straße in erster Linie aus Blöcken kontinentaler Kruste besteht. Dazwischen liegt eine 45 km breite Einheit aus neuer magmatischer oder aus stark magmatisch intrudierter, gedehnter, kontinentaler Kruste. Wir führen diese Einheit auf einen Einfluss des frühen nordatlantischen Manteldiapirs zurück.

Mit den neuen Informationen unserer Krustenmodelle konnte ich ein plattenkinematisches Modell entwickeln, welches auf bestehenden Rotationspolen basiert. Das Fehlen klarer magnetischer Spreizungsanomalien in der Baffin Bucht trotz der Präsenz von ozeanischer Kruste, ist vermutlich auf die Vielzahl an Störungen zurückzuführen. Dies fhrt zu kleinen Krustenfragmenten, die zueinander verschoben sind. Durch die Bewegungsänderung der grönländischen Platte im späten Paleozän wurden Kompressionskräfte aufgebaut. Diese haben vorerst im Bereich der Ungava Verwerfung (der prä-Eozänen Plattengrenze) zu Deformationen geführt. Anschließend muss sich eine

neue Transformstörung gebildet haben - die Hudson Störungszone.

Um abzuschätzen zu welchem Zeitpunkt ein Wasseraustausch durch die Davis Straße möglich war und wie sich die Labrador See entwickelte, habe ich eine paläo-bathymetrische Rekonstruktion erstellt. Hierzu habe ich die Stratigraphie der neu gewonnenen seismischen Daten mit publizierten Interpretationen und Bohrdaten zusammengeführt. Mit dem sogenannten "backstripping" Verfahren berechne ich die Entlastungsflexur der Lithosphäre, die Dekompaktion von Sedimenten, die Effekte durch Meeresspiegeländerungen und die thermische Subsidenz der Lithosphäre. Paläo-Lokationen der Profile und die Altersstruktur der Kruste wurden aus unserem neuen plattenkinematischen Modell abgeleitet.

Obwohl die paläo-bathymetrischen Gitter mit hohen Unsicherheiten behaftet sind, können wir schlussfolgern, dass die Davis Straße in prä-Eozäner Zeit die Labrador See von der Baffin Bucht getrennt hat. Es ist wahrscheinlich, dass bereits seit dem Paläozän der frühe Westgrönlandstrom eine Ringströmung ähnlich der heutigen Situation in der Labrador See verursachte. Unsere Berechnungen können in Paläo-Ozenmodellen verwendet werden und somit helfen Paläo-Klimamodelle zu verbessern.

# Summary

The Baffin Bay and the Labrador Sea are located between Greenland and Canada. Both basins evolved from Cretaceous to Eocene times. They are linked by the bathymetric high of Davis Strait, which limits the water transport between both basins.

The Labrador Sea is an extinct rift system of the early North Atlantic. Oceanic crust has been identified from magnetic spreading anomalies. It is also proposed that the crust of Baffin Bay is oceanic. But no clear magnetic spreading anomalies are detected and therefore the presence of stretched continental crust is also possible. A similar controversy exists on the nature of the Davis Strait crust. Thick oceanic crust as well as continental fragments are debated. The tectonic evolution of the area is an important factor for the role of Davis Strait as a polar gateway in palaeocean models.

In 2008 and 2010 research expeditions to the Davis Strait and Baffin Bay were undertaken to collect geophysical data on the tectonic evolution of this area. Here, I present P-wave velocity and density models of a 710-km-long line in southern Baffin Bay and of a 315-km-long line in the central Davis Strait. The models are supported and complemented by seismic reflection and magnetic anomaly data.

The models support results of previous studies: southern Baffin Bay is underlain by oceanic crust of 7.5 km thickness on average. The crust is covered by sediments of up to 6 km thickness. Conjugate to breakup volcanics off Baffin Island, we find seaward dipping reflector sequences in the seismic reflection data of the Greenland margin. We conclude, that the opening of southern Baffin Bay was accompanied by volcanism. The Davis Strait is also characterized by volcanism - along most of the profile basalt flows are imaged. The models reveal that the Davis Strait consists mainly of sections of continental crust. These are saparated by a 45-km-wide unit of new igneous or highly intruded, stretched, continental crust. We account this feature to an influence of the early North Atlantic mantle plume.

With the new information of our crustal models, I developed a plate kinematic model. Although southern Baffin Bay is underlain by oceanic crust, magnetic spreading anomalies are probably missing due to many fractures. These lead to small scale crustal sections which are shifted to each other. Due to the reorientation of the Greenland plate in the Late Paleocene, compressional forces were compensated in the Davis Strait. These probably resulted first in a deformation within the Ungava Fault Complex (the pre-Eocene plate boundary) and then caused the evolution of a new transform fault, the Hudson Fracture Zone.

To estimate at what time a water transport was possible via the Davis Strait and how the Labrador Sea basin evolved, I calculated palaeobathymetry grids. I compiled published and new seismic data with information from drill sites. In a backstripping routine, I calculated the effects of flexural unloading for the lithosphere, of sediment

decompaction, of global sea-level changes, and of thermal subsidence of the lithosphere. Palaeolocations of the profiles and the age structure of the crust are derived from our recent plate kinematic model.

Although the grids are characterized by great uncertainties, we can conclude that the Davis Strait separated the Labrador Sea from the Baffin Bay in pre-Eocene times. We propose that, similar to today, an early West Greenland Current formed a cyclonic circulation in the early Labrador Sea basin since the Paleocene. Our palaeobathymetric reconstruction can be used in palaeocean models and improve palaeoclimate reconstructions.

# Contents

# List of Figures

# List of Tables

# Chapter 1

# Introduction and Motivation

## 1.1   Polar Gateways

One of the main tasks for geosciences is to understand the factors that control our climate. Besides human generated changes, such as the concentration of climate forcing gases in the atmosphere, natural changes like the distribution of land masses, the patterns of global wind systems and ocean circulations are of great interest. The heat transfer by ocean currents plays a major role in the climate system, which can easily be recognized by the mild temperatures in Ireland and Great Britain due to the warm Gulf Stream.

Ocean currents transport great amounts of thermal energy between the latitudes. As oceanic gateways limit the water transport between different oceans, they are key features in the global circulation pattern and need special attention. The polar regions act as energy sinks and play an important role in the global climate system.

Today, the oceanic currents that control the heat transfer between the polar and the temperate zones are the Antarctic Circumpolar Current in the south and the North Atlantic and East Greenland Current along with several smaller currents in the north (Fig. 1.1). The Antarctic Circumpolar Current evolved after the opening of the Drake Passage and the deepening of the Tasman Gateway in the Mid Eocene to Oligocene (e.g. Livermore et al., 2007; Stickley et al., 2004). The circulation prevents an invasion of warmer water masses to the Antarctic coast and is thought to be the controlling factor for the evolution of an icecap on Antarctica. The dominating currents in the Arctic Ocean are the Beaufort Gyre and the Transpolar Drift (Fig. 1.1). Warm waters flow into the Arctic Ocean from the North Atlantic Current and to a smaller extent from the North Pacific through the shallow Bering Strait. Cold water is transported into the Atlantic by the East Greenland Current and by a shallow water exchange across the Canadian Archipelago and the Baffin Bay-Labrador Sea system. While the Polar Ocean was connected to the world oceans throughout the Mesozoic, it was probably isolated from Late Cretaceous to Early Paleogene (Marincovich Jr. et al., 1990). An exchange of deep water
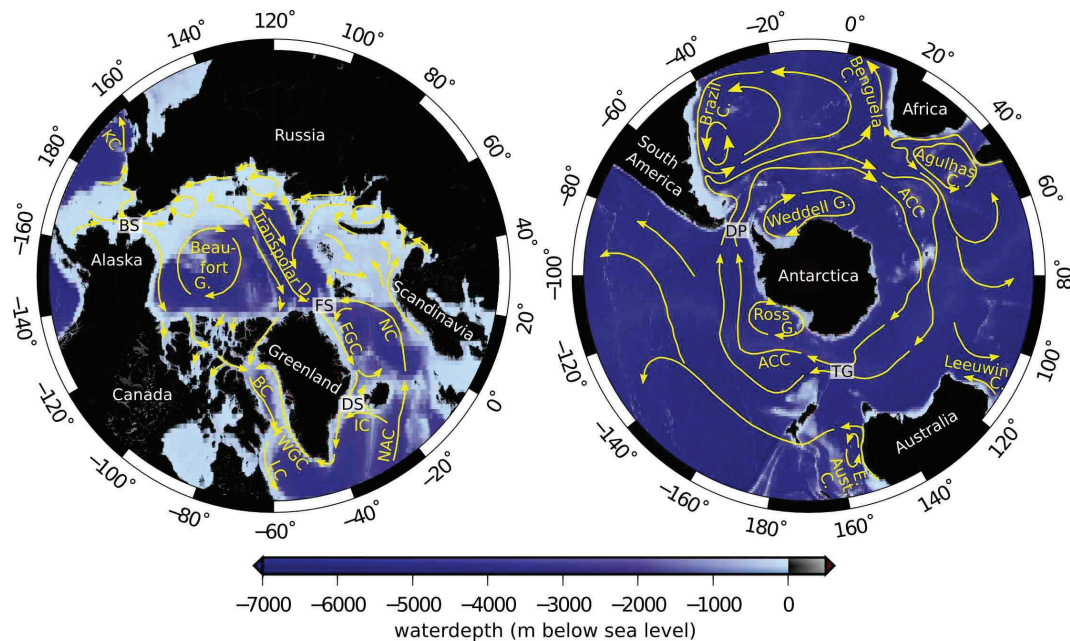
**Figure 1.1:** Bathymetry of the Arctic and Antarctic (GEBCO_08 Grid, Version 20090202, http://www.gebco.net) with direction of ocean currents in yellow; redrawn after Rekacewicz (2005); Rintoul et al. (2001). Abbreviations are: C. (Current), G. (Gyre), D. (Drift), KC (Kamchatka Current), BC (Baffin Current), LC (Labrador Current), WGC (West Greenland Current), EGC (East Greenland Current), IC (Irminger Current), NAC (North Atlantic Current), NC (Norwegian Atlantic Current), BS (Bering Strait), FS (Fram Strait), DS (Denmark Strait), ACC (Antarctic Circumpolar Current), E. Aust. C. (East Australian Current), DP (Drake Passage), TG (Tasman Gateway).

with the North Atlantic established between Early Oligocene and Mid Miocene via the Fram and Denmark Strait (Marincovich Jr. et al., 1990; Engen et al., 2008). The Baffin Bay-Labrador Sea system evolved from Cretaceous to Eocene times (e.g. Chalmers & Pulvertaft, 2001) and is subject of this study. The tectonic evolution is discussed in detail in the following section.

## 1.2 Evolution of the Baffin Bay - Labrador Sea System

The Labrador Sea is an extinct rift system of the early northern Atlantic. While the North Atlantic still opens between Greenland and Europe, seafloor spreading between Canada and Greenland ceased in the Late Eocene (Srivastava, 1978). The rift system of the Labrador Sea is connected to the Baffin Bay basin via the Davis Strait (Fig. 1.2). While the Labrador Sea and the Baffin Bay exceed water depths of 2000 m, the Davis Strait is a bathymetric high with less than 700 m water depth (GEBCO_08 Grid, Version

20090202, http://www.gebco.net). It is characterized by the Ungava Fault Complex, a major transform fault, that is easily recognized in regional gravity data by a series of positive anomalies (e.g. Funck et al., 2007; Gregersen & Skaarup, 2007; Gerlings et al., 2009), Fig. 1.2. Oblique to the Ungava Fault Complex runs the Hudson Fracture Zone and both meet north of the Davis Strait (e.g. Chalmers & Pulvertaft, 2001). The Hudson Fracture Zone was first recognized in magnetic anomaly data by Srivastava (1978), but is often neglected in newer literature (e.g. Sørensen, 2006; Gregersen & Skaarup, 2007; Dickie et al., 2011; Oakey & Chalmers, 2012).

Greenland separated from the North American Plate in the Mesozoic. Dyke swarms that are attributed to rifting of the Labrador Sea margins are dated to Late Triassic to Early Cretaceous (Larsen et al., 2009; Watt, 1969). Seafloor spreading first started at magnetic chron 33 (Roest & Srivastava, 1989) or at chron 27N (Chalmers & Laursen, 1995). This is between 80 to 62 Ma according to the timescale of Gradstein et al. (2004), which is used throughout the text for dating. After Paleocene spreading, the motion of the Greenland plate changed to a more northward direction, during magnetic chron 24R (Early Eocene, Srivastava (1978)). This change coincided with the onset of seafloor spreading between Europe and Greenland (Chalmers & Pulvertaft, 2001). Seafloor spreading ceased by magnetic chron 13 (Early Oligocene, (Srivastava, 1978; Chalmers & Laursen, 1995)).

The Labrador Sea and the Baffin Bay basins offer a unique opportunity to study different crustal structures. While the Labrador Sea is underlain by oceanic crust of 7 km thickness (Chian & Louden, 1994), central Baffin Bay is underlain by abnormally thin crust of only 4 km thickness (Keen & Barrett, 1972). The Davis Strait crust is interpreted as 22-km-thick oceanic crust by Keen & Barrett (1972). Chalmers & Pulvertaft (2001) argue that the crust is continental.

The Labrador Sea and Baffin Bay margins are characterized by different processes during their evolution. In the northern Baffin Bay and the southern Labrador Sea, serpentinized mantle material forms the transition from stretched continental to oceanic crust, Fig. 1.3 (Jackson & Reid, 1994; Reid & Jackson, 1997; Chian & Louden, 1994). This implies an amagmatic rifting and breakup process, while the Davis Strait area is characterized by volcanism. Tertiary volcanics crop out onshore of Baffin Island at Cape Dyer, which are related to the breakup process (Clarke & Upton, 1971; MacLean et al., 1978). At Disko Island and Nuussuaq Peninsula, Greenland, Early Tertiary volcanics are related to the Iceland mantle plume, which Greenland passed (Storey et al., 1998). Offshore, basalt flows can be traced as sea-ward dipping reflector sequences at the Baffin Island margin (Skaarup et al., 2006). P-wave models of the crust include a high velocity lower crust in the Davis Strait area, interpreted as magmatic underplating (Gohl & Smithson, 1993; Funck et al., 2007; Gerlings et al., 2009). Magmatic underplatings are mafic bodies attached to the crust in regions of intensive melt production due to thermal anomalies in the mantle. Funck et al. (2007) and Gerlings et al. (2009)
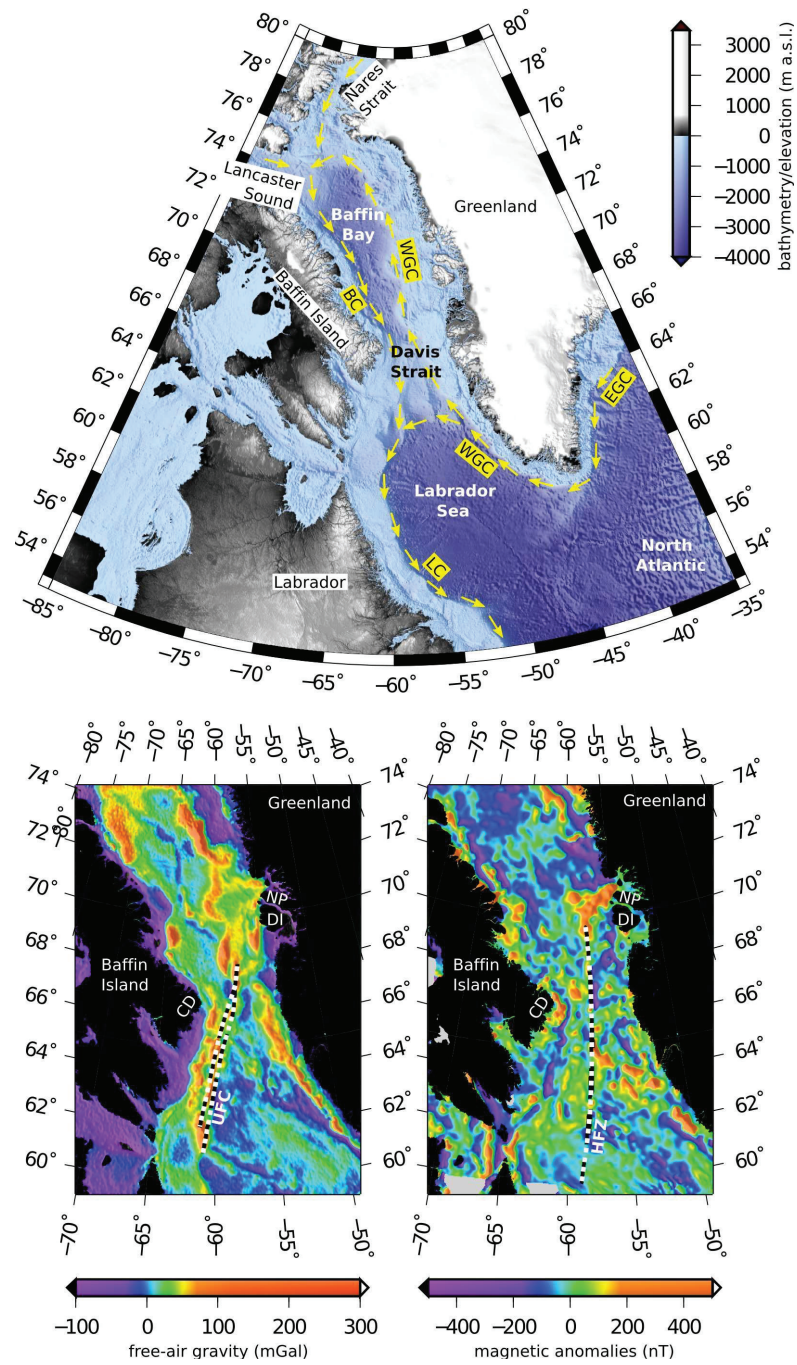
**Figure 1.2: (Top) Bathymetric map of the Baffin Bay, Davis Strait, and Labrador Sea area (GEBCO_08 Grid, Version 20090202, http://www.gebco.net) with place names and direction of oceanic currents. BC (Baffin Current), LC (Labrador Current), WGC (West Greenland Current), EGC (East Greenland Current). (Bottom left) Free-air gravity anomalies derived from satellite altimetry (Sandwell & Smith (2009), version 18.1); UFC (Ungava Fault Complex), CD (Cape Dyer), NP (Nuussuaq Peninsular), DI (Disko Island). (Bottom right) Magnetic anomalies (EMAG2 V2, Maus et al. (2009)); HFZ (Hudson Fracture Zone).**

interpret the underplated crust in southern Davis Strait as a product of the early North Atlantic - Iceland mantle plume (lines NUGGET-1 and -2 in Fig. 1.3).

## 1.3 Research Questions

Chalmers & Pulvertaft (2001) provide a detailed overview of the geologic evolution of the Labrador Sea, Davis Strait and Baffin Bay area. In the following, I only summarize some of the most important results that help to set the research questions in the following paragraphs and the papers in chapters 4, 5, and 6 into context.

### 1.3.1 Crust of the Southern Baffin Bay

While magnetic spreading anomalies in the Labrador Sea clearly characterize this as oceanic crust (Fig. 1.3, (e.g. Srivastava, 1978; Roest & Srivastava, 1989; Chalmers & Laursen, 1995)), magnetic spreading anomalies in southern Baffin Bay are debated. Jackson et al. (1979) first reported magnetic lineations in central Baffin Bay. Due to the scarce data no identification of magnetic chrones was possible. Recently, Oakey & Chalmers (2012) re-interpreted the magnetic data in context with a plate tectonic reconstruction. They interpret short magnetic lineations as results of Paleocene spreading in the central Baffin Bay.

Keen & Barrett (1972) interpret abnormally thin oceanic crust in the central Baffin Bay from sonobuoy readings (locations in Fig. 1.3). Rice & Shade (1982) and Jackson et al. (1992) also identify oceanic type crust in central Baffin Bay from seismic reflection data. At the EGU Assembley in Vienna, 2007, Chalmers and Oakey first presented a geologic map that includes the Baffin Bay area with oceanic crust of two spreading phases (Fig. 1.3). This map is now part of the "Map of the Arctic" by Harrison et al. (2008) and was recently published in Oakey & Chalmers (2012). This geologic map is mainly based on potential field data with additional information from seismic reflection lines.

**Although oceanic crust is proposed to underlay Baffin Bay, no clear magnetic spreading anomalies are detected. Is there stretched continental crust or is there oceanic crust in southern Baffin Bay? What is the extent of crustal units? How did southern Baffin Bay evolve tectonically?**

### 1.3.2 Crust of the Davis Strait

Similar to southern Baffin Bay, the nature of the crust in the Davis Strait is disputed. Keen & Barrett (1972) first interpreted a 22-km-thick pile of oceanic crust from
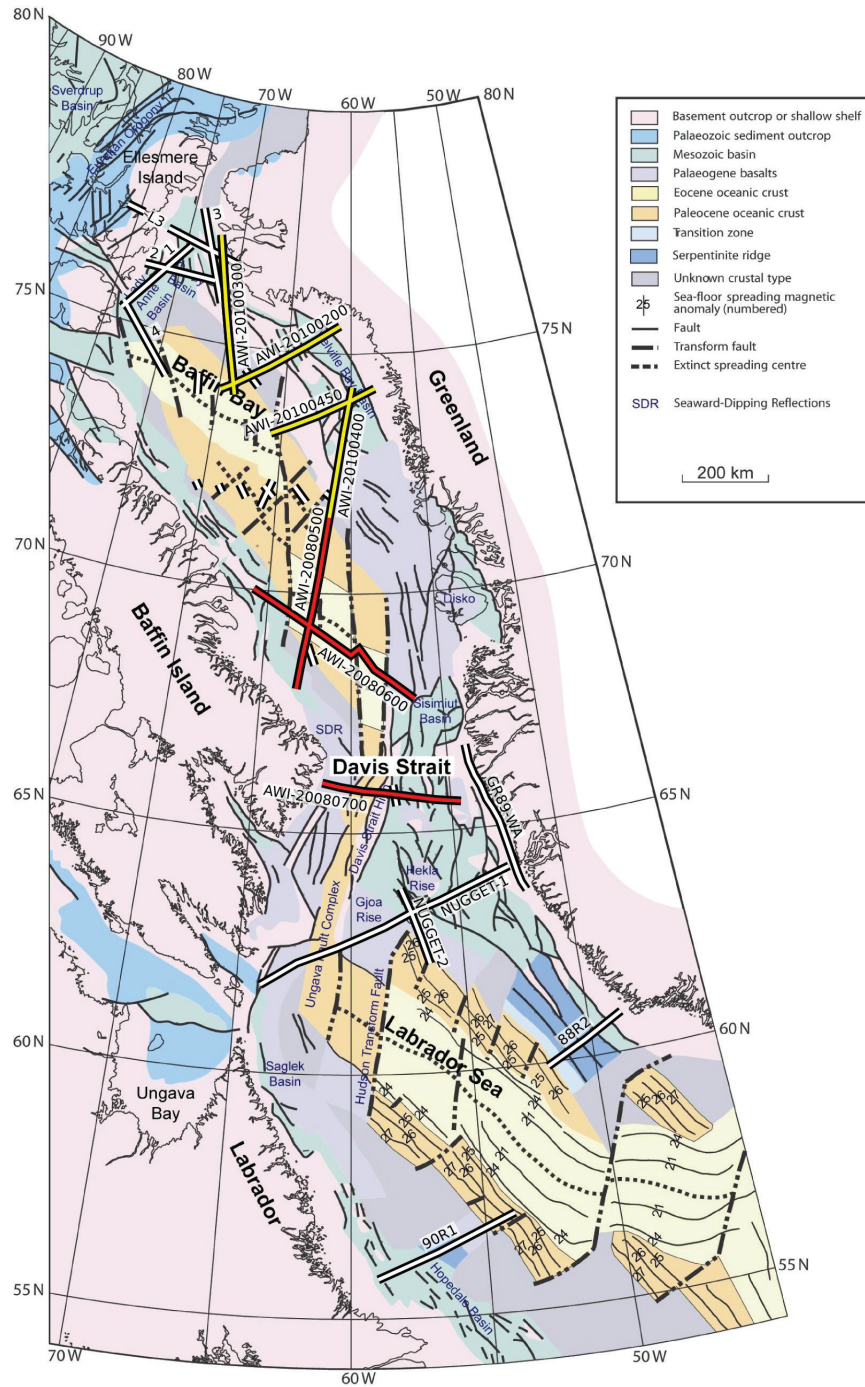
**Figure 1.3: Geologic map (Chalmers & Oakey, 2007) and locations of seismic refraction profiles; in white are published profiles, in red new data from cruise leg MSM09/3, in yellow leg ARK XXV/3; L3 (Funck et al., 2006); 1, 3 (Jackson & Reid, 1994); 2, 4 (Reid & Jackson, 1997); short lines in central Baffin Bay and Davis Strait (Keen & Barrett, 1972); GR89-WA (Gohl & Smithson, 1993); NUGGET-1 (Funck et al., 2007); NUGGET-2 (Gerlings et al., 2009); 88R2 (Chian & Louden, 1994); 90R1 (Chian et al., 1995).**

sonobuoy readings. Srivastava et al. (1982) interpret the Davis Strait High as a continental fragment, which is enclosed by oceanic crust. Chalmers & Pulvertaft (2001) argue from sequence stratigraphy that the Davis Strait crust is continental. A recent seismic refraction profile in the southern Davis Strait reveals that stretched continental crust is separated by a 140-km-wide section of oceanic crust (line NUGGET-1, Fig. 1.3, Funck et al. (2007)). This section of oceanic crust coincides with the location of the Ungava Fault Complex. Oakey & Chalmers (2012) compiled these informations in a geological map (Fig. 1.3).

**What type of crust underlies the central Davis Strait? Is there a similarity to the published model in the southern Davis Strait? What is the tectonic evolution of the Davis Strait area?**

### 1.3.3 Palaeobathymetry of the Davis Strait

The Davis Strait limits the water transport between the Labrador Sea and the Baffin Bay. Part of the West Greenland Current passes the strait and brings warmer waters into the Baffin Bay. Cold waters from the Arctic Ocean enter the Baffin Bay via Nares Strait and Lancaster Sound. The cold Baffin Current transports these waters southwards across the Davis Strait. Here, they form the Labrador Current and enter the Atlantic Ocean.

**Which role did the Davis Strait play as a polar gateway in the past? At what time was a water transfer possible between the Labrador Sea and the Baffin Bay? What was the palaeobathymetry of the Davis Strait area?**

To asses these research questions, new geophysical data were collected. The data acquisition and the evaluation procedures are briefly described in the following chapter. Chapters 4, 5, and 6 are the paper contributions I made during my dissertation. Each manuscript deals with one of the research topics listed above. Overall conclusions and an outlook are given in chapter 7.

# Chapter 2

# Dataset, Methods & Processing

## 2.1  New Geophysical Data

The new data that are evaluated in this study were collected during the cruise leg MSM09/3 of the research vessel Maria S. Merian in 2008 (Gohl et al., 2009) and during the leg ARK XXV/3 of the research icebreaker Polarstern in 2010 (Damm, 2010).

The cruise of 2008 was a cooperation of the Alfred Wegener Institute for Polar and Marine Research (AWI) and the Federal Institute for Geosciences and Natural Resources (BGR) with the Geological Survey of Denmark and Greenland (GEUS) and the Canadian Dalhousie University. The cruise was part of a project called DAVIS GATE of the International Polar Year (IPY 2007/2008) Lead Project *Plate Tectonics and Polar Gateways in the Earth System (Plates & Gates)*. Survey area was the southern Baffin Bay and the Davis Strait. The cruise of 2010 was a cooperation of the AWI and the BGR with focus on the central and northern Baffin Bay. Unfortunately, the acquisition of data was limited to Greenland waters only due to permitting reasons.

On both expeditions, high resolution seismic reflection and wide-angle seismic refraction data were acquired to analyze the sediment cover and the crustal structure. Gravity and magnetic anomaly data were collected to complement crustal modelling and to search for seafloor spreading anomalies and indications of volcanism. Additionally, multibeam bathymetry and sediment echosounding were recorded. At several locations of the Greenland margin, the geothermal heat flux was measured during ARK XXV/3.

For my dissertation, I first developed a crustal and tectonic model in the southern Baffin Bay. The deep-crustal seismic line AWI-20080500 with the extension-line AWI-20100400 was set up across proposed Paleocene and Eocene oceanic crust with an Eocene spreading centre (Fig. 1.3). Secondly, I developed a crustal and tectonic model in the central Davis Strait. Seismic line AWI-20080700 crosses the strait and the Ungava Fault Complex (Fig. 1.3). For a calculation of the palaeobathymetry, I
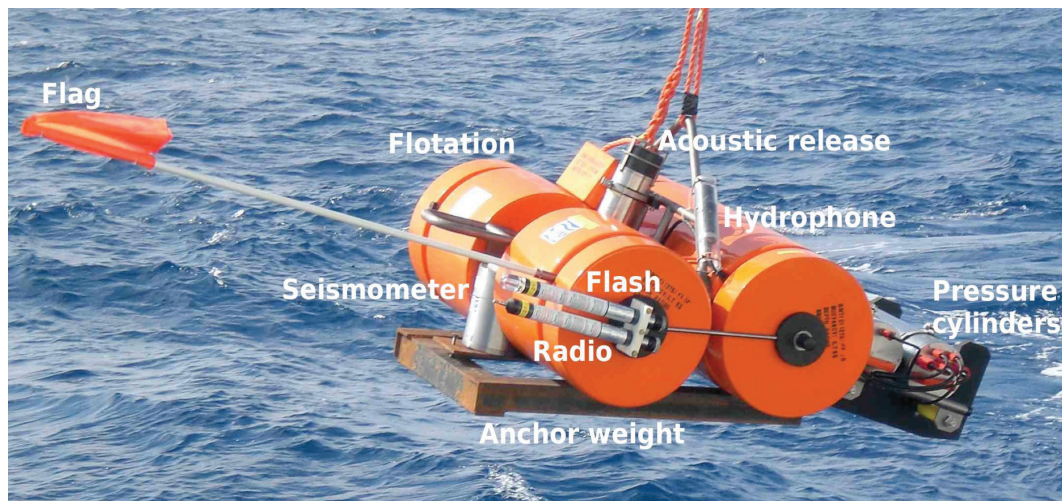
**Figure 2.1: OBS used during ARK XXV/3 with components labelled (Damm, 2010).**

thirdly interpreted new seismic reflection lines (BGR08-301, -304, and -319), compiled a dataset of existing interpretations, and developed a backstripping routine.

## 2.2 Data Acquisition

### 2.2.1 Seismic Refraction Survey with Ocean Bottom Seismometers (OBS)

Fig. 2.1 displays the components that compose an OBS during deployment. Four channels of data are acquired by a 3-component seismometer and an additional hydrophone. In this study, only data of the hydrophone or of the z-component of the seismometer are used. S-wave modelling of the x- and y-components was not persued due to limited data quality. Technical details of the OBS and the air-guns are listed in chapters 4 and 5 and in the cruise reports (Gohl et al., 2009; Damm, 2010). In the following I summarize the typical actions during the setup of a seismic refraction survey.

- OBS are deployed along a profile and sink to the ground due to the additional weight of an anchor.

- Seismic pulses are emitted by air-guns along the profile (Fig. 2.2). The seismometers and hydrophones of the OBS receive the motion and data are recorded on a hard drive within a pressure cylinder (Fig. 2.1).

- After completion of the profile, the vessel returns to the first OBS location.

**Figure 2.2: (Left) G-Gun used during ARK XXV/3. (Right) A cluster of six G-Guns and two additional G-Guns are towed by Polarstern during the seismic refraction survey of ARK XXV/3. Fotos from M. Koch, 2010.**

- An acoustic signal is transmitted to open the releaser unit - a device that holds the anchor fixed to the instrument.

- Disconnected from the anchor weight, the OBS floats up and can be collected from the surface. The vessel can continue to the next OBS location.

- Data that are stored on the hard drive are transferred to a PC.

The continuous data files, that are recorded by the seismometers and hydrophones, are cut into traces of 60 s length, according to the shot time. Because the OBS drifted in the water column after deployment, the actual position has to be determined. This process is called relocalization. The direct wave is picked and the shortest travel time is shifted to 0-offset. The OBS section is then ready for traveltime picking.

## 2.2.2 Multichannel Seismic Reflection (MCS) Survey

During a marine seismic reflection survey, seismic pulses are generated by air-guns towed by a vessel. The receiving unit is a streamer - a chain of hydrophones that is also towed by a vessel. Data are recorded on-board and demultiplexed. A real-time quality control is set up, where the operator can check the signal recorded by a single hydrophone (channel) and the functionality of all channels. After completion of a survey, the seismic data are transferred from tape or hard drive to a PC and merged with navigation information. Subsequent processing steps usually include frequency filtering, velocity analysis, normal move-out correction, stacking, multiple supression, and migration. The technical details of the equipement and the processing steps are listed in chapters 4, 5, 6 and in the cruise reports (Gohl et al., 2009; Damm, 2010).

### 2.2.3 Potential Field Data

Sea gravimeter systems were operated during both cruises. The instruments were located at the gravimeter rooms of each vessel and logged data continuously. To account for the drift of the instruments, calibration measurements were performed at the start and at the end of each cruise. For these calibrations a separate gravimeter is used at reference locations. The magnetic anomaly data that are presented in this study were acquired by towed systems. During the seismic reflection surveys, magnetometers were towed on a cable behind the vessel. A detailed description of the gravimeters and magnetometers is given in the cruise reports (Gohl et al., 2009; Damm, 2010).

## 2.3 Modelling

### 2.3.1 P-wave Velocity Model

I developed the P-wave velocity models in chapter 4 and 5 by following a standard procedure, which I will outline here only briefly. First, traveltimes have to be picked in the seismic sections of the OBS. Subsequently a P-wave velocity model is obtained by forward modelling (Fig. 2.3).

For the picking of phases I used the software "zp" (Barry Zelt), which is a free software that can be downloaded at http://www.soest.hawaii.edu/users/bzelt/zp/ zp.html. Another common software is zplot (Colin Zelt), http://terra.rice.edu/department/faculty/ zelt/fast.html. Traveltimes of refracted and reflected signals are picked and referred to as phases of a specific layer. While reflected phases appear as hyperbolas in the seismic sections, refracted phases are straight or slightly bent lines with an apparent seismic layer-velocity as the inverse of the slope (Fig. 2.3).

I obtained the P-wave velocity structure by forward modelling using the software "rayinvr" (Zelt & Smith (1992); Zelt (1994), Fig. 2.3). The model has to be set up carefully, taking into account the total model length and the positions of relocated OBS along this line. The dip of refracted phases is an indication of the average P-wave velocity within a layer, while reflected phases mark layer boundaries (Fig. 2.3). P-wave velocity and thickness are assigned manually to each layer from top to bottom and are varied in a trial and error procedure until a best fit for all phases is obtained. Rayinvr offers the possibility to run an inversion for selected model nodes. I used the inversion algorithm within single layers to obtain a better fit and statistical values on the quality of the model. Rayinvr is a well established algorithm that is widely used (e.g. Chian et al., 2001; Mjelde et al., 2005; Funck et al., 2007; Voss et al., 2009).
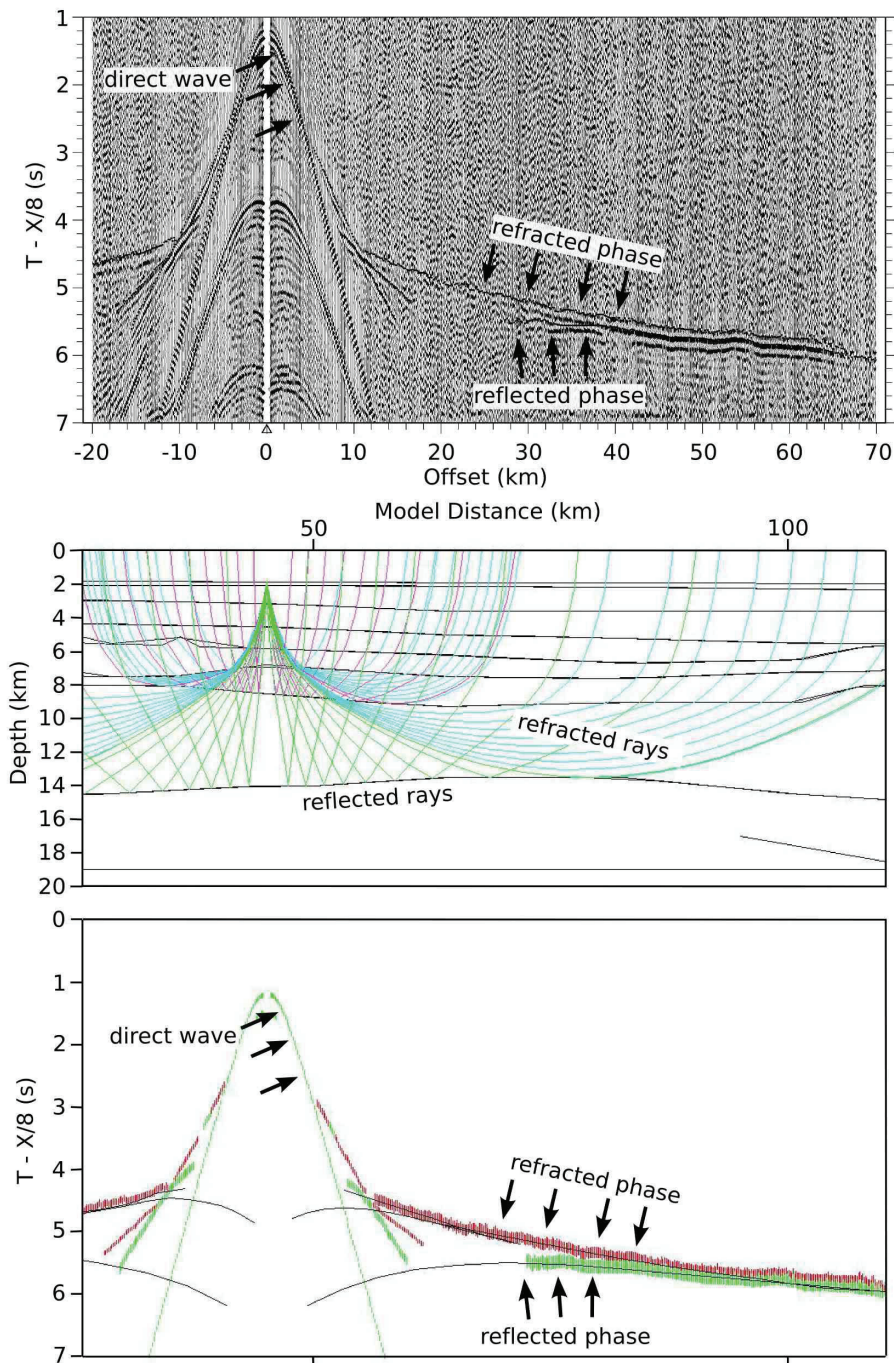
**Figure 2.3: (Top) Seismic section of OBS 6, line AWI-20080500. (Bottom) During forward modelling with "rayinvr" the model layers and calculated ray paths are displayed in a window above the picked travel times (green and red bars) and calculated times (thin black lines).**

13

### 2.3.2 Gravity Model

The density models were developed in a collaboration with by Dr. Ingo Heyde, BGR, from the free-air gravity data. For a better understanding, I will summarize our procedure briefly. Density modelling was accomplished by forward modelling and a subsequent inversion with the software GM-SYS (Northwest Geophysical Associates, Inc.). We used a first version of a P-wave velocity model as starting model. The layer boundaries were used directly, while we calculated average P-wave velocities of each layer to transfer them into densities. A compilation of P-wave velocities and corresponding densities is given in Barton (1986). We applied an inversion of the density values to this starting model, which usually resulted in a better fit of the calculated to the measured data. We kept density values fixed within a range that was corresponding reasonably to the P-wave velocity values. Where layer boundaries were not constrained by the P-wave velocity model, we adjusted these to fit the gravity data and subsequently adjusted the P-wave velocity model. In several iterations we were able to obtain models that satisfied the seismic refraction and the gravity data.

### 2.3.3 Palaeobathymetry

To calculate the palaeobathymetry of the Davis Strait area, I collected published stratigraphy from seismic lines to enlarge our dataset from cruise leg MSM09/3. As most original data could not be recovered by the authors, I digitized most information from the published figures. All authors pick different horizons, but the Base Neogene, Base Cenozoic, and Mid Cretaceous Unconformity are mapped by most authors. By analysis of the crosspoints of profiles, it is possible to check the depth of each horizon and to decide if it is misinterpreted.

Several programs exist that perform backstripping. A program by N. Cardozo performs backstripping at a single point, e.g. a drill site, and is freely available at http://www.ux.uis.no/~nestor/work/programs.html. The package "balpal" was used at AWI in a previous study (Ehlers, 2009; Ehlers & Jokat, 2013). It was developed by C.N. Wold at GEOMAR, Kiel, 1994, to calculate a palaeobathymetry on grids. Unfortunately it is limited to oceanic crust and consists of more than 40 subroutines, that are difficult to manage. Commercial seismic interpretation software can perform backstripping along profiles, but this was not available to me.

I developed a backstripping routine along profiles that accounts for flexual unloading (isostasy), sediment decompaction, and subsidence due to sea-level changes. It is written in Fortran.90 and can handle up to 10 sediment layers. It can be downloaded at: https://dl.dropbox.com/u/53905623/backstripping_routine_suckro.zip. The advantage of calculations along a profile is that the result can easily be checked by plotting the backstripped profile with the original (Fig. 2.4). The backstripped sediment cover can subsequently be gridded. To account for the thermal subsidence of the crust, I di-
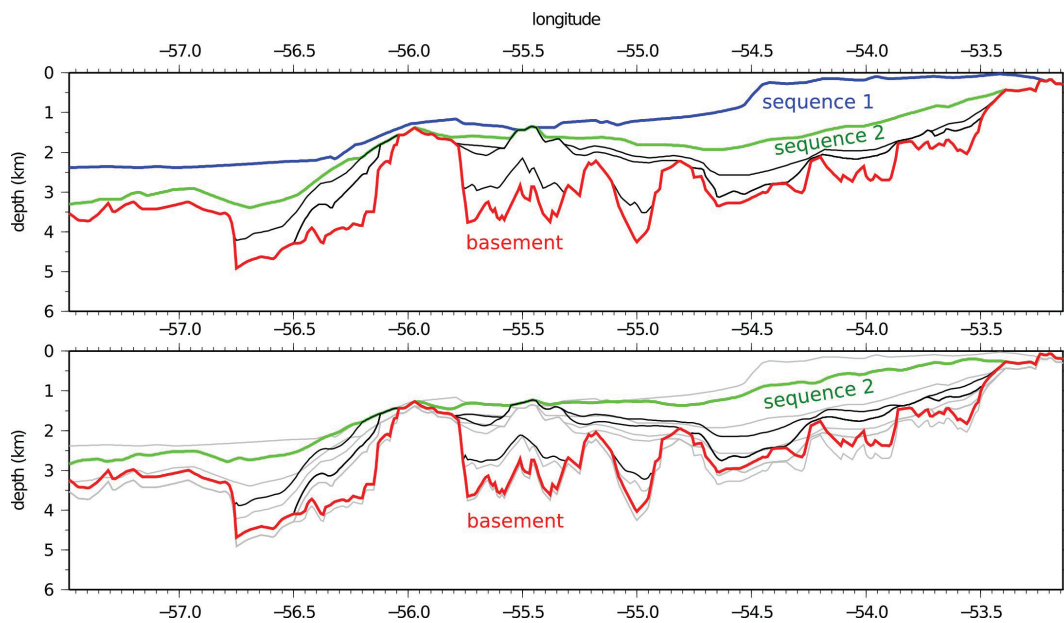
**Figure 2.4: (Top) Original stratigraphy along line BGR77-06 (Chalmers et al., 1993). (Bottom) The same line after backstripping of the first sedimentary sequence; original stratigraphy underlain in grey.**

vided it into sections of the same age and type within a tectonic model. The subsidence is then calculated at several positions and also gridded. The combination of both grids produces the palaeobathymetry. The calculations and formulas are described in chapter 6 and appendix C.2

# Chapter 3

# Contributions to Scientific Journals

**The crustal structure of southern Baffin Bay: implications from a seismic refraction experiment**

S.K. Suckro, K. Gohl, T. Funck, I. Heyde, A. Ehrhardt, B. Schreckenberger, J. Gerlings, V. Damm, and W. Jokat

In this paper, we present a P-wave velocity and a density model in the southern Baffin Bay along with MCS and magnetic anomaly data. The models show that the basin is underlain by oceanic crust of normal thickness (7.5 km), extending for at least 305 km. From a P-wave velocity increase at the Greenland margin and the occurrence of sea-ward dipping reflector sequences, we conclude that the margins are volcanic. With our new crustal models we develop a plate tectonic model, which suggests minor changes to the map of Chalmers & Oakey (2007).

I calculated the P-wave velocity model, developed the plate kinematic model, processed part of the MCS data, and wrote the manuscript. Karsten Gohl supervised the work and was Chief Scientist during MSM09/3. Thomas Funck relocalized the OBS deployed during MSM09/3 and explained P-wave velocity modelling to me. Ingo Heyde completed the density modelling. Axel Ehrhardt processed part of the MCS data. Bernd Schreckenberger provided the magnetic anomaly data. Joanna Gerlings assisted in the collection of seismic data and represents the Dalhousie University as cooperation partner in the project. Volkmar Damm was Chief Scientist during ARK XXV/3. Wilfried Jokat agreed to the profile-setup during ARK XXV/3. All authors revised the manuscript and contributed to the results in several discussions.

**The Davis Strait crust - a transform margin between two oceanic basins**

S.K. Suckro, K. Gohl, T. Funck, I. Heyde, B. Schreckenberger, J. Gerlings, and V. Damm

*Geophysical Journal International (2013)*, **193**(1), p. 78-97,
doi: 10.1093/gji/ggs126

We present a P-wave velocity and a density model in the central Davis Strait along with MCS and magnetic anomaly data. The line is mostly underlain by continental crust with a 45-km-long section that is similar to an oceanic section along a line in the southern Davis Strait (Funck et al., 2007). With a plate kinematic model we can demonstrate the evolution of the Ungava Fault Complex and the Hudson Fracture Zone. Given that the poles of rotation are correct, the Hudson Fracture Zone must have played a far greater role than previously assumed.

I calculated the P-wave velocity model, developed the plate kinematic model, and wrote the manuscript. Karsten Gohl supervised the work and was Chief Scientist during MSM09/3. Thomas Funck relocalized the OBS. Ingo Heyde completed the density modelling. Bernd Schreckenberger provided the magnetic anomaly data. Joanna Gerlings and Volkmar Damm assisted in the collection of seismic data and represent the Dalhousie University and BGR as cooperation partners in the project. All authors revised the manuscript and contributed to the results in several discussions.

**Palaeobathymetric reconstruction of the Davis Strait area - a polar gateway between Canada and Greenland**

S.K. Suckro, K. Gohl, and V. Damm
*to be submitted to Palaeogeography, Palaeoclimatology, Palaeoecology (2013)*

We estimate the palaeobathymetry of the Davis Strait area from Mid Cretaceous to Late Eocene. To accomplish this, we compiled seismic stratigraphy and drill site information for a backstripping routine and used a plate tectonic model for thermal subsidence calculations. The palaeobathymetry grids show that the Davis Strait probably prevented a water transfer between the Labrador Sea and the Baffin Bay before the Late Eocene. It is likely that a cyclonic current, similar to today, was present in the Labrador Sea since the Paleocene.

I re-interpreted the new MCS data, compiled the dataset from the literature, developed the procedure for the calculation of a palaeobathymetry, and wrote the manuscript. Karsten Gohl supervised the work and was Chief Scientist during MSM09/3. Volkmar Damm assisted in the collection of seismic data and represents the BGR as cooperation partner in the project. All authors revised the manuscript and contributed to the results in several discussions.

# Chapter 4

# The crustal structure of southern Baffin Bay: implications from a seismic refraction experiment

Sonja K. Suckro[1], Karsten Gohl [1], Thomas Funck[2], Ingo Heyde[3], Axel Ehrhardt[3], Bernd Schreckenberger[3], Joanna Gerlings[4], Volkmar Damm[3], Wilfried Jokat[1]

[1] Alfred Wegener Institute for Polar and Marine Research (AWI), Am Alten Hafen 26, 27568 Bremerhaven, Germany

[2] Geological Survey of Denmark and Greenland (GEUS), Øster Voldgade 10, 1350 Copenhagen K, Denmark

[3] Federal Institute for Geosciences and Natural Resources (BGR), Stilleweg 2, 30655 Hanover, Germany

[4] Dalhousie University, Department of Earth Sciences, 1459 Oxford Street, Halifax, N.S., Canada

# 4.1 Summary

Baffin Bay represents the northern extension of the extinct rift system in the Labrador Sea. While the extent of oceanic crust and magnetic spreading anomalies are well constrained in the Labrador Sea, no magnetic spreading anomalies have yet been identified in Baffin Bay. Thus, the nature and evolution of the Baffin Bay crust remain uncertain. To clearly characterize the crust in southern Baffin Bay, 42 ocean bottom seismographs were deployed along a 710-km-long seismic refraction line, from Baffin Island to Greenland. Multichannel seismic reflection, gravity, and magnetic anomaly data were recorded along the same transect. Using forward modelling and inversion of observed traveltimes from dense airgun shots, a P-wave velocity model was obtained. The detailed morphology of the basement was constrained using the seismic reflection data. A 2-D density model supports and complements the P-wave modelling. Sediments of up to 6 km in thickness with P-wave velocities of 1.8 - 4.0 $\mathrm{km\,s^{-1}}$ are imaged in the centre of Baffin Bay. Oceanic crust underlies at least 305 km of the profile. The oceanic crust is 7.5 km thick on average and is modelled as three layers. Oceanic layer 2 ranges in P-wave velocity from 4.8 - 6.4 $\mathrm{km\,s^{-1}}$ and is divided into basalts and dykes. Oceanic layer 3 displays P-wave velocities of 6.4 - 7.2 $\mathrm{km\,s^{-1}}$. The Greenland continental crust is up to 25 km thick along the line and divided into an upper, middle, and lower crust with P-wave velocities from 5.3 - 7.0 $\mathrm{km\,s^{-1}}$. The upper and middle continental crust thin over a 120-km-wide continent-ocean transition zone. We classify this margin as a volcanic continental margin as seaward dipping reflectors are imaged from the seismic reflection data and mafic intrusions in the lower crust can be inferred from the seismic refraction data. The profile did not reach continental crust on the Baffin Island margin, which implies a transition zone of 150 km length at most. The new information on the extent of oceanic crust is used with published poles of rotation to develop a new kinematic model of the evolution of oceanic crust in southern Baffin Bay.

Keywords: plate motions, continental margins: divergent, crustal structure, Arctic region

## 4.2  Introduction

Baffin Bay is located between the Canadian Baffin Island and Greenland. It represents the northern extension of the rift system in the Labrador Sea, from which it is separated by the bathymetric high of Davis Strait (Fig. 4.1). Although the opening of the Northeast Atlantic is an ongoing process, the opening of the Labrador Sea and Baffin Bay ceased in mid Eocene times (Chalmers & Pulvertaft, 2001). Since then, subsidence and sedimentation are the dominant geologic processes in these basins.

The crustal structure and evolution of the Labrador Sea have been studied in detail (Chian & Louden, 1994; Chian et al., 1995; Chalmers & Pulvertaft, 2001). Magnetic spreading anomalies can clearly be identified in the central Labrador Sea and models of oceanic spreading have been proposed (Srivastava, 1978; Roest & Srivastava, 1989; Oakey, 2005). However the identification of the oldest magnetic spreading anomaly remains enigmatic. Roest & Srivastava (1989) use chron 33 in their model, which dates to 74 - 82 Ma after Gradstein et al. (2004), while Chalmers & Laursen (1995) argue that magnetic anomaly 27N is the oldest one observed (62 Ma after Gradstein et al. (2004).

The extent of oceanic, transitional, and continental crust in the northern Labrador Sea has been mapped with two seismic refraction lines (Funck et al., 2007; Gerlings et al., 2009). Along NUGGET line 1 a 140-km-long segment of oceanic crust is interpreted between continental blocks (Funck et al., 2007). A layer of magmatic underplating is modelled beneath the oceanic crust and for 200 km at the Greenland margin (Funck et al., 2007). NUGGET line 2 images the transition from continental to oceanic crust (Gerlings et al., 2009).

Although the evolution of Baffin Bay is closely related to the evolution of the Labrador Sea, no clear magnetic spreading anomalies are identified there. Therefore, the nature and evolution of oceanic crust in Baffin Bay remain uncertain.

A first comprehensive study on the nature of Baffin Bay crust is provided by Keen & Barrett (1972). From sonobuoy recordings, the crust of the central basin is interpreted as abnormally thin oceanic crust. Rice & Shade (1982) and Jackson et al. (1992) identify oceanic crust in northern Baffin Bay from seismic reflection lines.

In northern Baffin Bay five seismic refraction lines are located near Ellesmere Island and across Nares Strait (Fig. 4.1; Jackson & Reid 1994; Reid & Jackson 1997; Funck et al. 2006). Line 1 and 3 image a thinning of crystalline crust towards the basin but no oceanic crust (Jackson & Reid, 1994). Along line 4 (Fig. 4.1) serpentinized mantle is interpreted which implies an amagmatic continental margin (Reid & Jackson, 1997).

Mainly from potential field data, Chalmers & Oakey (2007) compiled a tectonic map of the Baffin Bay and Labrador Sea region. This is incorporated in the Geological Map of the Arctic (Harrison et al., 2008), but will be quoted as Chalmers & Oakey (2007) in the following. The locations of extinct spreading centres in Baffin Bay are oriented along distinct free-air gravity lows, striking northwest - southeast, as previously proposed by Chalmers & Pulvertaft (2001) and also visible in Fig. 4.1. Chalmers &
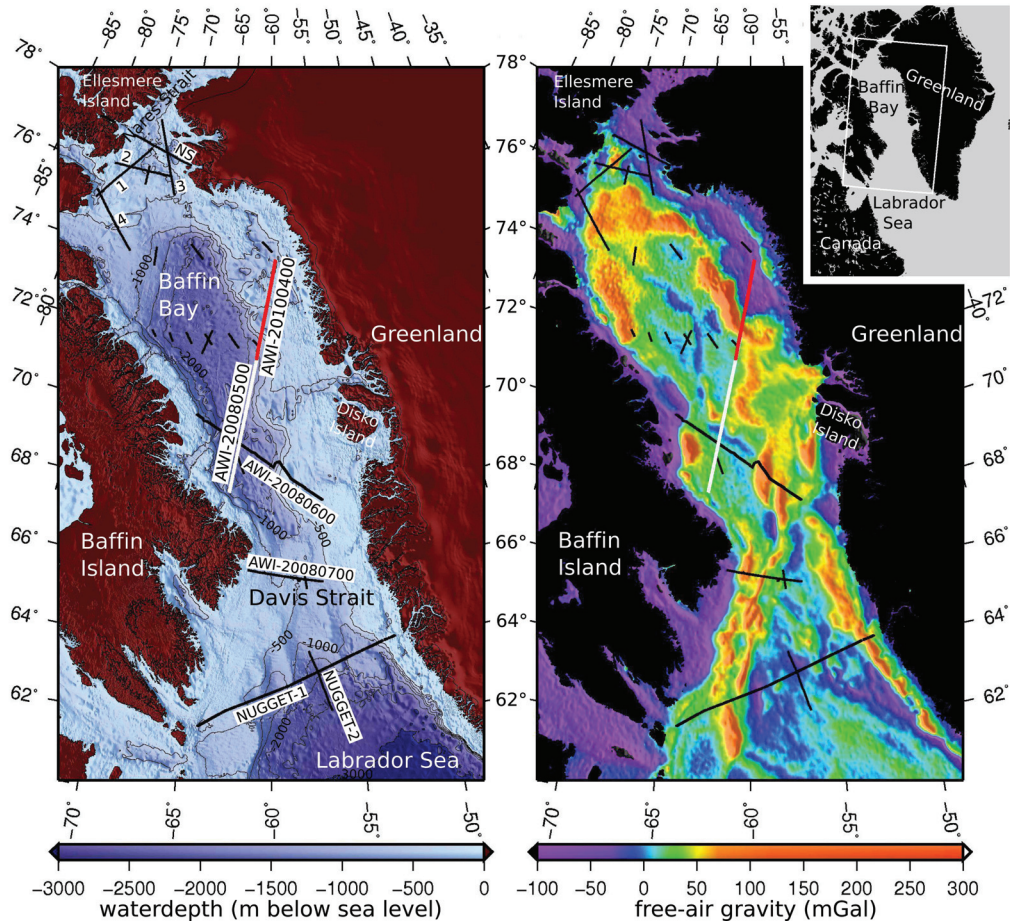
**Figure 4.1:** (Left) Bathymetric map of the Baffin Bay area (GEBCO_08 Grid, Version 20090202, http://www.gebco.net) with place names and locations of published seismic refraction data. The profiles discussed in this paper are marked in white and red (Gohl et al., 2009; Damm, 2010), black dots and short black lines mark sonobuoy locations and profiles from Keen & Barrett (1972); all other data are seismic refraction lines; Numbers 1 to 4 are line 1 to 4 (Jackson & Reid, 1994; Reid & Jackson, 1997); NS is Nares Strait Line 3 (Funck et al., 2006); AWI-20080600 (Funck et al. (2012), submitted); AWI-20080700 (Gohl et al. (2009), in preparation); NUGGET-1 and -2 (Funck et al., 2007; Gerlings et al., 2009). (Right) Free-air gravity anomalies derived from satellite altimetry (Sandwell & Smith (2009), version 18.1) of the offshore area of Baffin Bay. The same locations as in the left map are marked.
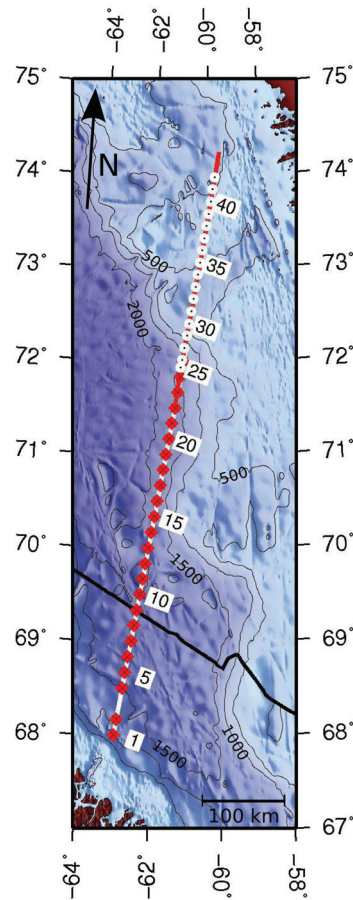
**Figure 4.2: Locations of OBS along line AWI-20080500 (white line with red OBS locations) and AWI-20100400 (red line with white OBS locations); OBS 3 did not record data and is therefore not marked; line AWI-20080600 is marked in black; bathymetry map from GEBCO_08 Grid, Version 20090202, http://www.gebco.net.**

Oakey (2007) differentiate Paleocene from Eocene oceanic crust due to a change of direction in sea-floor spreading.

In order to clearly characterize the type and extension of the crust in Baffin Bay, we present data from ocean bottom seismographs (OBS) along a 710-km-long seismic refraction line in southern Baffin Bay (Figs 4.1, 4.2). The line is oriented across the proposed location of an extinct spreading centre and oceanic crust of Paleocene and Eocene age (Chalmers & Oakey, 2007). Multichannel seismic reflection (MCS) data are used to model the detailed morphology of the basement. Magnetic field data are analysed for indications of magnetic spreading anomalies and volcanic intrusions. Additional density modelling was performed using shipboard gravity data to complement the P-wave model. This analysis now allows for the characterization of the crustal affinity in south-

23

ern Baffin Bay. From previous plate reconstruction models (Roest & Srivastava, 1989; Oakey, 2005; Müller et al., 2008), we chose the poles of rotation from Oakey (2005) and with our new data, develop a kinematic model for the evolution of oceanic crust in southern Baffin Bay.

## 4.3 Tectonic background of the opening of the Labrador Sea and Baffin Bay

Baffin Bay and the Labrador Sea formed during Paleocene to Eocene times when the Greenland plate first separated from the North American craton and subsequently from Eurasia (Chalmers & Pulvertaft, 2001; Tessensohn & Piepjohn, 2000). The opening history of Canada and Greenland is derived from magnetic spreading anomalies in the North Atlantic and Labrador Sea by various authors (Srivastava, 1978; Roest & Srivastava, 1989; Chalmers & Laursen, 1995). Srivastava (1978) first dated magnetic spreading anomalies in the Labrador Sea and proposed a single, linear spreading centre in Baffin Bay. Roest & Srivastava (1989) modified the previous reconstruction and suggested two spreading centres in Baffin Bay, separated by a transform fault. Jackson et al. (1992) again proposed a single spreading centre. The latest opening reconstruction from Oakey (2005) uses the isochrones from Roest & Srivastava (1989) in the Labrador Sea and the geometry of fracture zones.

The initiation of extension between Canada and Greenland is dated to 223 - 150 Ma from dykes in Southwest Greenland (Larsen et al., 2009). Following extension, regional rifting emplaced > 400-km-long dyke swarm in a coast-parallel fracture system in Southwest Greenland from 140 - 133 Ma (Watt, 1969). The duration of rifting is disputed, as the timing of initial breakup remains uncertain. The oldest undisputed magnetic spreading anomaly is chron 27N (Chalmers & Laursen, 1995).

The motion of the Greenland plate relative to the North American plate changed at magnetic chron 24 from an eastward motion to a more northeastward motion, indicated by the orientation of magnetic spreading anomalies (Srivastava, 1978; Roest & Srivastava, 1989; Oakey, 2005). The breakup between East Greenland and Northwest Europe is also dated to chron 24 (Talwani & Eldholm, 1977; Olesen et al., 2007) and may thus have caused the change in motion of the Greenland plate. According to Storey et al. (1998), the reorientation of spreading caused a volcanic pulse at 54.8 - 53.6 Ma in the Disko Island area. An older volcanic pulse is identified at 60.7 - 59.4 Ma and correlated with the arrival of the Greenland-Iceland mantle plume (Storey et al., 1998). Spreading ceased in the Labrador Sea between chrons 20 and 13 (Srivastava, 1978), while spreading between Greenland and Eurasia and the opening of the Northeast Atlantic is ongoing.

**Table 4.1: Parameters of seismic refraction measurements.**

|  | MSM09/3 (2008) | ARK-XXV/3 (2010) |
|---|---|---|
| OBS type | 3-component Mark seismometers, 4.5 Hz natural frequency, 1 hydrophone | 3-component broad-band Güralp seismometers, 60 s natural period, 1 hydrophone |
| OBS spacing | approx. 18 km | approx. 12 km |
| Seismic source | array of 16 G.Guns$^{TM}$ and 2 Bolt$^{TM}$ guns | array of 6 G.Guns$^{TM}$ and 2 G.Guns$^{TM}$ |
| Total source volume | 114.8 litres, 7006 in$^3$ | 68.2 litres, 4160 in$^3$ |
| Shot interval | 60 s | 60 s |

## 4.4 Data acquisition

The seismic and potential field data presented in this study consist of two profiles (Fig. 4.1, 4.2), acquired during the research cruise MSM09/3 of RV Maria S. Merian in 2008 (line AWI-20080500, Gohl et al. 2009) and the cruise ARK-XXV/3 of RV Polarstern in 2010 (line AWI-20100400, Damm 2010). While AWI-20080500 and AWI-20100400 denote seismic refraction lines, BGR08-304 and BGR10-309 refer to seismic reflection, gravity, and magnetic anomaly data along the same lines. The survey in 2008 was designed to cross the proposed location of an extinct Eocene spreading centre as well as various units of oceanic and transitional crust, according to the tectonic map of Chalmers & Oakey (2007). On the 2010 cruise, the line from 2008 was extended to image the transition from thin crust in the centre of the basin to continental crust on the Greenland shelf.

The 24 southernmost ocean bottom seismometers (OBS) belong to line AWI-20080500, an additional 17 OBS were deployed along line AWI-20100400. An overlap of 72 km of both profiles was chosen to ensure overlapping ray coverage in the deep crust. Acquisition parameters of both surveys are listed in Table 4.1. On both seismic refraction lines, multichannel seismic reflection (MCS) data were acquired. Parameters of the MCS setup are summarized in Table 4.2.

Gravity data were recorded in 2008 with the KSS31M and in 2010 with the KSS31 sea gravimeters (Bodensee Gravitymeter Geosystem GmbH) at 1 Hz sampling rate. To reference the shipboard gravity data connection measurements were carried out with a LaCoste&Romberg land gravity meter at the beginning and end of each cruise (Gohl et al., 2009; Damm, 2010). Magnetic field data were recorded on RV Maria S. Merian with an Overhauser SeaSPY marine magnetometer system towed approximately 600 m behind the vessel. On the Polarstern cruise, an Overhauser SeaSPY marine gradient magnetometer system consisting of two sensors at 150 m distance was used. The use of a gradiometer allows for the elimination of the diurnal variations induced by solar storms

**Table 4.2: Parameters of MCS measurements.**

|                        | MSM09/3 (2008)                    | ARK-XXV/3 (2010)                  |
| ---------------------- | --------------------------------- | --------------------------------- |
| Active streamer length | 3450 m                            | 3750 m                            |
| Number of channels     | 276                               | 300                               |
| Sampling rate          | 2 ms                              | 2 ms                              |
| Recording length       | 14 s                              | 13 s                              |
| Seismic source         | array of 16 G.Guns$^{TM}$         | array of 6 G.Guns$^{TM}$          |
| Total source volume    | 50.8 litres, 3100 in$^3$          | 51.1 litres, 3120 in$^3$          |
| Operation pressure     | 100 - 135 bar                     | 150 bar                           |
| Shot interval          | 18 s                              | 15 s                              |

during the survey (Roeser et al., 2002). Multi-beam bathymetry data were recorded during both cruises. In this study, we only use the centre beam for depth of the seafloor in the P-wave velocity and density models. Research vessel Maria S. Merian is equipped with an EM-120 multi-beam echo-sounder for continuous mapping of the seafloor while on research vessel Polarstern a Hydrosweep DS-2 swath system was operated. For calibration of the depth measurements, sonic log profiles were acquired on both cruises.

## 4.5 Seismic data

### 4.5.1 Processing of seismic data

Raw data from the OBS recorders were merged with navigation data, transferred to SEGY-format, cut according to the shot interval into 60 s traces, and the OBS locations were more accurately determined using direct arrivals. We picked all refracted and reflected signals with the software ZP (by B. Zelt), using a bandpass filter of 4 - 15 Hz applied for the near offset signals ($\pm 30$ km distance from the OBS) and 4 - 10 Hz for more distant signals. Picking errors of 0.02 to 0.50 ms were assigned manually for each phase.

In the MCS data, we mapped the basement for the P-wave velocity and density model (Fig. 4.3). We processed line BGR08-304 with the software package FOCUS$^{TM}$ and line BGR10-309 with ProMAX$^{TM}$. The processing steps are listed in Table 4.3.

### 4.5.2 P-wave modelling

We obtained a P-wave velocity structural model with the software RAYINVR (Zelt & Smith, 1992) by forward modelling and subsequent inversion of each layer (Figs 4.4, A.1 - A.4). The detailed basement morphology was constrained using the high
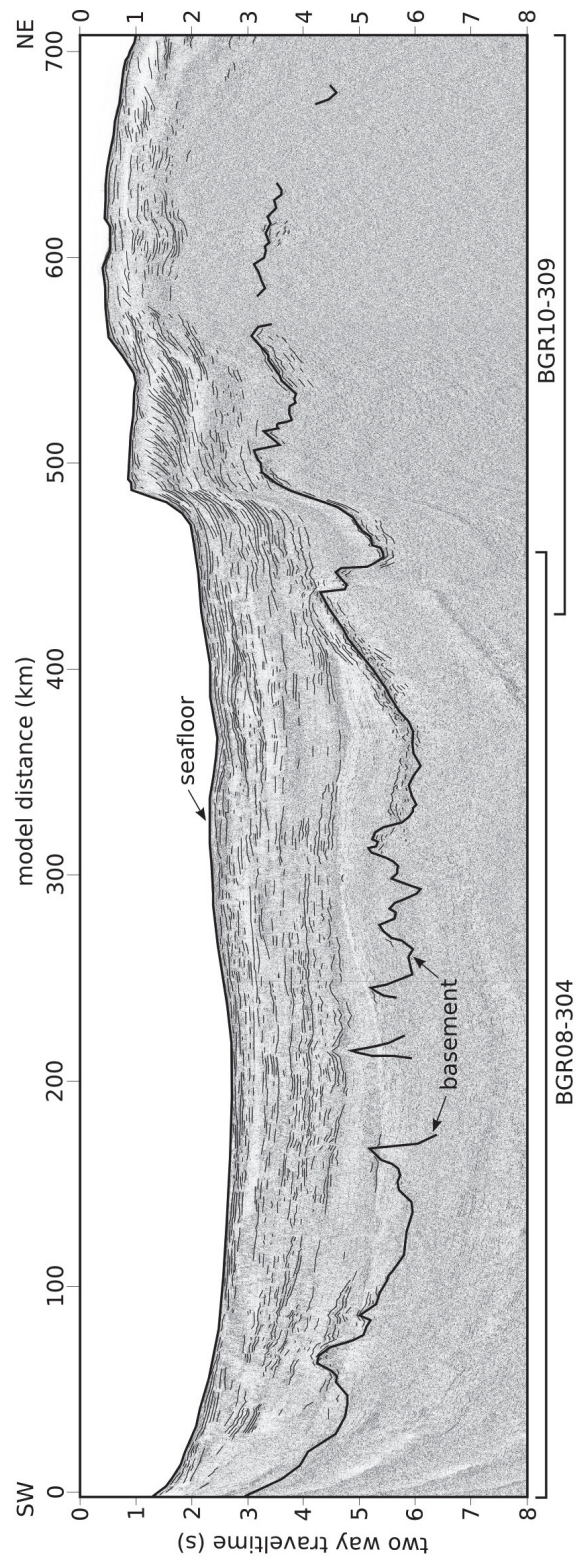
**Figure 4.3: MCS data along line BGR08-304 & BGR10-309 with a line drawing.**

27

**Table 4.3: Processing of the MCS lines.**

| FOCUS™ processing of line BGR08-304 | ProMAX™ processing of line BGR10-309 |
|---|---|
| - Resampling: 4 ms | - Resampling: 4 ms |
| - Geometry: CMP binning of 6.25 m | - Geometry: CMP binning of 6.25 m |
| - Interactive velocity analysis | - Bandpass filter: 4-8-80-160 Hz |
| - Gain: spherical divergence | - Gain: spherical divergence |
| - Bandpass filter: 2-7-90-120 Hz | - Prestack deconvolution |
| - Multiple suppression: fk filter "zmult" | - Interactive velocity analysis |
| - Normal move out (NMO) correction | - Surface related multiple estimation |
| - Stack | - NMO correction |
| - Kirchhoff migration | - Stack |
| - Coherency filter after two way travel-time of first multiple | - Kirchhoff migration |

resolution MCS data (Fig. 4.3). From the model distance of 560 to 708 km, the depth of basement is modelled with OBS data only, as the basement is not clearly visible on the MCS line. At OBS 34 to 41, we modelled deep crustal reflections from water multiples. At OBS 42, a multiple reflection within the sediment cover was used. In areas lacking refracted phases, velocity values were interpolated from constrained velocity nodes nearby.

Refracted and reflected phases in the sedimentary layers are grouped in the following to $P_{sed}$ and $P_{sed}P$, respectively. The name of the reflected phase always refers to a reflection at the base of a layer. Beneath the sediments, phases of a layer that we later interpret as basalts are encountered and named $P_b$ and $P_bP$. Apart from the basaltic layer, we divide the crust into three layers: upper crust / dykes ($P_{c1}$ and $P_{c1}P$), middle crust ($P_{c2}$ and $P_{c2}P$), and lower crust / oceanic layer 3 ($P_{c3}$). Oceanic layer 2 comprises basalt and dyke phases. Reflections from the Moho are named $P_mP$, refractions in the mantle $P_n$ and reflections from floating reflectors in the mantle $P_nP$. Phases modelled from multiples in the water column and in the sediment package are identified with superscripts $^w$ and $^s$ (Figs A.1 - A.4).

Figs 4.5 and 4.6 display sections from different parts of the model where data quality and the corresponding raytracing were good. In Fig. 4.5 sediment phases are visible to 16 - 20 km offset and modelled with a 4 to 5 km thick sedimentary cover. Although no $P_b$ or $P_bP$ phases are observed in OBS 6, it was necessary to introduce the basalts layer in order to match the basement on the MCS data. The thickness of the basalt layer was determined from the delay required for the crustal phases. OBS 20 does display a $P_b$ phase. Due to the overlay of sediment and crustal phases at the basement, signals from the basaltic layer are often hidden. OBS 6 recorded a strong $P_mP$ phase from 30 -
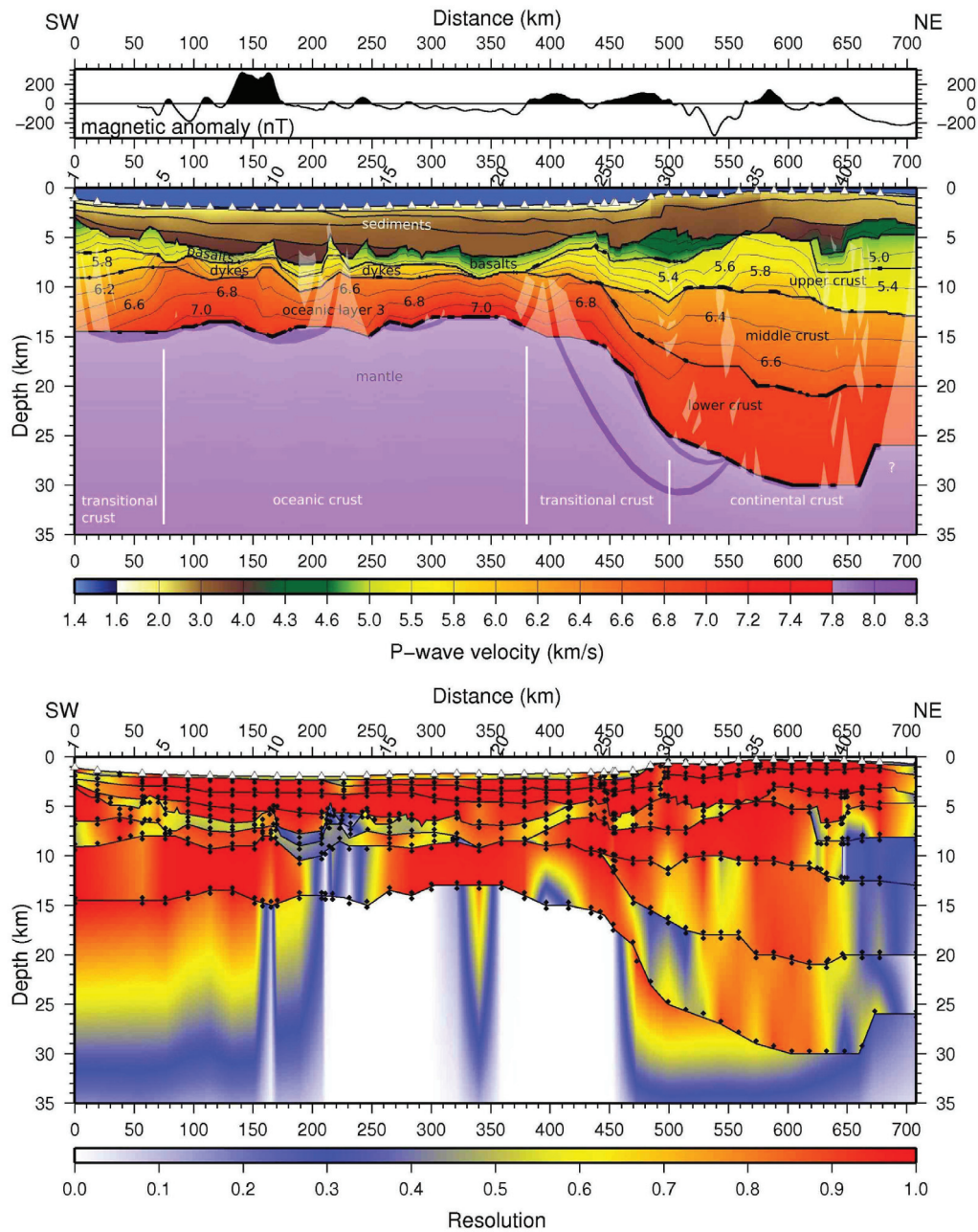
**Figure 4.4: (Top) Magnetic anomaly data along the presented line. (Centre) P-wave velocity model. White triangles indicate OBS locations; rotated numbers are OBS numbers; numbers on contour lines are P-wave velocities in km s$^{-1}$; thick layer boundaries mark discontinuities that are constrained by reflections; white shaded areas are not passed by rays. (Bottom) Grid of the diagonal values of the resolution matrix of the P-wave velocity model. Velocity nodes are displayed with black dots and are shifted inside the layers to indicate their affiliation; white triangles indicate OBS locations; rotated numbers are OBS numbers.**

70 km offset. This runs into the $P_{c3}$ refraction and coincides with this phase for offsets greater than 50 km. OBS 20 also detected a $P_mP$ phase, but it is much weaker and best visible in the multiple at 8 s travel-time. Between offsets -50 to -45 km, a $P_n$ phase was modelled. As there are only few picks for this phase, an accurate determination of the mantle velocity is not possible. In Fig. 4.6, OBS 29 is displayed as an example for raytracing in three-layered crust with the refractions $P_{c1}$, $P_{c2}$, and $P_{c3}$. OBS 40 is chosen as an example for modelling from multiples (Fig. 4.6). The grey dashed rays of the $P_{c2}P$ and $P_mP$ phases are reflected at the seafloor and at the water surface, before propagation in the subsurface. Apart from a $P_b$ phase, these multiples are the only signals at offsets greater than 30 km. A reason for the missing crustal phases can be the absorption of energy by an upper crustal basaltic layer.

Fig. 4.7 shows the ray coverage in the different layers to assess how well the model is constrained. P-wave velocities of the sediments are well constrained by refractions with the exception of the lowermost sediment layer between the model distances of 280 to 420 km. The thickness of this layer is constrained solely by reflections off the basement. The basalts are constrained by $P_b$ and $P_bP$ phases for the first 80 km of the model and from a distance of 300 km to the end of the model. In the area between, the layer is needed to model the basement from the MCS data and to account for the delay of other crustal traveltimes. The upper crust and dykes are well constrained by rays between the model distances of 20 to 170 km and 380 to 620 km. Outside these areas only sparse reflections mark the lower boundary of this layer. The middle crust is mainly modelled from reflections found as multiples. The velocity structure was extrapolated from $P_{c2}$ phases at the beginning of the mid-crustal layer (distance 440 to 520 km). Velocities in the lower crust are well constrained from the model distances of 40 to 190 km, 250 to 380 km, and 400 to 480 km. At the Baffin Island margin, the velocities are gradually lowered landwards to correspond with the density decrease in the gravity model. On the Greenland margin (distance 480 to 708 km), the velocity at the top of the lower crust was increased slightly with respect to the middle crust to create a velocity impedance that could generate various $P_{c2}P$ phases. $P_mP$ phases constrain the depth of the Moho along most of the profile. $P_n$ phases are detected for some stations from distance 0 to 320 km. Northeast of the model distance of 320 km, only OBS 36 recorded a mantle refraction (Fig. 4.7).

Table 4.4 summarizes statistical values as a measure of quality for the model's fit to the picked traveltimes. The root mean square (RMS) traveltime error is calculated by RAYINVR (Zelt & Smith, 1992) from the misfit between calculated and picked traveltimes. The normalized $\chi^2$ is a measure of how well the calculated traveltimes are within range of the assigned pick uncertainties and should ideally be one. The P-wave velocity model presented here has a normalized $\chi^2$ value of 2.3 and an RMS traveltime error of 112 ms for modelling without multiples. Typical RMS traveltime errors can be in the range of 80 ms (Bullock & Minshull, 2005) to 153 ms (Lau et al.,
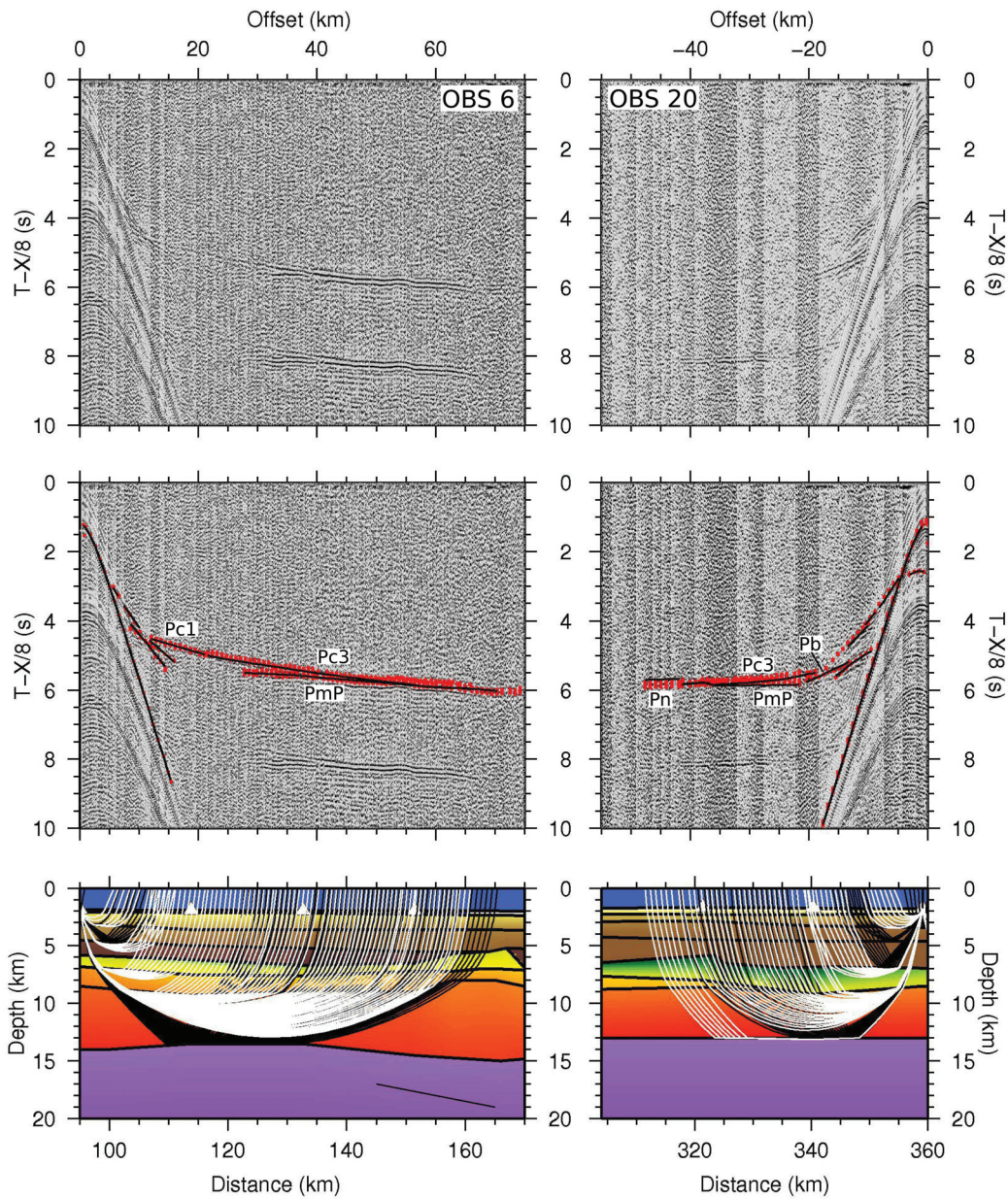
**Figure 4.5:** (Top) Part of seismic sections from OBS 6 and 20, plotted with a reduction-velocity of $8\,\mathrm{km\,s^{-1}}$ and a bandpass-filter of 4 - 10 Hz. (Centre) The same sections with picked signals (red bars with bar length according to assigned pick uncertainty) and modelled phases (black lines). Often phases of the lower crust and mantle are stronger in the multiple, as the data from OBS 20 show. (Bottom) Raytracing in the P-wave velocity model; refracted waves in white, reflected waves in black; for clarity only every fifth ray is drawn; colour scale of the P-wave velocity model according to Fig. 4.4: blue - water, brown - sediments, green - basalts, orange - dykes, red - oceanic layer 3, purple - mantle; white triangles mark OBS locations.

31
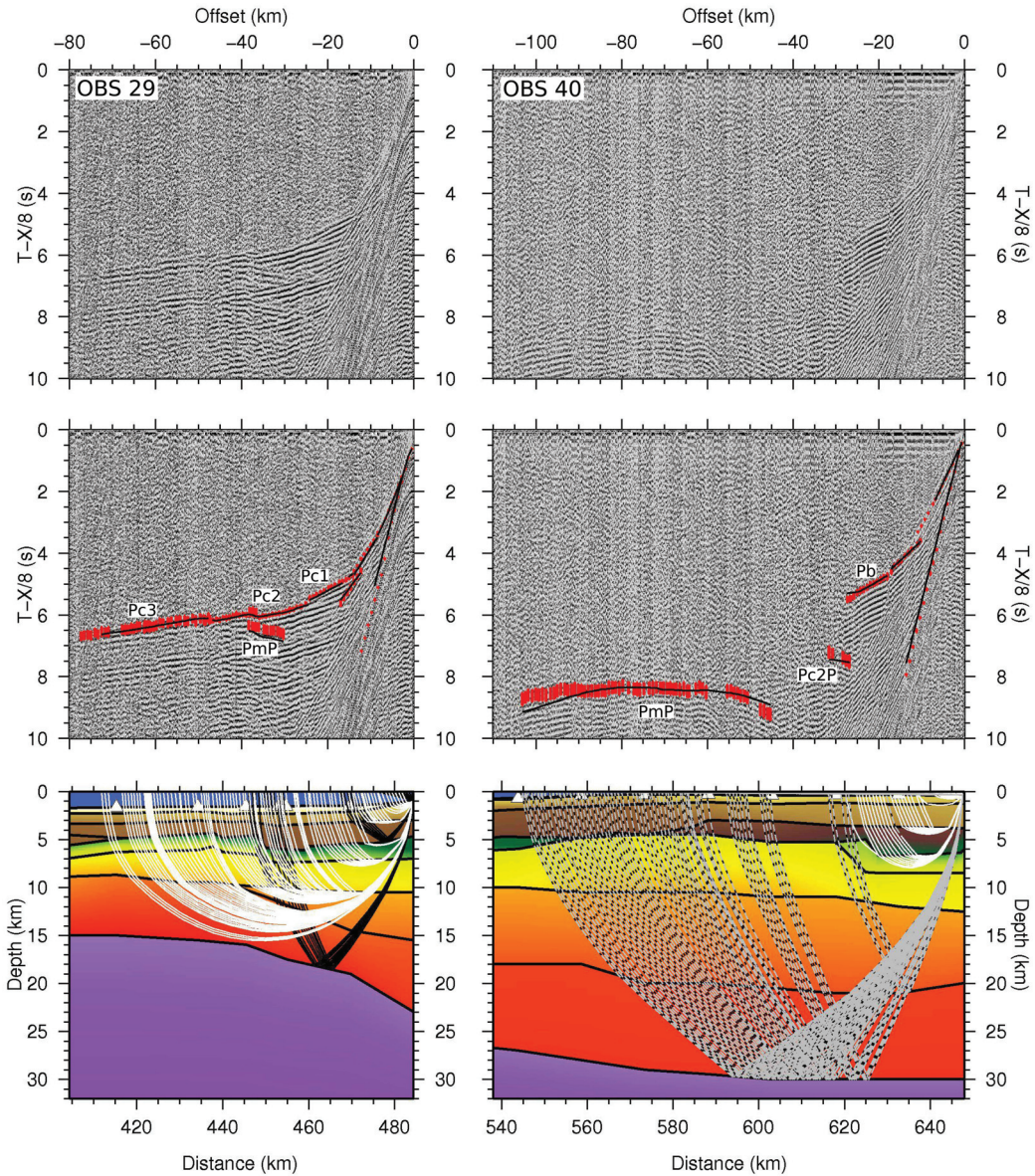
**Figure 4.6: (Top) Part of seismic sections from OBS 29 and 40, plotted with a reduction-velocity of $8\,km\,s^{-1}$ and a bandpass-filter of 4 - 10 Hz. (Centre) The same sections with picked signals (red bars with bar length according to assigned pick uncertainty) and modelled phases (black lines). (Bottom) Raytracing in the P-wave velocity model; refracted waves in white, reflected waves in black, those derived from the water multiple with gray dashes; for clarity only every fifth ray is drawn; colour scale of the P-wave velocity model according to Fig. 4.4: blue - water, brown - sediments, green - basalts, yellow - upper crust, orange - middle crust, red - lower crust, purple - mantle; white triangles mark OBS locations.**
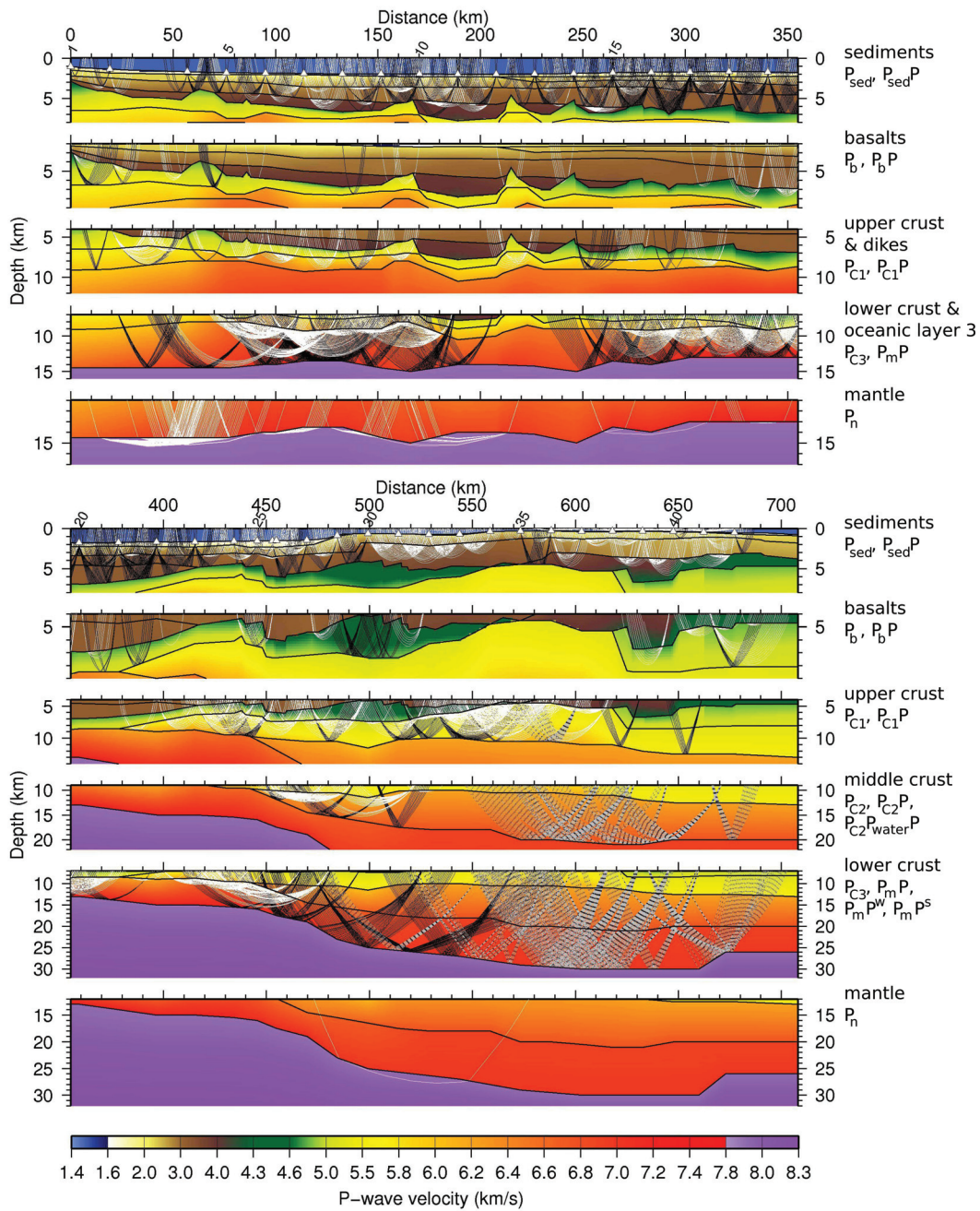
**Figure 4.7:** Ray coverage of the P-wave velocity model with refracted waves in white, reflected waves in black, and rays derived from multiples with grey dashes. For clarity, the model is split in two 355-km-long segments and only every fifth ray is plotted. Each panel displays the phases labeled on the right side.

33

**Table 4.4: Statistical values of the P-wave velocity model calculated by rayinvr and dmplstsqr for the inversion of each layer. For the inversion of a layer only the rays specifying this layer were activated. Rays from the direct arrival are not taken into account.**

| Phase | Number of picks | Pick uncertainty (ms) | RMS (ms) | Normalized $\chi^2$ |
|---|---|---|---|---|
| $P_{sed}$ | 5555 | 47 | 60 | 2.328 |
| $P_{sed}P$ | 3370 | 55 | 81 | 2.232 |
| $P_b$ | 927 | 75 | 78 | 2.039 |
| $P_bP$ | 446 | 73 | 83 | 1.585 |
| $P_{c1}$ | 3527 | 82 | 96 | 1.881 |
| $P_{c1}P$ | 753 | 128 | 148 | 1.954 |
| $P_{c1}P^w$ | 126 | 150 | 130 | 0.752 |
| $P_{c2}$ | 602 | 134 | 138 | 2.135 |
| $P_{c2}P$ | 233 | 190 | 114 | 0.774 |
| $P_{c2}P^w$ | 487 | 200 | 157 | 0.618 |
| $P_{c2}P^s$ | 197 | 200 | 142 | 0.504 |
| $P_{c3}$ | 3876 | 82 | 109 | 2.207 |
| $P_mP$ | 3367 | 117 | 218 | 3.361 |
| $P_mP^w$ | 1507 | 222 | 500 | 4.133 |
| $P_n$ | 1224 | 114 | 184 | 2.286 |
| total without multiples | 23880 | 80 | 111 | 2.315 |
| total with multiples | 26197 | 92 | 135 | 2.367 |

2006). Normalized $\chi^2$ values can be higher than 3.7 (Voss et al., 2009), depending on the data quality and assigned pick uncertainty.

Fig. 4.4 shows the diagonal values of the resolution matrix as a color grid. These values are calculated at the velocity nodes and provide a measure of how well a velocity value is constrained by all rays passing though it. Lutter & Nowack (1990) refer to values greater than 0.6 as well resolved, which is true for most of the model. Perturbation of single velocity and boundary nodes gives an uncertainty of modelled P-wave velocities and layer thicknesses. The P-wave velocity of the sediment layers and the basalts-layer is constrained to $\pm 0.1 \, \text{km s}^{-1}$. As the basement is constrained by the MCS data, this boundary can only be varied by $\pm 0.1 \, \text{km}$. The P-wave velocities of the upper and middle crust are constrained to $\pm 0.2 \, \text{km s}^{-1}$ and their boundaries to $\pm 0.2 \, \text{km}$. Where the lower boundary of the middle crust is only modelled from multiples, the uncertainty can reach $\pm 1.0 \, \text{km}$. The lower crust is constrained to $\pm 0.1 \, \text{km s}^{-1}$ and $\pm 0.5 \, \text{km}$. Where it is modelled from multiples these values can be twice as high.

### 4.5.3 Results and interpretation of the P-wave model

The P-wave velocity model (Fig. 4.4) shows a thick sedimentary layer (up to 6 km) in the centre of the basin from the model distance of 170 to 200 km. Average velocities of the **sediment** layers range from $1.8 \, \text{km s}^{-1}$ at the top to $4.0 \, \text{km s}^{-1}$ at the bottom. The basement morphology varies on the profile from smooth segments in the deep sea environment to fault-block features and rough segments at the Greenland continental shelf (northeast of the model distance of 430 km, Fig. 4.3). Three distinct basement highs at the distances of 170, 215, and 245 km dominate the basement morphology in the centre of the basin.

The first crustal layer, which we interpret as **basalts** from the model distance of 0 to 560 km has velocities ranging from $4.2 - 5.7 \, \text{km s}^{-1}$ (Fig. 4.4). Along the NUGGET line 1 some 600 km to the south, P-wave velocities in the same range ($4.2 - 5.8 \, \text{km s}^{-1}$, Funck et al. (2007)) were interpreted as basalts and are confirmed by drill holes. Although there are no drill holes along our line, we adopt this interpretation. The layer we interpret as **dykes** from the model distance of 0 to 330 km ranges in velocities from $5.5 - 6.4 \, \text{km s}^{-1}$. This interpretation is supported by Gilbert & Salisbury (2011), who report a P-wave velocity range of $5.65 - 6.61 \, \text{km s}^{-1}$ for upper and lower dykes in oceanic crust from samples. From the model distance of 380 to 708 km, the layer interpreted as **upper crust** displays velocities of $5.1 - 6.1 \, \text{km s}^{-1}$ and thickens northeastwards. The **middle crust** is only present from a distance of 440 km northeastwards. The P-wave velocities range from $6.1 - 6.7 \, \text{km s}^{-1}$, but are only constrained for the southeastern 80 km by $P_{c2}$ phases (Fig. 4.7). **Oceanic layer 3** has P-wave velocities of $6.3 - 7.2 \, \text{km s}^{-1}$ and is 4 - 7 km thick. P-wave velocities of the **lower crust**, from distance 520 to 708 km, are modelled with $6.9 \, \text{km s}^{-1}$ and 6 - 10 km thickness. The velocity at the top of the **mantle** is kept constant at $7.9 \, \text{km s}^{-1}$.

The thickness and velocity structure of the crystalline crust, including basalts, upper, middle, and lower crust, allow a classification into oceanic, transitional, and continental crust.

#### Oceanic crust

We interpret oceanic crust from model distances of 75 to 380 km. Due to differences in the oceanic layer 2, comprising basalts and dykes, we separate the oceanic crust into five segments that are described in the following section. Fig. 4.8 shows vertical velocity profiles of these oceanic sections in comparison with a data review by White et al. (1992). The compiled data by White et al. (1992) represent oceanic crust in the Atlantic, which formed between 59 - 127 Ma.

85 to 155 km and 255 to 330 km:
The crust is 7 - 8.5 km thick. Oceanic layer 2 is 1 - 2.5 km thick and has a P-wave
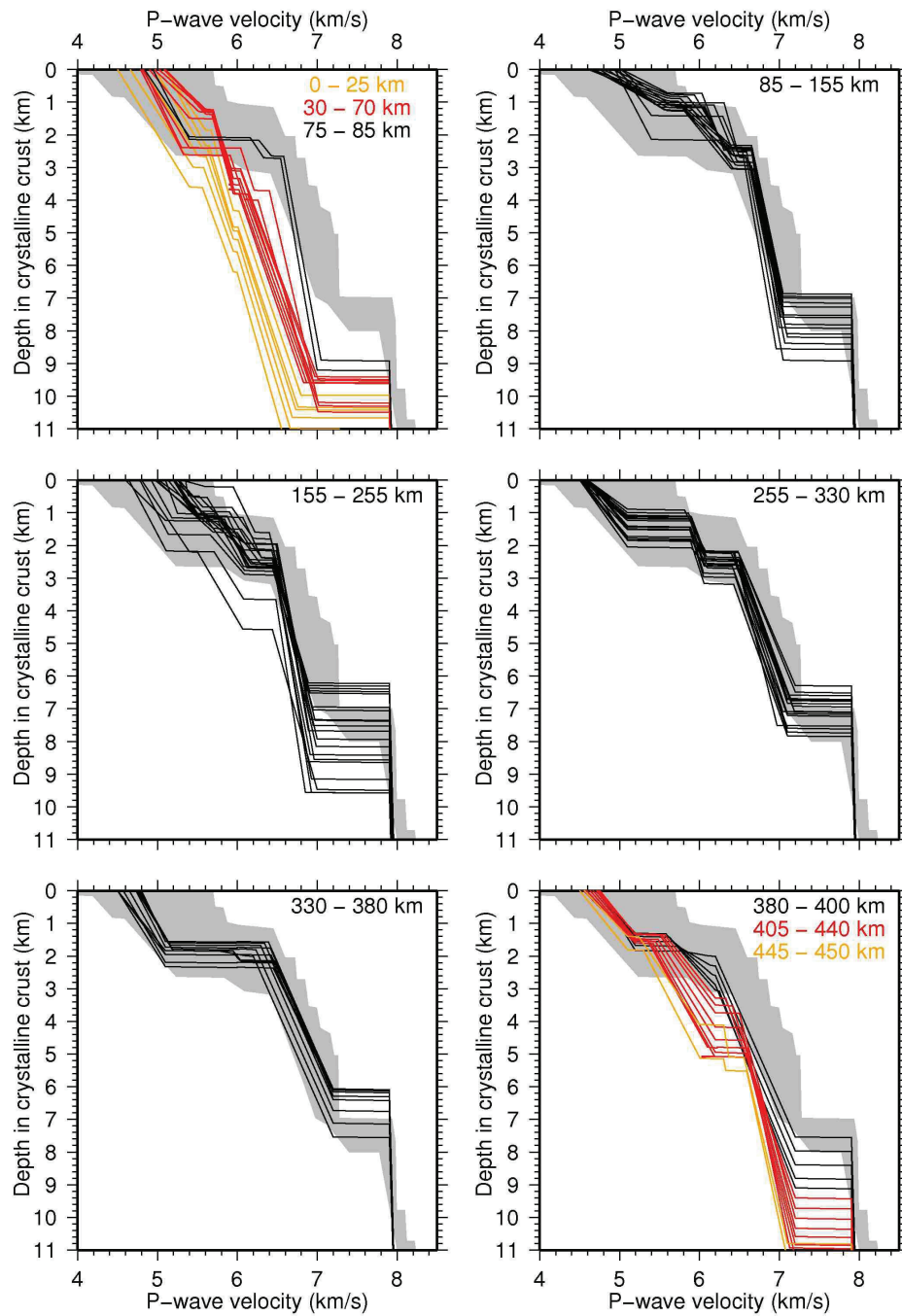
**Figure 4.8: Velocity-depth profiles from different segments of the crystalline crust in the P-wave velocity model, taken every fifth kilometer. Thin black lines are velocity-depth profiles from the model distances labeled in the upper right corner of each pannel. Gray shaded is the area outlined by the data compilation from White et al. (1992) of Atlantic oceanic crust from 59 - 127 Ma.**

velocity range from 4.8 - 6.4 km s$^{-1}$. Oceanic layer 3 is 4.5 - 6.1 km thick with P-wave velocities of 6.4 - 7.1 km s$^{-1}$. Fig. 4.8 shows, that thickness and velocity structure are compatible with oceanic crust.

155 to 255 km:

In the centre of southern Baffin Bay lies the deepest basin along the profile (Fig. 4.4, from model distance 170 to 200 km) with basement ridges on both sides. The velocity structure does not vary significantly from the previously described sections. From distance 190 to 210 km, the crust is only 6 km thick with a thickening of the oceanic layer 3 to both sides. Due to the thinner crust and the deep basin, we propose that this part of the profile represents an extinct spreading centre. Notable is also the symmetry of the Moho topography to this axis. Adjacent to the location of the extinct spreading centre, the crust thickens to 9 km, due to a thickening of oceanic layer 3 by 3 km and ridges in oceanic layer 2. The changes in thickness are well illustrated by the variability of velocity-depth-profiles in Fig. 4.8.

75 to 85 km and 330 to 380 km:

Along the model distance of 330 to 380 km, the crust is very homogeneous with respect to basement morphology and to thickness (6 - 7.5 km). In contrast to the previously mentioned segments, oceanic layer 2 is not divided into two layers. The basaltic layer with velocities of 4.7 - 5.1 km s$^{-1}$ lies directly on the oceanic layer 3 with velocities of 6.3 - 7.2 km s$^{-1}$. The small segment from the model distance of 75 to 85 km has a crustal thickness of 8.5 km. In oceanic layer 2, the basaltic layer thickens while the layer of dykes thins to only 0.5 km.

**Continental crust**

500 to 710 km, Greenland:

The crust is 21 - 23.5 km thick and consists of an upper, middle, and lower crust with an additional upper crustal layer landward from a model distance of 620 km. Velocities of the upper crust average to 5.5 km s$^{-1}$ and decrease northeastwards. The middle crust is modelled with 6.3 - 6.7 km s$^{-1}$ and the lower crust with 6.9 s$^{-1}$. Both layers are kept homogeneous in their velocity structure as they are not well constrained by the OBS data. $P_{c2}P$ phases indicate an impedance contrast at the middle to lower crust boundary, which can also exceed the modelled velocity contrast of 0.2 km s$^{-1}$, but cannot be quantified due to missing raycoverage. The modelled velocity trend of the crust fits well to the P-wave velocity range that Christensen & Mooney (1995) report for extended continental crust. They report P-wave velocity ranges of 4.7 - 6.5 km s$^{-1}$ for upper crust, 6.6 - 6.8 km s$^{-1}$ for middle crust, and 6.8 - 7.2 km s$^{-1}$ for lower crust. The minimum of the global average of 30.5±5.3 km thickness (Christensen & Mooney, 1995) exceeds the thickness of 23 km found here by only 2.2 km.

37

Landward of the model distance of 620 km, a layer with P-wave velocities of 5.0 km s$^{-1}$ is modelled on top of the upper crust. The lower boundary of this layer is only constrained by one reflection (Figs 4.4 and 4.7). The P-wave velocities of this layer can equally be interpreted as basalts or consolidated sediments (Fox et al., 1973; Castagna et al., 1985). As the MCS data do not image the basement on this part of the profile well, no interpretation from the basement morphology can be given.

**Transitional crust**

We here use the term "transitional crust" where thickness and / or velocity structure of the crystalline crust vary significantly from that of oceanic and stretched continental crust.

380 to 500 km, Greenland:
The crust thickens from 8 - 21 km. At a model distance of 380 km an upper crustal layer appears with an average P-wave velocity of 5.5 km s$^{-1}$. It thickens from 0 - 4 km over a distance of 60 km with decreasing P-wave velocities further landward. At the model distance of 440 km, a mid-crustal layer appears, which thickens from 0 - 5 km. Noticeable is also the rise of P-wave velocities in the lower crust by 0.4 km s$^{-1}$ northeast of a model distance of 430 km, which is consistent with an increase in mafic content. The MCS data show a basement morphology with block faulting after a model distance of 430 km (Fig. 4.3) and from the distance of 390 to 410 km seaward dipping reflectors are imaged (Block et al., 2012).

The comparison with the data compilation from White et al. (1992) in Fig. 4.8 shows, that the oceanic character of the velocity distribution in the crust is well preserved up to a model distance of 400 km. From distance 405 km northeastwards, the thickening of upper and lower crust lead to a mismatch with the oceanic velocity-depth function from White et al. (1992). Though the type "oceanic crust" can be extended to a model distance of 400 km, we interpret the area southwest of 380 km as clear oceanic crust and the area northeast as transitional crust.

0 to 75 km, Baffin Island:
Toward the Baffin Island shelf, the crystalline crust thickens from 8 -11 km. Upper and lower crust shift to lower P-wave velocities southwestward, which is consistent with a decreasing amount of mafic material. Velocity-depth functions from model distances of 0 to 25 km differ from the compilation of White et al. (1992) due to slow P-wave velocities in the upper crust and thick basalts (Fig. 4.8). From distance 30 to 70 km, an increase of P-wave velocities in the upper crust and a decreasing thickness of the basalts are modelled, and an oceanic character develops. Unfortunately, this part of the profile is not well covered by the OBS data and will be discussed in connection with the density modelling.

**Table 4.5: Corrections applied to the gravity data.**

- time shift due to overcritical damping of the sensor
- conversion from instrument reading units to mGal
- tie to world gravity net IGSN 71 with connection measurements
- correction for the Eötvös effect with navigation data
- correction for instrument drift during the cruise
- subtraction of normal gravity (GRS80)

## 4.6 Gravity data

### 4.6.1 Processing and modelling of the gravity data

Several processing steps were applied to the gravity data to obtain the free-air gravity anomalies for subsequent modelling (Table 4.5). The forward modelling of gravity data was accomplished with the software GM-SYS (Northwest Geophysical Associates, Inc.). To set up a starting model, we used the geometry and velocity distribution of the P-wave velocity model. We calculated average P-wave velocities for each layer and converted them to density, according to the data synthesis from Barton (1986). To simplify the model, we combined the three upper sedimentary layers into one density unit (Fig. 4.9). However, we included a lateral variation from $2140\,\mathrm{kg\,m^{-3}}$ to $2250\,\mathrm{kg\,m^{-3}}$ between the model distances of 490 to 580 km in accordance with the higher average P-wave velocities in this part of the model. To obtain a best fit between modelled and observed free-air gravity anomalies, the density values were inverted while the geometry was kept fixed. The inverted density values differ only slightly from the initial values and all lie within the range from Barton (1986). During modelling, we compared the density and the P-wave model and adjusted layer boundaries in either to obtain an optimal correspondence between both. Generally, the correspondence between the P-wave velocity and density models is excellent, except between the model distances of 200 to 260 km and 440 to 560 km where the geometry of the layer boundaries had to be changed to reproduce the high observed gravity values. The geometry at the ends of the profile were edited to account for the regional gravity field. The RMS difference between the observed and modelled gravity is 2.03 mGal on average with a 6.63 mGal maximum at the distance of 483 km (Fig. 4.9).

### 4.6.2 Results and interpretation of the density model

The mean free-air gravity value is 24 mGal on the first 460 km of the profile (Fig. 4.9), except for the model distance of 190 km where -6 mGal were measured. Across the transition to continental crust on the Greenland shelf, the free air gravity rises to 97 mGal and then drops to negative values to the northeast with a minimum value of -93 mGal.
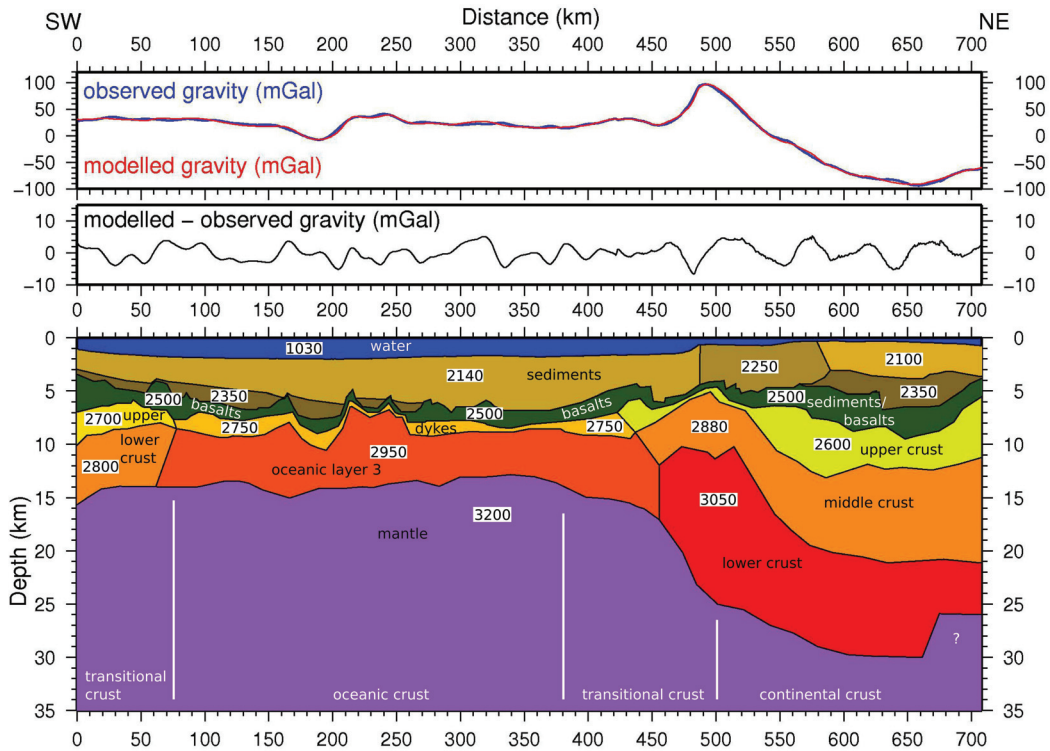
**Figure 4.9: (Top) Observed and modelled free-air gravity data (blue and red respectively). (Centre) Difference of modelled and observed gravity. (Bottom) Density model; numbers inside the layers indicate density values in $\mathrm{kg\,m^{-3}}$.**

Along the profile the sediment density varies from 2100 - 2250 $\mathrm{kg\,m^{-3}}$ on top of a 2350 $\mathrm{kg\,m^{-3}}$ dense lower sediment layer. The density of the basalts (2500 $\mathrm{kg\,m^{-3}}$) on oceanic, transitional, and continental crust is kept constant, while the other crustal layers vary in density along the profile.

From model distances of 75 to 430 km the dykes are modelled with 2750 $\mathrm{kg\,m^{-3}}$. Oceanic layer 3 is modelled by a 2950 $\mathrm{kg\,m^{-3}}$ dense body, extending from distance 70 to 450 km. From distance 200 to 260 km, the boundary of oceanic layer 2 and 3 differs significantly from the P-wave velocity model. This can represent the actual thickening of the oceanic layer 3, or it can indicate an increase in denser material at this location. As the OBS data do not cover this section well, the density model will be emphasized in the discussion.

The crust of the Baffin Island shelf, from a model distance of 0 to 75 km, is modelled with 2700 $\mathrm{kg\,m^{-3}}$ and 2800 $\mathrm{kg\,m^{-3}}$ beneath the basalts. These are lower density values than are needed at the adjacent oceanic crust. The transition to lower densities supports the interpretation of this section as transitional crust, which was already indicated by the P-wave model, but uncertain due to poor raycoverage. The density model already

40

indicates a thickening of the crust to Baffin Island with a deeper Moho at the beginning of the profile. This thickening was not imaged by the OBS data, as the profile was not extended further landward.

From a model distance of 430 km to the northeast, the upper crust is modelled with 2600 kg m$^{-3}$ and a mid-crustal layer is modelled with 2880 kg m$^{-3}$ from the distance of 440 km to the end of the model. These values are lower than the densities of the adjacent oceanic layers and thus separate these units. The lower crust displays high density values of 3050 kg m$^{-3}$, which indicate a mafic composition. Unlike the P-wave model, the density model displays denser middle-crust-material at shallower depth at a model distance of 460 to 530 km. An increase of dense material near the surface is needed to model the distinct higher values of a free-air gravity anomaly at the shelf break. A strong gravity high is observed at various shelf breaks, named "sedimentation anomaly" according to Watts & Fairhead (1999). If a 2-D model is oriented perpendicular to the shelf break, the density contrast between water and sediments is sufficient to model this anomaly. As our line runs oblique to the Greenland shelf (Fig. 4.1), it is likely, that a 3-D effect of the shelf break leads to the modelled upward arch of dense material in the 2-D model.

## 4.7    Magnetic field data

On profile BGR08-304, the reference field values of the IGRF-10 were removed from the measured magnetic total intensity values to obtain residual anomaly values. On profile BGR10-309 the reference field IGRF 11 was used. In the overlapping range, the BGR10-309 data were shifted to the BGR08-304 data to obtain a constant anomaly level. Finally, the anomalies on the combined profile were adjusted to meet the mean level of two published magnetic maps (Verhoef et al., 1996; Maus et al., 2009) by adding a constant value of 100 nT.

It was not possible to derive the distribution of oceanic and continental crust from the pattern of the magnetic anomalies alone (Fig. 4.4). Except for a distinct anomaly around the model distance of 150 km, the oceanic crust is characterized by small amplitudes and shorter wavelengths, while longer wavelengths and higher amplitudes dominate the transitional and continental crust. Despite the thick sediment cover, we had expected to find indications for magnetic spreading anomalies and a distinction for oceanic and continental crust.

## 4.8    Plate kinematic model

For the plate reconstruction we used GPlates (Boyden et al. (2011), www.gplates.org), which visualizes plate motion on a sphere. We compare published poles of rotation from
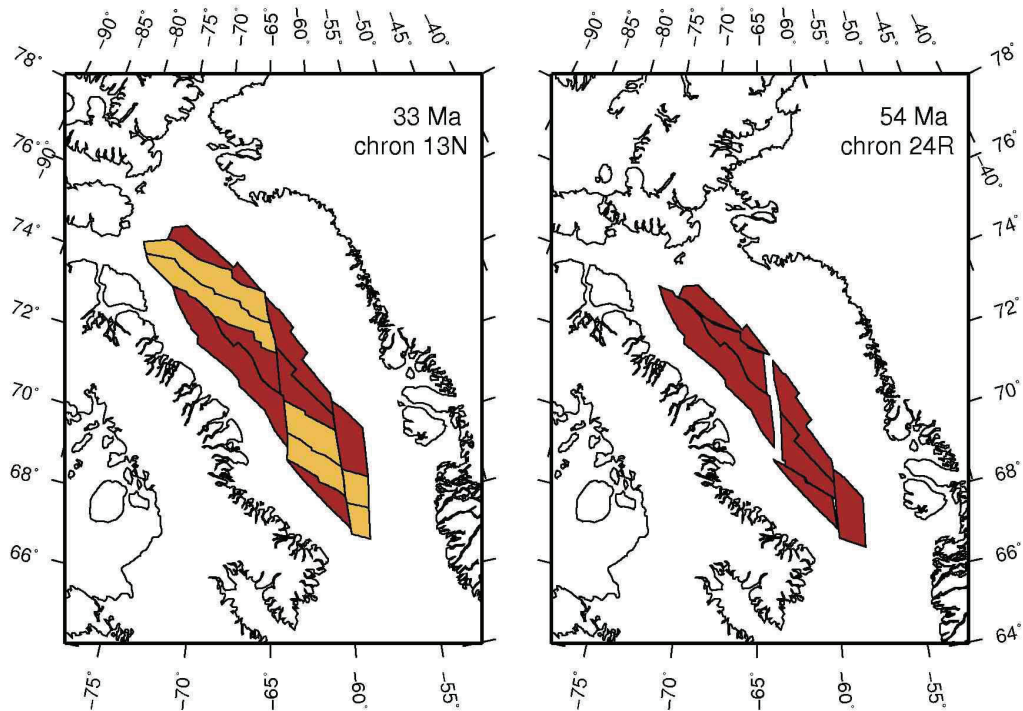
**Figure 4.10: Distribution of oceanic crust from Chalmers & Oakey (2007). Dark brown segments are Paleocene oceanic crust, light brown segments are Eocene oceanic crust. The configuration at 33 Ma (left) is also valid for today. At 54 Ma (right) the greatest gap occurs in Paleocene oceanic crust with the poles of rotation from Oakey (2005).**

Roest & Srivastava (1989), Oakey (2005), and the compilation from GPlates (Müller et al. (2008), version 1.0.1). In the reconstruction from GPlates, Baffin Island is moving as a microplate from 95.2 to 33.5 Ma. As we did not find any evidence of this, we kept Baffin Island fixed to the North American continent and, therefore, refer to a modified GPlates reconstruction.

The location of extinct spreading centres and the extent of oceanic crust were proposed previously by Srivastava (1978), Roest & Srivastava (1989), Jackson et al. (1992), Tessensohn & Piepjohn (2000), Geoffroy et al. (2001), and Chalmers & Oakey (2007). We digitized the crustal segments from the detailed tectonic map from Chalmers & Oakey (2007) with ArcGIS[TM], and displayed the evolution of these segments for the different reconstructions to verify the tectonic map.

42

## 4.8.1   Results and interpretation of the plate kinematic model

We rotated the segments of oceanic crust from the tectonic map from Chalmers & Oakey (2007) in GPlates with the rotation poles from Roest & Srivastava (1989), Oakey (2005), and the modified GPlates rotation (Müller et al., 2008). All sets of rotation poles lead to a gap in Paleocene oceanic crust (Fig. 4.10). The gap has a maximum width of 44 km for the rotation poles from Oakey (2005), of 57 km for the poles from Roest & Srivastava (1989), and of 88 km for the modified GPlates poles (Müller et al., 2008). This indicates, that either the rotation poles need to be re-calculated, or that the tectonic map from Chalmers & Oakey (2007) needs modifications. Deriving a new set of rotation poles from our data is not possible but the tectonic map from (Chalmers & Oakey, 2007) can be modified.

To explain the missing oceanic crust in the Paleocene, we outline the extent of oceanic crust at different stages in the reconstruction from Oakey (2005). To date the rotation poles, that are given in magnetic anomaly chrons, we use the time scale from Gradstein et al. (2004).

On the Greenland shelf, we kept the eastern boundary of oceanic crust as proposed by Chalmers & Oakey (2007), which is within an error of 5 km to the boundary we derived from the P-wave velocity and density models of this study. At the Baffin Island shelf, we used the more detailed continent-ocean boundary (COB) from Skaarup et al. (2006), which was derived from seismic reflection data (Fig. 4.11). At the location of our profile, we modified the COB from Skaarup et al. (2006) according to our interpretation by placing it 17 km further seaward (at a model distance of 75 km). This is 11 km further landward than the COB proposed by Chalmers & Oakey (2007). The location where we interpret the extinct spreading centre corresponds within 5 km with the location of the southern Eocene spreading centre given by Chalmers & Oakey (2007). We orientate the spreading centre along a pronounced low in the free-air gravity data (Fig. 4.11). The northern Eocene spreading centre was also placed along a distinct gravity low. No assumptions can be made on the extent of oceanic crust in northern Baffin Bay due to a lack of constraining data. By rotating the Greenland plate back to its position at 47 and 54 Ma, we mapped the extent of oceanic crust, avoiding gaps and overlaps. For the Paleocene oceanic crust, we introduce a spreading centre by dividing the oceanic crust in two equal parts. This differs from the spreading centre from Chalmers & Oakey (2007), who postulate more oceanic crust on the Baffin Island margin (Fig. 4.10). As we did not find indications for asymmetric spreading, we preferred a spreading centre that produces equal parts of oceanic crust. An uneven distribution of oceanic crust can be indicated by clear magnetic spreading anomalies, which are not observed here. We introduced three spreading centre segments, as the outline of oceanic crust from Chalmers & Oakey (2007) indicates fracture zones in the centre of the Paleocene crust.

Fig. 4.12 illustrates the evolution of oceanic crust in Baffin Bay, according to the results of this study with the rotation poles from Oakey (2005). At 61 Ma (chron 26R),
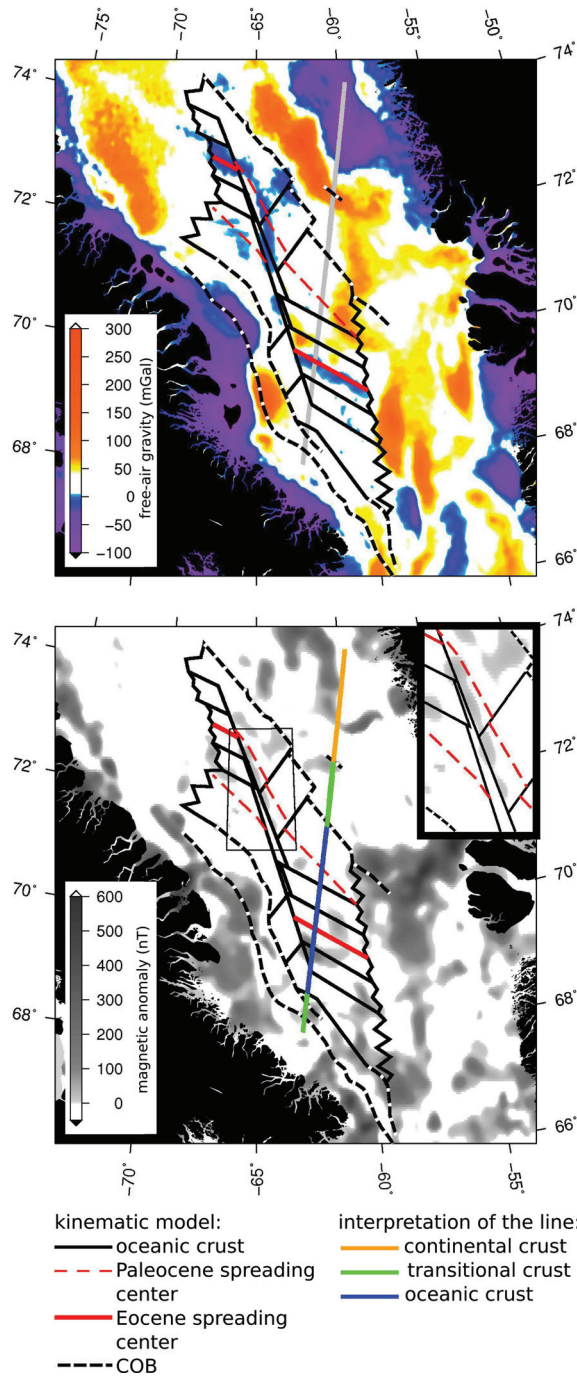
**Figure 4.11: (Top)** Features of our kinematic model and the location of the presented line (grey) on top of satellite derived free-air gravity data (Sandwell & Smith (2009), version 18.1). **(Bottom)** Features of our kinematic model and the location of the presented line with interpretations of the crustal character on top of magnetic anomaly data (EMAG2 V2, Maus et al. (2009)). Closeup in the upper right: positive magnetic anomaly at the location of the transform fault.
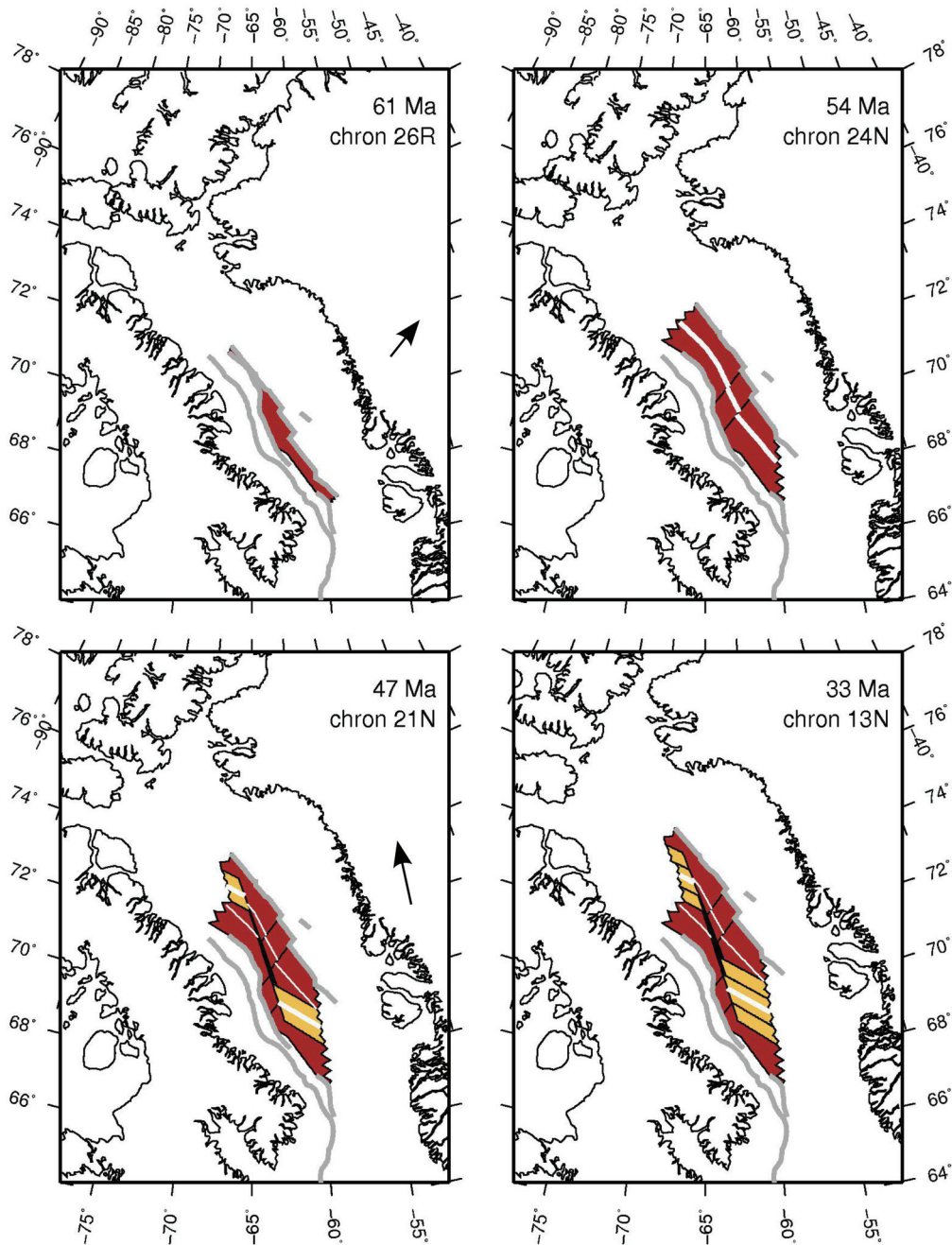
**Figure 4.12: Evolution of oceanic crust in southern Baffin Bay with rotation poles from Oakey (2005). Thick grey lines outline the continent - ocean transition: on the Baffin Island margin from Skaarup et al. (2006), modified at the location of our line; on the Greenland margin from Chalmers & Oakey (2007). The extent of transitional crust is marked on the Greenland margin only at the location of our line. Paleocene oceanic crust is marked in dark brown, Eocene oceanic crust in light brown, spreading centres in white. Arrows indicate the motion of Greenland relative to the North American plate.**

45

oceanic crust begins to form due to east-west extension. At magnetic chron 24N (54 Ma) the direction of extension changes to a southeast-northwest direction. This direction change marks the change from Paleocene to Eocene spreading. The Paleocene oceanic crust breaks into several fragments as two Eocene spreading centres evolve, connected by a major transform fault. At chron 13N (33 Ma), seafloor spreading ceases.

## 4.9 Discussion

### 4.9.1 Oceanic crust

Our P-wave and density models show that the basin is mostly underlain by oceanic crust with an average thickness of 7.5 km. Keen & Barrett (1972) report abnormally thin crust of 4 km thickness from sonobuoy readings in the centre of Baffin Bay, along a line at 72°N, 200 km northwest from our line (Fig. 4.1). We suggest, that the northward decrease in crustal thickness indicates a decrease in magma production.

The oceanic crust in Baffin Bay developed during two stages with different spreading directions (Oakey, 2005; Chalmers & Oakey, 2007). Our profile is perpendicular to the Eocene spreading centre, which we locate in the P-wave velocity and density model at a model distance of 190 to 210 km (Figs 4.4, 4.9). From GPlates, the Paleocene spreading centre is located at a model distance of 300 km (Fig. 4.12) but we prefer to place it at 292 km (Fig. 4.13) where a depression is visible in the basement (Figs 4.4, 4.9).

Oceanic layer 2 consists of basalts and dykes, which are modelled as individual layers. While the basalts layer is always modelled, the dykes were not modelled as a separate layer from a distance of 330 to 380 km, and only as a very thin layer from the model distance of 75 to 85 km in the P-wave velocity model. These are the regions closest to transitional crust and could indicate a change in material due to spreading or alteration. Where basalts and dykes are modelled as separate layers, only few reflections indicate that there is a significant velocity contrast between them. It is unlikely that oceanic layer 2 does not contain dykes. So where they are not modelled as separate layer, the velocity structure does not allow for discrimination and the velocity contrast between basalts and dykes is more continuous.

In the centre of the basin, north of the extinct Eocene spreading centre, the density model shows a thickening of oceanic layer 3 from the distances of 200 to 260 km, which is not resolved by the OBS data. This thickening of the lower crust is equivalent to an increase of dense material at this location. The accumulation of dense material and/or the thickening of oceanic layer 3 can be the result of volcanic activity (Jokat & Schmidt-Aursch, 2007) or it can represent the natural variability of oceanic crust. As positive free-air gravity anomalies are present 30 km north and south of our line (Fig. 4.1), the influence of a 3-D effect also needs to be considered.
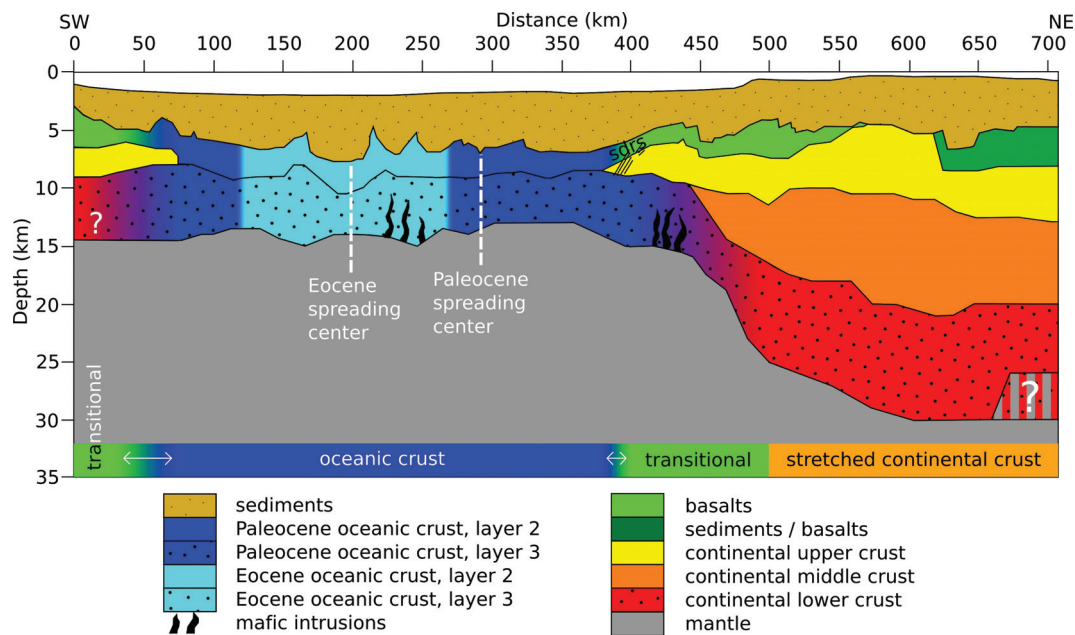
**Figure 4.13: Geologic interpretation of the P-wave and density model.**

In the oceanic domain, a symmetric magnetic anomaly pattern around the inferred extinct spreading centre at distances 190 to 210 km would be expected. Such an anomaly pattern is not observed, neither for the Eocene nor for the Paleocene spreading. As the oceanic crust in Baffin Bay is highly fragmented, the identification of magnetic spreading anomalies will remain difficult. Fragmentation is caused by the change in spreading direction at magnetic chron 24 (Figs 4.11, 4.12; Srivastava (1978); Roest & Srivastava (1989); Oakey (2005)) and by the offset due to small fractures that accompany spreading.

The high amplitude magnetic anomaly at model distances of 130 to 170 km remains enigmatic, because neither the P-wave velocity nor the density model indicate a significant difference in material composition. The kinematic model shows that this part of oceanic crust lies at the transition from Paleocene to Eocene crust and at the southern termination of the major transform fault, linking the northern and southern Eocene spreading centres. The magnetic anomaly data imply, that this region was subject to volcanism, when the spreading direction changed and the transform motion initiated. This region is structurally complex and 3-D effects need to be considered.

### 4.9.2 Greenland continental crust

According to the definition from Christensen & Mooney (1995), stretched continental crust is interpreted from a model distance of 500 to 710 km. On the nearby NUGGET

47

line 1 (Fig. 4.1), south of Davis Strait, a 10-km-thick layer of P-wave velocities similar to our middle crust is also interpreted as middle crust (6.4 - 6.6 km s$^{-1}$) on the Greenland margin (Funck et al., 2007). A 5-km-thick lower layer of 6.6 - 6.8 km s$^{-1}$ is interpreted as lower crust (Funck et al., 2007). Although the middle crust velocities are similar in both models, the lower crust velocities differ by 0.2 km s$^{-1}$. This difference is within the assigned error and as both models are separated by 1100 km along the margin, a variation in composition is not unlikely.

If a greater impedance contrast was modelled between middle and lower crust, for example an average P-wave velocity of 7.3 km s$^{-1}$ is assumed for the lowest crustal layer, this layer would be 2 km thicker. It would also be interpreted differently, as P-wave velocities higher than 7.2 km s$^{-1}$ indicate magmatic underplating (White & McKenzie, 1989). This interpretation would mean, that middle crust directly overlies an underplated body of 12 km thickness. On the nearby NUGGET line 1 (Fig. 4.1) a section of the Greenland margin is modelled with an underplated body with a P-wave velocity of 7.4 km s$^{-1}$ and 5 km thickness below middle crust (Funck et al., 2007). Although the velocity structure is similar, the thickness of the underplating is only one third. Underplating of 9 - 16 km thickness is modelled under stretched continental crust on the East Greenland margin, north of the Jan Mayen Fracture Zone along seismic refraction lines (Voss & Jokat, 2007). Together with seaward dipping reflector sequences of the initial break-up along 20 - 50 km distance (Hinz et al., 1987), the profiles are interpreted to indicate a weak-magmatic evolution of the northeastern Greenland margin (Voss et al., 2009). As the P-wave velocity structure of the lower crust is not resolved by the OBS data on our line, an interpretation of stretched continental lower crust with middle crust overlying an underplate is possible.

The Moho has a steep step of 4 km at a model distance of 660 to 675 km, that was introduced due to $P_mP$ phases from three OBS (Figs 4.7, A.4). The recorded reflections could have also been modelled as an inner crustal reflection. Although the density model also included the steep Moho dip, a flattened boundary would only cause minor changes in the gravity fit. A step of 4 km in the Moho should be isostatically compensated by a depression in the basement, which was not observed. From the available data it cannot be differentiated between a Moho-step and an inner crustal reflection.

### 4.9.3 Greenland transitional crust

Passive margins are typically characterized as volcanic or magma-poor margins. Ocean-continent transitions of magma-poor margins often display a gradual increase of P-wave velocities from the basement to mantle depth without an abrupt Moho transition due to complete serpentinization of mantle material (Chian & Louden, 1994; Reid & Jackson, 1997; Minshull, 2009). We find $P_mP$ phases in the OBS data as well as phases from a layered crust. Therefore, the crust cannot consist completely of serpentinized mantle material. Characteristics of a volcanic margin typically are a high velocity lower crust

(magmatic underplating) and seaward dipping reflector sequences of flood basalts, that formed at the initial break-up (Hopper et al., 2003; Mjelde et al., 2005; Voss et al., 2009). Seaward dipping reflectors of flood basalt are imaged on the MCS data from 390 - 410 km (Block et al., 2012), supporting an interpretation as volcanic margin, as does the discussion on magmatic underplating in the previous section.

If the volcanic seaward dipping reflectors found along our line are products of the initial breakup, their counterpart should be found on the Baffin Island margin. According to our kinematic model, these should be located at the Baffin Island coast at 68 - 68.5°N. Skaarup et al. (2006) mapped seaward dipping reflectors from MCS lines in this area, but do not report any at this location. In the case that no counterpart exists, the Greenland seaward dipping reflectors may be sequences of a later volcanic phase. Studies of the Southeast Greenland margin also report volcanic seaward dipping reflectors on oceanic crust, 180 km seaward of the continent-ocean-boundary (Hopper et al., 2003). Therefore, seaward dipping reflectors are not necessarily related to the initial break-up.

P-wave velocities in the lower crust rise by $0.3\,\mathrm{km\,s^{-1}}$ at the model distance of 410 to 450 km. This can indicate increased mafic composition, as mafic intrusions are often encountered at volcanic margins (Minshull, 2009). The density modelling does not require an increase of denser material at this location but this is likely because the density difference is too small to cause a misfit between the observed and calculated gravity values.

### 4.9.4 Baffin Island transitional crust

The comparison with velocity-depth profiles from White et al. (1992) shows, that the crust displays oceanic type velocities northeast of a model distance of 30 km (Fig. 4.8). This is the location, where Skaarup et al. (2006) place the limit of oceanic crust. As the thickness of layers 2 and 3 are not typical according to the compilation from White et al. (1992), we only interpret oceanic crust northeast of 75 km.

The lower crust of the Baffin Island transitional zone has P-wave and density values similar to the middle continental crust of the Greenland side. Regardless of this similarity, it is marked as lower crust in Fig. 4.13 as it directly overlies the mantle.

A pronounced thickening of crust that would indicate continental crust is not observed, although the profile ends at a distance of 75 km from the Baffin Island coast. The extent of transitional crust can therefore add up to a maximum of 150 km, which is in the same range as the extend of transitional crust at the Greenland margin (120 km).

### 4.9.5 Evolution of southern Baffin Bay

We introduce several changes to the tectonic map of Chalmers & Oakey (2007) (Fig. 4.10). In our kinematic model, we define the extent of oceanic crustal segments dif-

ferently to prevent gaps in oceanic crust at all times. Based on our P-wave velocity and density model (Figs 4.4, 4.9) we shift the COB at the Baffin Island shelf 11 km westwards, shift the Eocene spreading centre 5 km northwards, and reaffirm the extent of transitional crust at the Greenland margin. We shift the Paleocene spreading centre 20 km southwestwards to obtain equal spreading (Fig. 4.12). In our kinematic model, the major transform fault, that connects the northern and southern Eocene spreading centres, is rotated by approximately 6° counter clockwise with respect to the north-south trending transform fault, that Chalmers & Oakey (2007) propose. Chalmers & Oakey (2007) orient the transform fault along a gravity low in the centre of Baffin Bay (Fig. 4.11). In our model, the transform fault is in the range of the gravity low, but does not fit it exactly. Instead it lies on a positive magnetic anomaly, that has previously been recognized by Oakey (2005) (Fig. 4.11). We suggest, that the magnetic high is a product of volcanic activity along the major transform fault.

## 4.10   Conclusions

We present P-wave velocity and density models along a 710-km-long transect in southern Baffin Bay (Figs 4.4, 4.9). With the new information from these models we develop a kinematic model of the evolution of oceanic crust with the rotation poles from Oakey (2005) (Fig. 4.12).

A minimum of 305 km of oceanic crust of Paleocene and Eocene age is interpreted from the P-wave velocity and density models. The oceanic crust is 7.5 km thick on average with a sediment package of up to 6 km thickness. From the comparison with Keen & Barrett (1972), we suggest a northward decrease of crustal thickness and therefore of magma production in Baffin Bay. From our models we are able to propose locations for the extinct Paleocene and Eocene spreading centres (Fig. 4.13). Although the profile is oriented along the direction of Eocene spreading, no typical seafloor spreading anomalies are found in the magnetic anomaly data (Fig. 4.4). Most likely the oceanic crust is too fragmented and covered by too much sediment to display a clear magnetic signature.

On the Greenland shelf, the models image 5 km of sediments on top of a 23-km-thick, three-layered, stretched continental crust (Fig. 4.13). The Greenland continental margin is classified as a volcanic margin as no evidence of serpentinized mantle material is found and seaward dipping reflectors are imaged on the MCS data (Block et al., 2012). Mafic intrusions in the lower crust are inferred from a P-wave velocity increase and support this interpretation. From the available data, the existence of an underplated body, typical for volcanic margins, is unclear. The crustal structure of the Baffin Island margin is only coarsely resolved by the data presented here as our line did not extent further landward.

Plate kinematic modelling showed that modifications to the tectonic map from

Chalmers & Oakey (2007) are necessary. The modified model that we present spans from late Cretaceous to the end of seafloor spreading (Fig. 4.12). Lows in the free-air gravity data can clearly be attributed to extinct spreading centres (Fig. 4.11). A distinct high in the magnetic anomaly data can be attributed to a major fracture zone that connects a southern and a northern spreading centre in Baffin Bay in the Eocene (Fig. 4.11).

## 4.11   Acknowledgments

# Chapter 5

# The Davis Strait crust - a transform margin between two oceanic basins

Sonja K. Suckro[1], Karsten Gohl [1], Thomas Funck[2], Ingo Heyde[3], Bernd Schreckenberger[3], Joanna Gerlings[2,4], Volkmar Damm[3]

[1] Alfred Wegener Institute for Polar and Marine Research (AWI), Am Alten Hafen 26, 27568 Bremerhaven, Germany

[2] Geological Survey of Denmark and Greenland (GEUS), Øster Voldgade 10, DK-1350 Copenhagen K, Denmark

[3] Federal Institute for Geosciences and Natural Resources (BGR), Stilleweg 2, 30655 Hanover, Germany

[4] Dalhousie University, Department of Earth Sciences, 1459 Oxford Street, Halifax, N.S., B3H 4R2, Canada

# 5.1 Summary

The Davis Strait is located between Canada and Greenland and connects the Labrador Sea and the Baffin Bay basins. Both basins formed in Cretaceous to Eocene time and were connected by a transform fault system in the Davis Strait. Whether the crust in the central Davis Strait is oceanic or continental has been disputed. This information is needed to understand the evolution of this transform margin during the separation of the North American plate and Greenland. We here present a 315-km-long east-west oriented profile that crosses the Davis Strait and two major transform fault systems - the Ungava Fault Complex and the Hudson Fracture Zone. By forward modelling of data from 12 ocean bottom seismographs, we develop a P-wave velocity model. We compare this model with a density model from ship-borne gravity data. Seismic reflection and magnetic anomaly data support and complement the interpretation. Most of the crust is covered by basalt flows that indicate extensive volcanism in the Davis Strait. While the upper crust is uniform, the middle and lower crust are characterized by higher P-wave velocities and densities at the location of the Ungava Fault Complex. Here, P-wave velocities of the middle crust are $6.6\,\mathrm{km\,s^{-1}}$ and of the lower crust are $7.1\,\mathrm{km\,s^{-1}}$ compared to $6.3\,\mathrm{km\,s^{-1}}$ and $6.8\,\mathrm{km\,s^{-1}}$ outside this area; densities are 2850 and $3050\,\mathrm{kg\,m^{-3}}$ compared to 2800 and $2900\,\mathrm{kg\,m^{-3}}$. We here interpret a 45-km-long section as stretched and intruded crust or as new igneous crust that correlates with oceanic crust in the southern Davis Strait. A high-velocity lower crust ($6.9 - 7.3\,\mathrm{km\,s^{-1}}$) indicates a high content of mafic material. This mantle derived material gradually intruded the lower crust of the adjacent continental crust and can be related to the Iceland mantle plume. With plate kinematic modelling, we can demonstrate the importance of two transform fault systems in the Davis Strait: the Ungava Fault Complex with transpression and the Hudson Fracture Zone with pure strike slip motion. We show that with recent poles of rotation most of the relative motion between the North American plate and Greenland took place along the Hudson Fracture Zone.

Keywords: plate motions, transform faults, continental margins: divergent, crustal structure, Arctic region

## 5.2 Introduction

The Davis Strait is located between Canada and Greenland and connects the Baffin Bay in the north with the Labrador Sea in the south (Fig. 5.1). The strait is a bathymetric high with water depths <700 m, while the water depth in the Baffin Bay and the Labrador Sea exceeds 2000 m. Prominent tectonic features of the Davis Strait are the Ungava Fault Complex and the Davis Strait High. A line of positive southwest-northeastward striking free-air gravity anomalies marks the location of the Ungava Fault Complex, a major transform fault (Funck et al. (2007); Gregersen & Skaarup (2007); Gerlings et al. (2009)). In the center of the strait, the Davis Strait High is characterized by outcropping basement between 66 - 67°N (Dalhoff et al., 2006).

The Davis Strait area has experienced Paleogene volcanism. Outcrops of volcanic sequences are located on Disko Island and the adjacent Nuussuaq Peninsula (Storey et al., 1998; Pedersen et al., 2006). On the Canadian margin, volcanics are mapped at Cape Dyer (Clarke & Upton, 1971) and offshore in seismic reflection data (Skaarup et al., 2006). Volcanics are drilled offshore at several wells as indicated in Fig 5.1 a.

The Davis Strait crust has long been a subject of debate. Sonobuoy readings reveal a 22 km-thick crust, which is interpreted as a thick pile of oceanic crust by Keen & Barrett (1972). Chalmers & Pulvertaft (2001) interpret the crust as continental, while Srivastava et al. (1982) argue that the Davis Strait High is a continental block and the adjacent basins are underlain by oceanic crust. A seismic refraction line in southern Davis Strait showed that continental crust is separated by a 140-km-wide zone of oceanic crust (NUGGET-1, Funck et al. (2007), Fig. 5.1 b).

To determine the nature of the crust in the central Davis Strait, a 226-km-long seismic refraction profile was recorded during the cruise MSM09/3 of RV Maria S. Merian in 2008 (Gohl et al., 2009). Additionally, multichannel seismic reflection (MCS), ship-borne gravity, and magnetic field data were collected on the same line with an additional 90-km-extend to the east. We here present the results of P-wave velocity and gravity forward modelling together with magnetic field and MCS data. The results are used in a plate kinematic model to determine the role of the Ungava Fault Complex in the evolution of the Davis Strait.

## 5.3 Tectonic background of the opening of the Labrador Sea and the Baffin Bay

The tectonic evolution of the Davis Strait is linked to the evolution of the Baffin Bay and the Labrador Sea. These have formed in the Cretaceous to Eocene during the separation of Greenland from the North American craton (e.g. Chalmers & Pulvertaft (2001), Tessensohn & Piepjohn (2000)). The time of initial rifting of North America and Green-
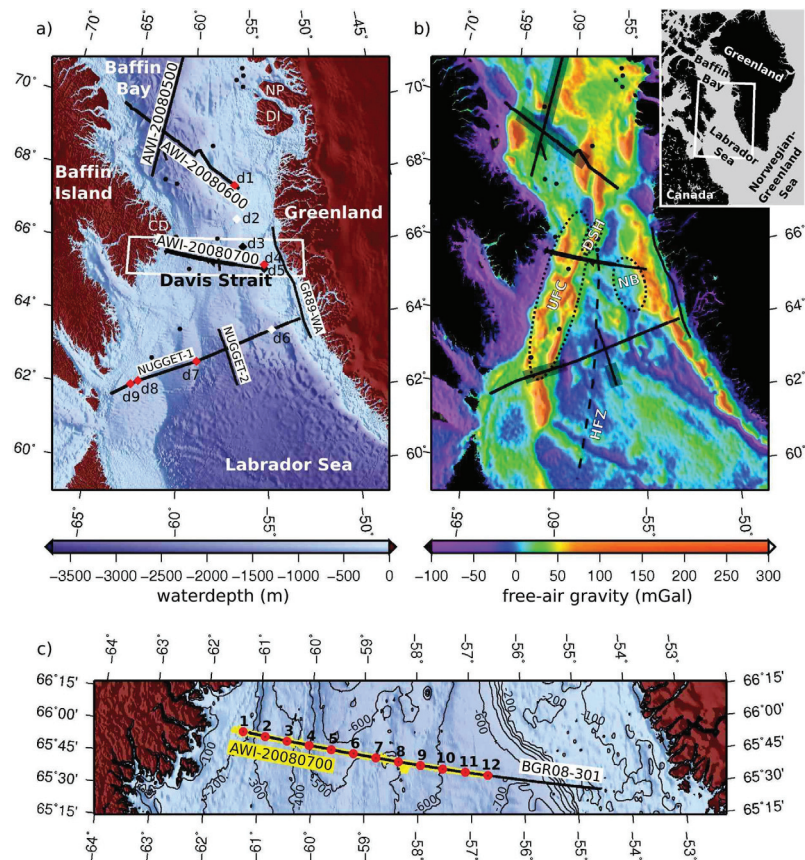
**Figure 5.1: a):** Bathymetric map of the Davis Strait area (GEBCO_08 Grid, Version 20090202, http://www.gebco.net) with place names and locations of wide-angle seismic data. Abbreviations are: (NP) Nuussuaq Peninsula, (DI) Disko Island, (CD) Cape Dyer. Line AWI-2008500, -600, -700 were acquired during the MSM09/3 cruise of RV Merian in 2008 (Gohl et al. (2009); Funck et al. (2012); Suckro et al. (2012)); black dots and short black lines are locations of sonobuoys and profiles of expandable sonobuoys from Keen & Barrett (1972); NUGGET-1 (Funck et al., 2007), NUGGET-2 (Gerlings et al., 2009), and GR89-WA (Gohl & Smithson, 1993) are seismic refraction lines; diamonds mark well locations: (d1) Hellefisk-1 , (d2) Ikermiut, (d3) Kangamiut-1, (d4) Nukik-2, (d5) Nukik-1, (d6) Qulleq-1, (d7) Gjoa G-37, (d8) Ralegh N-18, (d9) Hekja O-71; red diamonds: volcanics are drilled; black diamonds: Precambrian rocks are drilled; white diamonds: neither is drilled; all well information are from the BASIN database: www.basin.gdr.nrcan.gc.ca/wells/index_e.php. **b):** Free-air gravity anomalies derived from satellite altimetry of the offshore area (Sandwell & Smith, 2009), version 18.1; grey shaded areas mark the extend of oceanic crust on seismic refraction lines (Funck et al., 2007; Gerlings et al., 2009; Funck et al., 2012; Suckro et al., 2012); positive gravity anomalies that mark the Ungava Fault Complex (UFC) are circled, as is the Davis Strait High (DSH) and the Nuuk Basin (NB); location of the Hudson Fracture Zone (HFZ) after Chalmers & Pulvertaft (2001). **c):** Closeup of the coinciding seismic refraction line AWI-20080700 with OBS locations marked by red dots and line BGR08-301 with seismic reflection, gravity and magnetic anomaly data.

56

land is dated to earliest Cretaceous by Larsen et al. (1999) from dyke intrusions in southern West Greenland. On the Nuussuaq Peninsula, tectonic instability with three phases of uplift occurred in the Maastrichtian (Chalmers et al., 1999). The age of the oldest oceanic crust in the Labrador Sea is disputed. Roest & Srivastava (1989) date it to magnetic chron 33 (80 Ma after Gradstein et al. (2004), which is used throughout this paper for dating), while Chalmers & Laursen (1995) use chron 27N (62 Ma). Recent seismic refraction and gravity data have now confirmed Paleocene and Eocene oceanic crust in southern Baffin Bay (Funck et al., 2012; Suckro et al., 2012).

A first volcanic pulse at 60.7 - 59.4 Ma is identified from volcanics on Disko Island by Storey et al. (1998) and correlated with the arrival of the Greenland-Iceland mantle plume in the Davis Strait area. Funck et al. (2007) attribute a thick high-velocity lower crust in their P-wave velocity model of the NUGGET-1 line to the southward flow of plume material.

During magnetic chron 24R (55Ma), the relative motion of Greenland to the North American craton changed from east to northeast, as indicated by magnetic spreading anomalies in the Labrador Sea (Roest & Srivastava, 1989; Oakey, 2005). This caused new fractures and the breaking of Paleocene oceanic crust in the southern Baffin Bay and the evolution of new spreading centres in the Eoecene (Chalmers & Pulvertaft, 2001; Oakey, 2005; Suckro et al., 2012). The opening of the Norwegian-Greenland-Sea is dated to chron 24 (Talwani & Eldholm, 1977; Olesen et al., 2007)), therefore, Greenland moved as an independent plate from this time until the end of relative motion between Greenland and the North American craton (Tessensohn & Piepjohn, 2000). According to Storey et al. (1998) the reorientation of spreading caused a second volcanic pulse at 54.8 - 53.6 Ma in the Disko Island area.

Spreading ceased in the Labrador Sea at chron 13 (33 Ma) according to Srivastava (1978), while separation of Greenland and Eurasia and the opening of the Northeast Atlantic is still ongoing. Since then sedimentation and subsidence are the dominant geologic processes in the Baffin Bay and the Labrador Sea (Chalmers & Pulvertaft, 2001).

The Ungava Fault Complex consists of several northeast-southwest striking faults that are oriented along positive gravity anomalies in the Davis Strait (Fig. 5.1 b, Sørensen (2006)). The Ungava Fault Complex marks the northwestern border of oceanic crust in the Labrador Sea (Chalmers & Pulvertaft, 2001). It is interpreted as a transform system, linking sea-floor spreading in the Labrador Sea with spreading in the Baffin Bay (Rice & Shade, 1982; Chalmers & Pulvertaft, 2001). Skaarup et al. (2006) interpret the Ungava Fault Complex in the Davis Strait as the continent-ocean boundary of the Greenland plate. East of the Ungava Fault Complex runs the north-south striking Hudson Fracture Zone, which meets the Ungava Fault Complex in the Davis Strait (Chalmers & Pulvertaft, 2001). The Hudson Fracture Zone was first identified from magnetic anomaly data by Srivastava (1978).

**Table 5.1: Setup parameters of the seismic refraction survey.**

| | |
|---|---|
| OBS type | 3-component Mark seismometers, 4.5 Hz natural frequency, 1 hydrophone |
| OBS spacing | nominally 18 km |
| Seismic source | array of 16 G.Guns$^{TM}$ and 2 Bolt$^{TM}$ guns |
| Volume G.Gun$^{TM}$ array | 50.8 litres, 3100 in$^3$ |
| Operation pressure | 145 bar |
| Volume 2 Bolt$^{TM}$ guns | 64 litres, 3906 in$^3$ |
| Operation pressure | 120 bar |
| Total source volume | 114.8 litres, 7006 in$^3$ |
| Shot interval | 60 s |

**Table 5.2: Setup parameters of the seismic reflection survey.**

| | |
|---|---|
| Streamer length | 3450 m |
| Number of channels | 276 |
| Sampling rate | 2 ms |
| Recording length | 14 s |
| Seismic source | array of 16 G.Guns$^{TM}$ |
| Operation pressure | 100 - 135 bar |
| Total source volume | 50.8 litres, 3100 in$^3$ |
| Shot interval | 18 s |

## 5.4 Data acquisition

Seismic and potential field data of this study were acquired during the research cruise MSM09/3 of RV Maria S. Merian in 2008 (Gohl et al., 2009). The profiles presented here were set up to determine the crustal thickness and structure across the Davis Strait and the Ungava Fault Complex (Fig. 5.1).

We collected seismic refraction data along the 226-km-long profile AWI-20080700 with 12 ocean bottom seismometers (OBS) (Fig. 5.1 c). Technical details are listed in Table 5.1. On line BGR08-301 we recorded MCS and potential field data. BGR08-301 coincides with line AWI-20080700 and extends 90 km further eastwards (Fig. 5.1 c). Setup parameters of the MCS measurement are summarized in Table 5.2.

Gravity data were recorded with a KSS31M sea gravimeter (Bodensee Gravitymeter Geosystem GmbH) at 1 Hz sampling rate. To reference the ship borne gravity data, we carried out connection measurements on land with a LaCoste&Romberg gravity meter at the beginning and end of the cruise (Gohl et al., 2009). Magnetic field data were recorded with an Overhauser SeaSPY marine magnetometer system towed approximately 600 m behind the vessel.

**Table 5.3: Processing steps applied to the MCS data of line BGR08-301 in ProMAX[TM].**

- Resampling: 4 ms
- Apply geometry: common mid point binning of 6.25 m
- Bandpass filter: (4 -) 8 - 80 (- 160) Hz
- Velocity analysis
- Surface related multiple estimation
- Velocity analysis
- Predictive deconvolution
- Normal move out correction
- Stack
- Poststack Kirchhoff migration

## 5.5 Seismic data

### 5.5.1 Seismic reflection data

The MCS data is common depth point (CDP) sorted to 6.25 m and processed with ProMAX[TM] with the processing steps listed in Table 5.3. We were able to remove the first seafloor multiple by a surface related multiple estimation procedure. The trade off of this procedure is that primary signals are also partly absorbed (white band between 1 - 2 s from a model distance of 90 - 290 km, Fig. 5.2). Multiples that are not suppressed by this procedure are multiples of the basement at distances of 0 - 70 km and 95 - 135 km. At these locations the acoustic basement is close to the seafloor (less than 0.1 s two-way traveltime) and the remaining basement multiples can easily be confused with seafloor multiples. But their shape varies from the seafloor morphology, especially at 40 km and at 115 km model distance (Fig. 5.2).

We interpret the acoustic basement from the seismic reflection data in order to use it in the P-wave velocity and the density models. From distances of 70 - 95 and 165 - 325 km, the basement is the lowest continuous reflector and marks the base of stratified sedimentary sequences. From a distance of 135 - 165 km, we use the top of a series of high amplitude reflectors below a more transparent sediment succession. The base of these high amplitude reflectors cannot be defined from the seismic reflection data, but in combination with the P-wave velocity and density model an interpretation is discussed later. The deformation of sediments in this section will be discussed later and is therefore highlighted in closeup B of Fig. 5.2. As mentioned before, distances of 0 - 70 km and 95 - 135 km are only covered by very little sediment. Here, the basement morphology is best determined from the basement multiples. Dipping reflector sequences from a distance of 55 - 67 km are also better visible in the multiple (closeup A in Fig. 5.2).

59
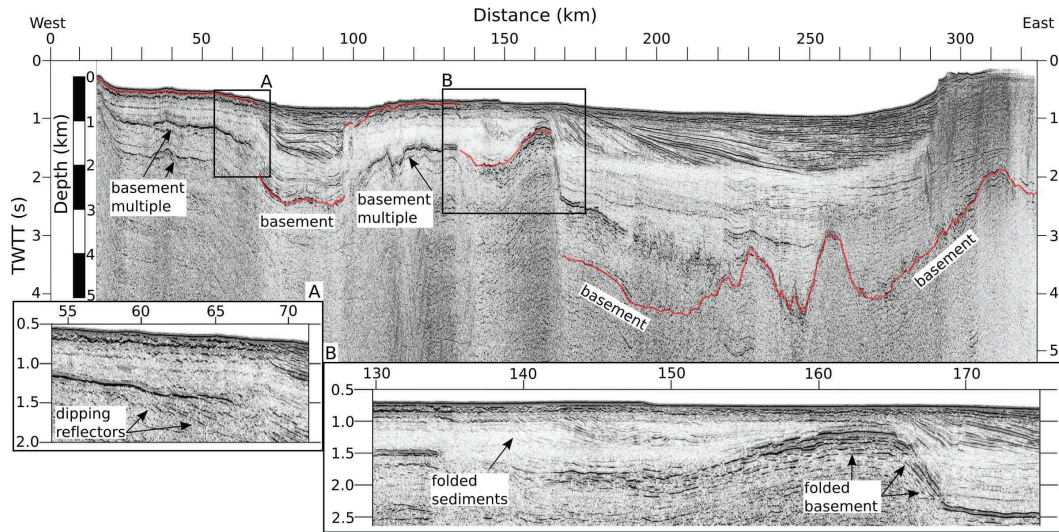
**Figure 5.2:** Final processing of MCS data along line BGR08-301; basement is marked in red; depth-scale is approximated by average P-wave velocities of sediments along the profile. Closeup A shows dipping reflectors in the basement multiple. Closeup B shows folded sediments.

**Table 5.4:** Statistical values of the P-wave velocity model calculated by rayinvr and dmplstsqr (Zelt & Smith, 1992). n is the number of observations; pick uncertainties are averaged for all observations; RMS is the misfit between calculated and observed traveltime; the normalized $\chi^2$ is a measure of how well calculated traveltimes are within the range of the pick uncertainty.

| Layer | n | Pick uncertainty (ms) | RMS (ms) | Normalized $\chi^2$ |
|---|---|---|---|---|
| $P_{sa}$ - $P_{sd}$ | 424 | 67 | 47 | 0.527 |
| $P_{sa}P$ - $P_{sd}P$ | 211 | 89 | 70 | 0.915 |
| $P_{se}$ | 644 | 82 | 48 | 0.401 |
| $P_{se}P$ | 288 | 90 | 99 | 1.040 |
| $P_{bas}$ | 84 | 92 | 46 | 0.278 |
| $P_{LVZ}P$ | 113 | 70 | 50 | 0.296 |
| $P_{c1}$ | 707 | 100 | 68 | 0.692 |
| $P_{c1}P$ | 188 | 115 | 100 | 1.006 |
| $P_{c2}$ | 2647 | 123 | 170 | 2.261 |
| $P_{c2}P$ | 429 | 166 | 153 | 0.764 |
| $P_{c3}$ | 1217 | 189 | 279 | 2.064 |
| $P_mP$ | 1286 | 158 | 351 | 4.682 |
| $P_n$ | 221 | 200 | 109 | 0.300 |
| total | 8459 | 131 | 177 | 1.965 |

## 5.5.2 P-wave velocity model

We relocalized the OBS positions with the arrival of the direct wave. All refracted and reflected signals were picked with the software zp (by B. Zelt, www.soest.hawaii.edu/users/bzelt/index.html), using a bandpass filter of 4 - 15 Hz applied for the near offset signals (30 km distance from the station) and 4 - 10 Hz for greater offsets. Picking errors were assigned manually to each phase, taking into account the signal to noise ratio. In Table 5.4 the assigned pick uncertainties are summarized for each phase. Refracted phases are named $P_{layer}$ and reflected phases $P_{layer}P$, except for the reflection at the Moho, $P_mP$, and the refraction in the upper mantle, $P_n$.

By forward modelling with the software rayinvr (Zelt & Smith, 1992) we obtained the P-wave velocity model in Fig. 5.3. Raycoverage of the single layers is displayed in Fig. 5.4; modelling of all stations is given in the appendix in Figs B.1 and B.2; examples of modelling for OBS 2, 8, and 11 are displayed in Figs 5.5 - 5.7. The modelled layers are described in the following paragraphs. The accuracy of the model depends on the data coverage and quality; typical uncertainties of the P-wave velocity are $\pm\,0.1\,\mathrm{km\,s^{-1}}$.

**water**: For the seawater we used an average velocity of $1.47\,\mathrm{km\,s^{-1}}$, which was calculated from a conductivity temperature density (CTD) measurement during the cruise (Gohl et al., 2009). We took the depth of the sea-floor from bathymetry data of the on-board multi-beam echo-sounder.

**sa, sb, sc, sd**: Sediment layers with P-wave velocities ranging from 1.5 to $3.5\,\mathrm{km\,s^{-1}}$ are determined from the OBS data (Fig. 5.3). The complex structure of the basement is incorporated from the high resolution MCS data (Fig. 5.2).

From a model distance of 68 - 100 km a sediment basin with P-wave velocities from 1.8 to $2.9\,\mathrm{km\,s^{-1}}$ is modelled from phases of OBS 4 and 5 (Figs 5.3 and 5.4). The sediment infill of the basin at a model distance of 135 - 165 km consists of two units. A 1-km-thick unit with P-wave velocities of 1.5 - $2.4\,\mathrm{km\,s^{-1}}$ overlies a 0.5-km-thick unit with an average P-wave velocity of $3.3\,\mathrm{km\,s^{-1}}$ (Fig. 5.3). The low velocity of the upper unit is extrapolated from the sediment package of the eastern basin. The lower sediment unit is confirmed by $P_{sd}$ phases of OBS 8 (Fig. 5.4). The sediments east of a model distance of 165 km, in the Nuuk Basin, are of similar character. A 2-km-thick sediment sequence with P-wave velocities of 1.5 - $2.6\,\mathrm{km\,s^{-1}}$ overlies a 1-km-thick unit with an average P-wave velocity of $3.3\,\mathrm{km\,s^{-1}}$ (Fig. 5.3). $P_{sb}$, $P_{sc}$, and $P_{sd}$ phases from OBS 9 to 12 confirm these sequences (Fig. 5.4).

**se**: We later interpret this layer, with P-wave velocities between 4.1 and $5.1\,\mathrm{km\,s^{-1}}$, partly as basalts and therefore name it here separately from the other sediment layers.

At a model distance of 0 - 68 km, this layer is modelled with P-wave velocities of 4.4 - $5.5\,\mathrm{km\,s^{-1}}$ according to $P_{se}$ phases of OBS 1, 2, and 4 (Figs 5.3, 5.4, and B.1). From a model distance of 35 - 50 km lies a body of higher velocities ($5.4\,\mathrm{km\,s^{-1}}$). From a model distance of 68 - 95 km, the layer **se** is modelled with 2 km thickness and is confirmed by $P_{se}$ phases of OBS 5 (Figs 5.3 and B.1). From a model distance of 95 - 135 km, the
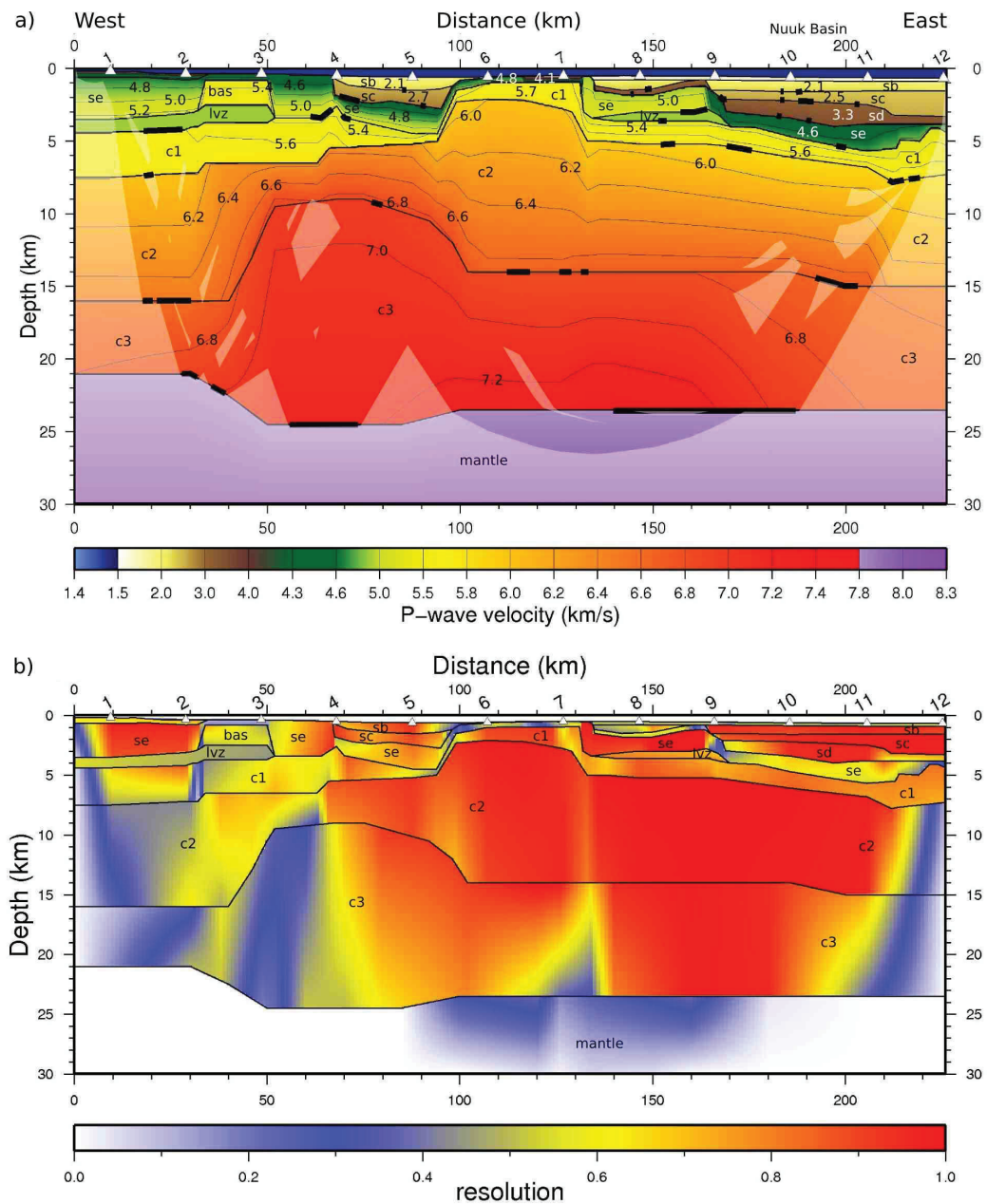
Figure 5.3: a): P-wave velocity model with layer names. Interpretation of the layers are: sb, sc, sd are sediments; se are basalts intercalated with sediments; bas is a basalt unit; lvz abbreviates low velocity zone and represents burried sediments; c1 is the upper crust, c2 the middle crust, c3 the lower crust. White triangles indicate OBS locations; rotated numbers are OBS numbers; numbers on contour lines are P-wave velocities in km s$^{-1}$; thick lines mark layer boundaries that are constrained by reflected phases; white shaded areas are not passed by rays. b): Gridded diagonal values of the resolution matrix of the P-wave velocity model. Layers are annotated; white triangles indicate OBS locations; rotated numbers are OBS numbers.

62
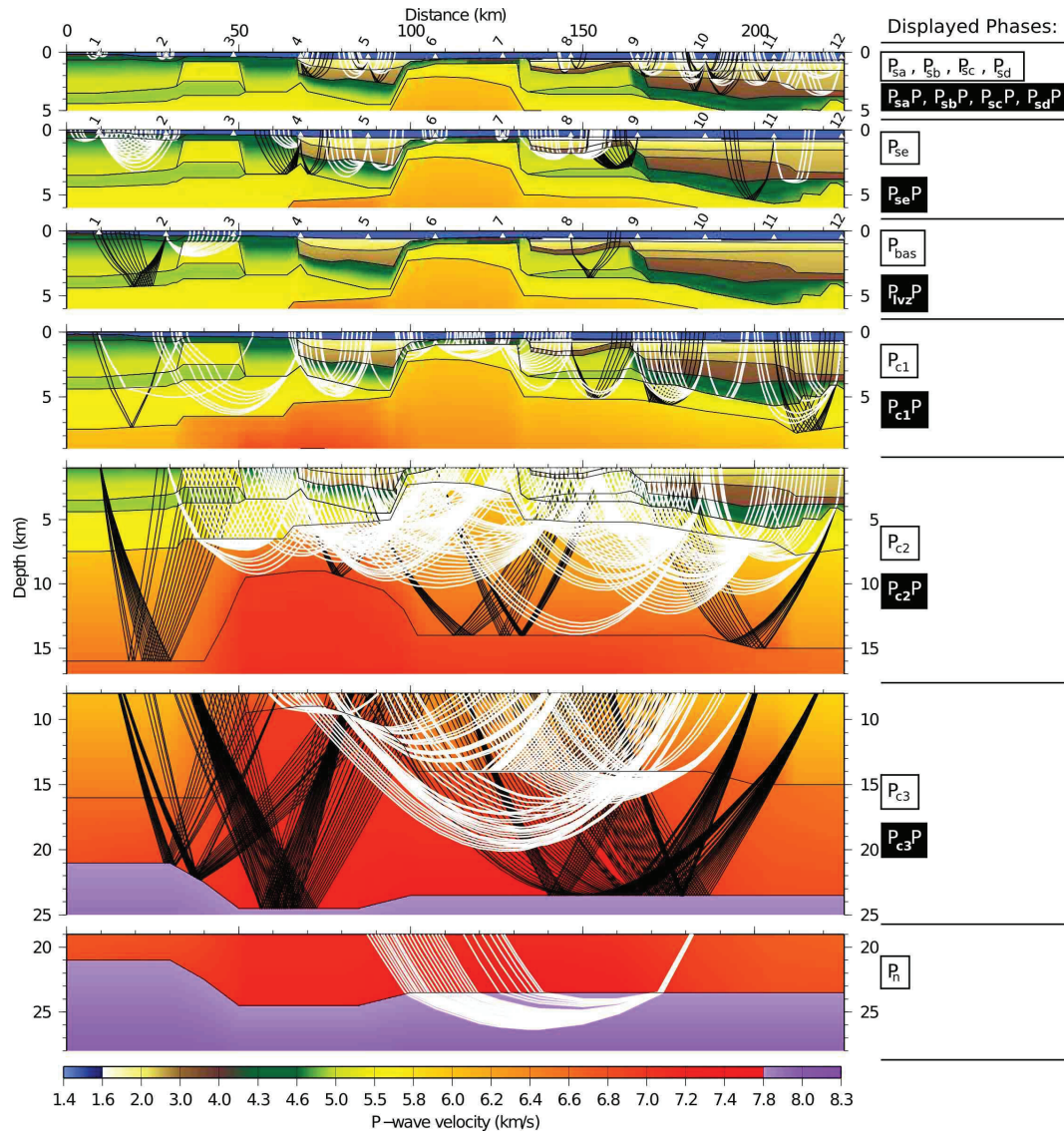
**Figure 5.4: Ray coverage of the different layers in the P-wave velocity model (Fig. 5.3). Refracted phases are displayed in white, reflected in black.**

63
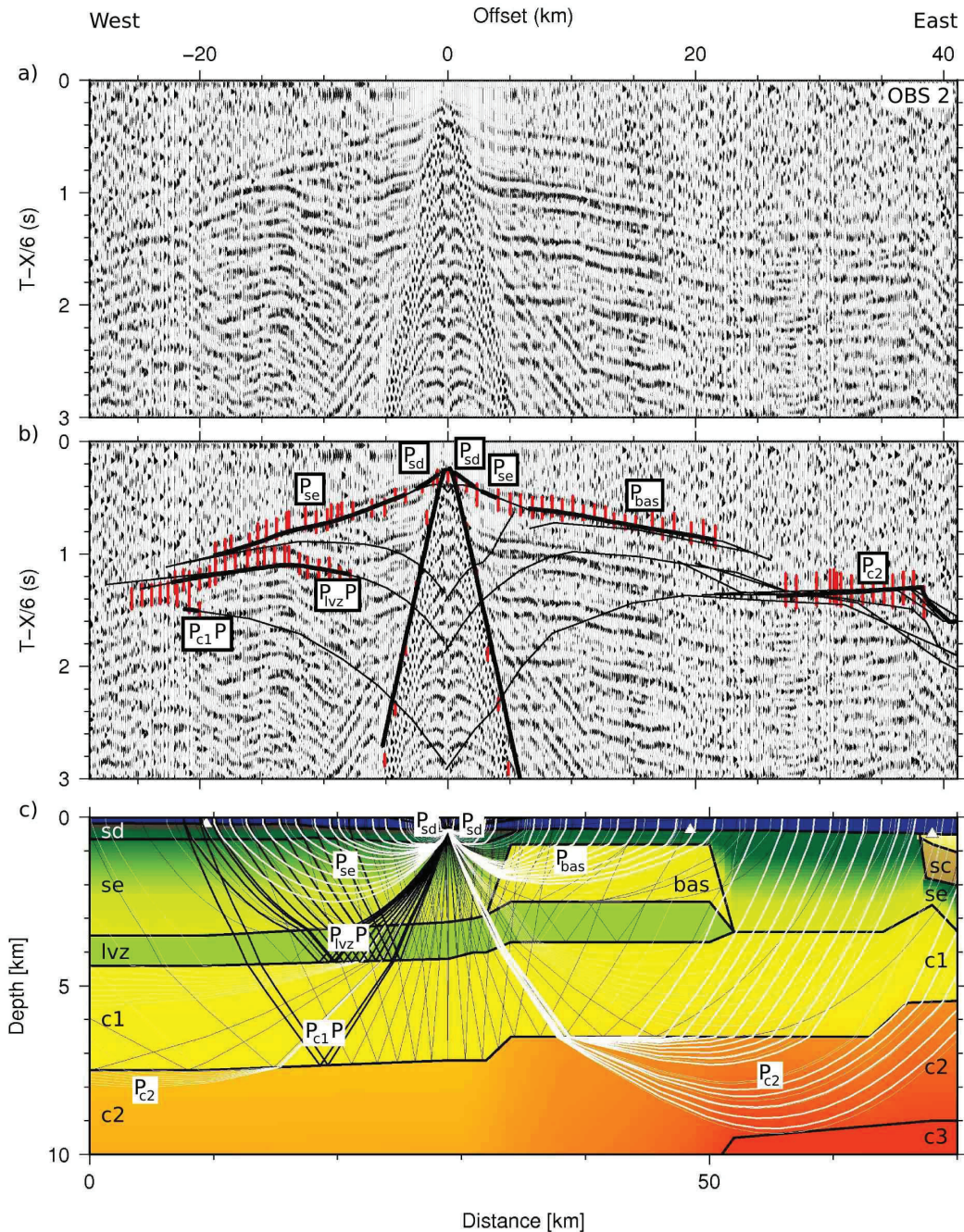
**Figure 5.5: a): Seismic section of OBS 2, displayed with a reduction velocity of $6\,\mathrm{km\,s^{-1}}$. b): The same seismic section with picks in red; the pick length corresponds to the assigned pick uncertainty; calculated traveltimes are displayed in black with thick black lines corresponding to the picks. c): P-wave velocity model with ray paths. Model layers are annotated; black rays indicate reflected phases, white rays refracted phases; thick lines correspond to the picks in the central panel.**

64
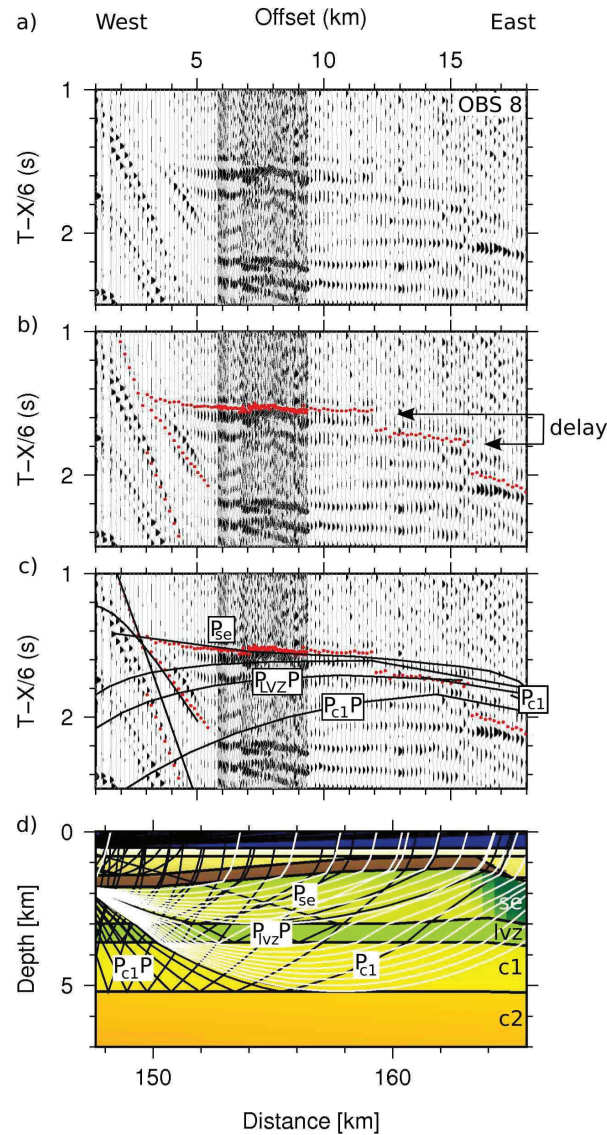
Figure 5.6: a): Cutout of the seismic section of OBS 8, displayed with a reduction velocity of $6 \, \text{km} \, \text{s}^{-1}$. b): the same seismic section with picks in red. c): The same seismic section with picks in red and calculated traveltimes in black. d): P-wave velocity model with ray paths; black rays indicate reflected phases, white rays refracted phases; model layers are annotated.
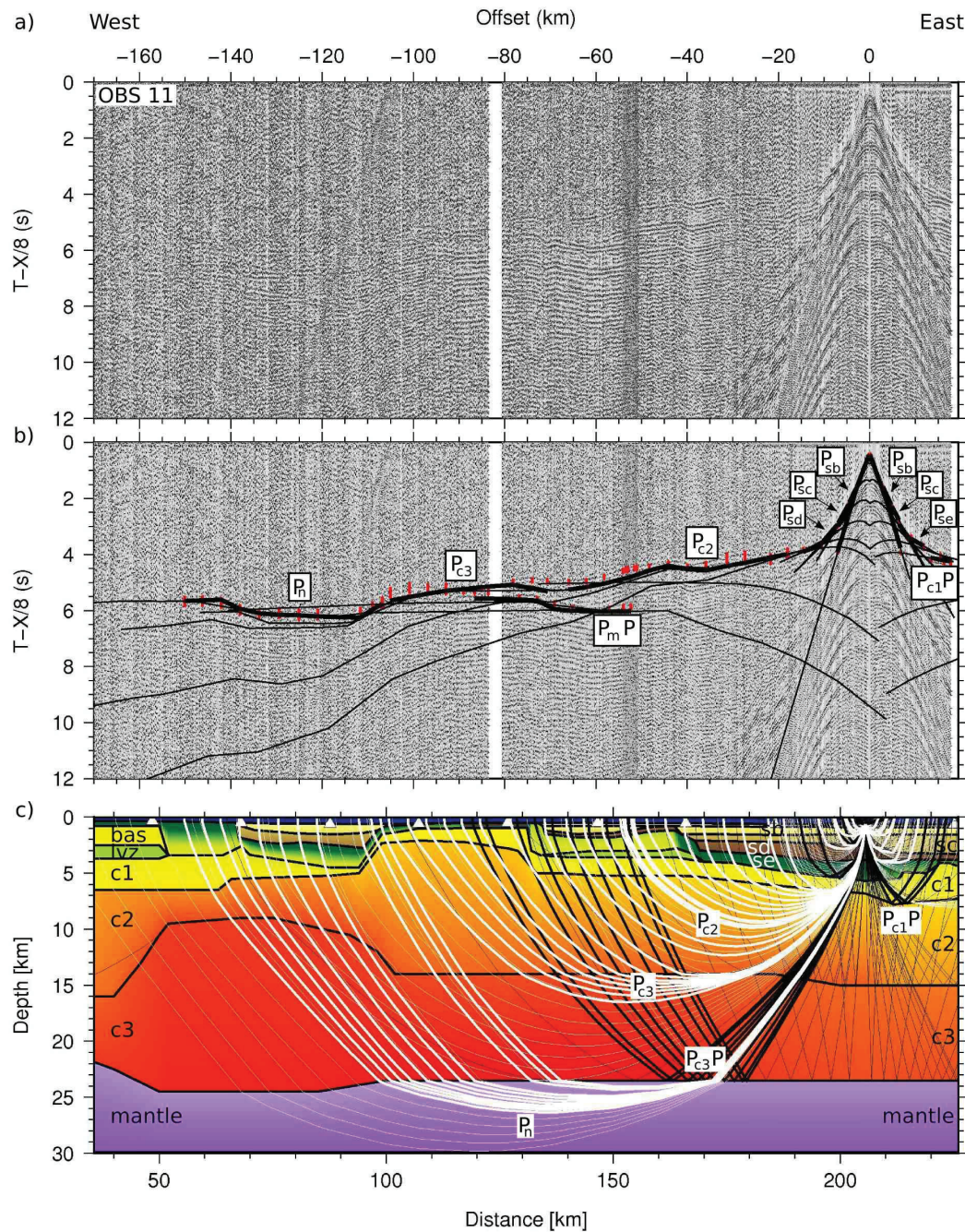
**Figure 5.7: a): Seismic section of OBS 11, displayed with a reduction velocity of $8\,\mathrm{km\,s^{-1}}$. b): The same seismic section with picks in red; the pick length corresponds to the assigned pick uncertainty; calculated traveltimes are displayed in black with thick black lines corresponding to the picks. c): P-wave velocity model with ray paths. Model layers are annotated; black rays indicate reflected phases, white rays refracted phases; thick lines correspond to the picks in the central panel.**

layer **se** is only 0.5 km thick and modelled with a P-wave velocity of 4.8 km s$^{-1}$ west of 117 km (Fig. 5.3). East of 117 km, a P-wave velocity of 4.1 km s$^{-1}$ is modelled. This velocity difference is needed to account for different $P_{se}$ phases from OBS 6 and 7. From a model distance of 135 - 165 km, the layer **se** is 2 km thick and modelled with 4.9 - 5.2 km s$^{-1}$, according to $P_{se}$ phases of OBS 8 (Figs 5.3, 5.4). The thickness is confirmed by OBS 9 (Fig. B.2). East of a model distance of 165 km, in the Nuuk Basin, the velocity structure is determined only by a $P_{se}$ phase of OBS 11 (Fig. 5.7), which indicates a P-wave velocity of 4.0 km s$^{-1}$.

**bas**: We modelled a separate body of higher P-wave velocities than the surrounding layer **se** from a refracted phase $P_{bas}$ of OBS 2 (Fig. 5.5). The average P-wave velocity is 5.4 km s$^{-1}$ and the thickness is 1.5 km.

**lvz**: Low velocity zones (LVZ) are modelled at a model distance of 0 - 50 km and of 135 - 170 km. Phases in OBS 1 and 2 indicate a LVZ at a model distance of 0 - 50 km by fading $P_{se}$ and $P_{bas}$ phases and by a delay of crustal phases (Figs 5.5 and B.1). We chose a velocity of 4.9 km s$^{-1}$ for the LVZ, as this is the average P-wave velocity of the surrounding layer **se**. The LVZ from a model distance of 135 - 170 km was introduced due to delayed phases in OBS 8 as shown in Fig. 5.6. The delay of 0.14 s is modelled with a 0.6-km-thick layer of P-wave velocity of 4.9 km s$^{-1}$. The P-wave velocity of the LVZ has to be smaller than 5.2 km s$^{-1}$, which is the velocity at the base of the overlying layer. We have chosen 4.9 km s$^{-1}$, which is the P-wave velocity at the top of the overlying layer se. It can therefore be interpreted as part of this layer, which is later interpreted as basalts intercalated with sediments.

**c1**: P-wave velocities of the first crustal layer range from 5.2 km s$^{-1}$ at the top to 5.8 km s$^{-1}$ at the base. The average P-wave velocity is 5.5 km s$^{-1}$, which is well confirmed by $P_{c1}$ phases throughout the model except for the western end of the model (Figs 5.3, 5.4). The thickness varies between 0.5 - 3.5 km along the profile.

From a model distance of 0 - 68 km, the upper crust (c1) is 2.5 - 3.0 km thick, while it thins from 3 to 0.5 km eastwards beneath the sediment basin from a model distance of 68 - 95 km (Fig. 5.3). From a model distance of 100 - 210 km, the thickness is more uniform with 1.5 - 2.0 km. East of a model distance of 210 km, a thickening to 3 km is modelled due to $P_{c1}P$ phases in OBS 11 and 12 (Figs 5.4 and B.2). The top of the upper crust (c1) is modelled from the basement interpretation of the MCS data from a model distance of 135 - 226 km (Figs 5.2 and 5.3).

**c2**: The second crustal layer is modelled with P-wave velocities of 5.9 - 6.7 km s$^{-1}$, except for a model distance of 40 - 95 km where it is characterized by higher P-wave velocities of 6.5 - 6.8 km s$^{-1}$ (Fig. 5.3). Here the middle crust (c2) is only 2.5 - 4 km thick, while it reaches 7.5 - 12 km thickness in the adjacent model parts. Except for the model boundaries, the velocity structure is well confirmed by $P_{c2}$ phases (Fig. 5.4). The velocity structure west of a profile distance of 40 km is only confirmed at the top of the layer by OBS 4 (Fig. B.1). The velocity at the bottom can thus be chosen in a

wide range. An extrapolation of high velocities, such as in the thin lower crust section from 40 - 95 km, did not lead to the required delay of later crustal phases. We thus adopt a lower velocity structure, similar to the model distances east of 95 km for the western profile termination. Also from model distances of 210 - 226 km, we use low P-wave velocities of 5.9 - 6.3 km s$^{-1}$ instead of 5.9 - 6.7 km s$^{-1}$ to model the delay of later arrivals. Fig. B.2 shows that the $P_mP$ phase in OBS 12 has travelled through crust with considerably lower P-wave velocities than the $P_mP$ phase in OBS 10 and 11.

**c3**: The third crustal layer has P-wave velocities between 6.5 and 7.4 km s$^{-1}$. Similar to the middle crust (c2), the lower crust (c3) is characterized by higher P-wave velocities in the centre of the model than at the sides (Fig. 5.3).

At a model distance of 50 - 160 km, P-wave velocity ranges from 6.8 to 7.4 km s$^{-1}$. At 190 - 226 km, the average velocity is considerably lower with only 6.7 km s$^{-1}$. This velocity reduction is necessary to account for the $P_mP$ phase in OBS 12. Fig. B.2 shows, that even slower velocities are necessary for modelling of OBS 12, but this would then change the fit of $P_{c3}$, $P_mP$ and $P_n$ phases in OBS 10 and 11 and we thus did not further lower the P-wave velocities. Similar to the modelling of the $P_mP$ phase of OBS 12, there is a misfit in the modelling of the $P_mP$ phase of OBS 1. Another possibility of modelling OBS 1 is with a deeper Moho at the eastern termination of the profile. Because this leads to a misfit with the gravity model and with data from OBS 4, we did not chose this option. At both profile terminations we chose the model that fits best to the data of OBS with good ray coverage and to the gravity model. The lower crust is well resolved from a model distance of 65 - 190 km by $P_{c3}$ and $P_mP$ phases (Figs 5.3, 5.4). From 0 - 65 km, modelling only depends on $P_mP$ phases (Fig. 5.4) and P-wave velocities are thus not well constrained. The depth of the Moho varies between 21and 24.5 km and is confirmed by various $P_mP$ phases (Fig. 5.4).

**mantle**: A P-wave velocity of 7.8 km s$^{-1}$ is modelled at the top of the mantle from a $P_n$ phase of OBS 11 (Figs 5.7 and B.2).

Table 5.4 summarizes statistical values as a measure of quality for the model's fit to the picked traveltimes. The root mean square traveltime (RMS) error is calculated by rayinvr from the misfit of calculated and picked traveltime. The normalized $\chi^2$ is a measure of how well the calculated traveltimes are within the range of the assigned pick uncertainties and should ideally be 1. The normalized $\chi^2$ of our model is 1.965, which is almost twice the ideal value. But a comparison with the P-wave velocity models of Mackenzie et al. (2005) ($\chi^2$ of 2.563) and Voss & Jokat (2007) ($\chi^2$ of 2.804 and of 3.049) shows, that $\chi^2$ values greater than 2 are not uncommon. The RMS error of our model is 177 ms, which is higher than the values of the before mentioned publications, which range from 137 to 164 ms. Especially phases from the lower crust contribute to the high RMS error. We think that the high RMS error is mainly due to the low signal to noise ratio of the OBS data. The model depicts a complex crust, which various vertical

**Table 5.5: Corrections applied to the gravity data.**

- time shift due to overcritical damping of the sensor
- conversion from instrument reading units to mGal
- tie to world gravity net IGSN 71 with connection measurements
- correction for the Eötvös effect with navigation data
- correction for instrument drift during the cruise
- subtraction of normal gravity (GRS80)

features where scattering of the deep phases can lower the signal amplitudes. Fig. 5.3 shows the diagonal values of the resolution matrix as a color grid. The resolution is a measure of how well a velocity value is constrained by all rays passing though it. The layers of the model are over all well resolved, except for the profile terminations.

## 5.6 Gravity and magnetic anomaly data

For free-air gravity anomalies, standard processing steps as listed in Table 5.5 were applied to the gravity data. We obtained a density model by forward modelling with the software GM-SYS (Geosoft, Inc.). For the starting model (Fig. 5.8 c), we used a simplified geometry of the P-wave velocity model. Line AWI-20080700 of the P-wave velocity model only extends up to a model distance of 226 km, while gravity data were recorded on line BGR08-301up to a model distance of 315 km. Density values were derived from average P-wave velocities according to Barton (1986). For simplicity we combined the upper three sediment layers with P-wave velocities of 1.7 - 2.9 $km\,s^{-1}$ to one density body of 2200 kg/m$^3$ (s1). The two underlying layers of 3.1 - 5.6 $km\,s^{-1}$ are combined to one layer of 2450 $kg\,m^{-3}$ density (s2). The basalt flow from a model distance of 35 - 50 km is added to the first crustal layer. We used the basement interpretation of the MCS data along the whole density model (Fig. 5.8 c).

Calculated free-air gravity values of the starting model are generally too high along the western part of the profile and too low at the eastern part (Fig. 5.8 b). We therefore divided the mantle at a model distance of 170 km into a body of 3200 $kg\,m^{-3}$ and of 3300 $kg\,m^{-3}$. Where this density change was not sufficient, we adjusted the layer boundaries. From a model distance of 117 - 135 km, we replaced the second sediment layer (2450 $kg\,m^{-3}$) by the first (2200 $kg\,m^{-3}$), to meet smaller free-air gravity values in this region. This density change is also indicated by a lateral change in P-wave velocities (4.8 - 4.1 $km\,s^{-1}$) along line AWI-20080700. Further, we adjusted the crustal layers east of a model distance of 225 km. This area is not covered by the P-wave velocity model, so only the depth of the basement is constrained by the MCS data. To fit the high free-air gravity values east of 270 km, we modelled a shallowing of the middle and lower crust.
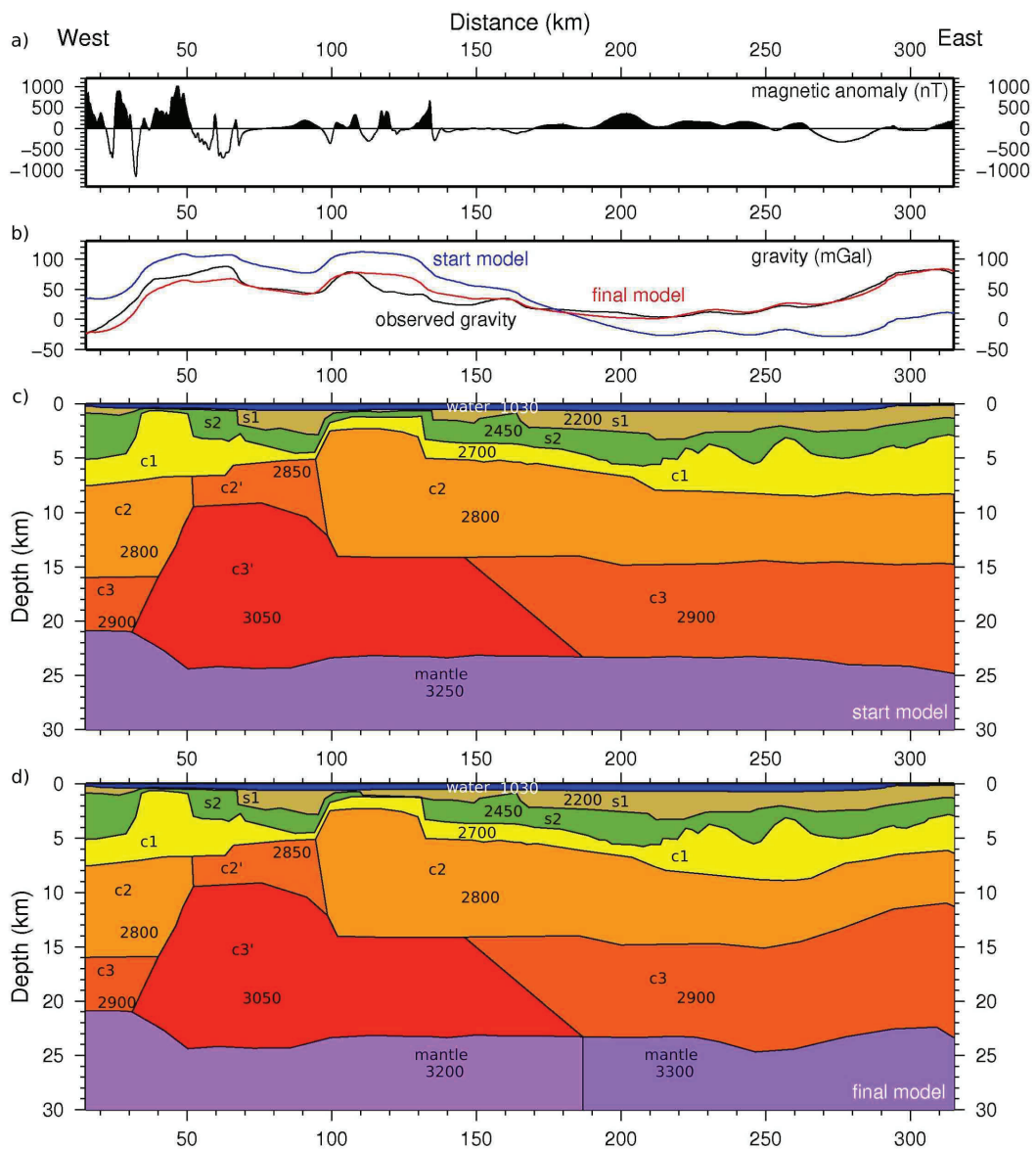
**Figure 5.8:** **a): Magnetic anomaly data along line BGR08-301. b): Free-air gravity data along line BGR08-301. Observed gravity in black, calculated gravity of the start model in blue (lower centre panel), of the final model in red (bottom panel). c): Start model of the density modelling; layer boundaries are taken from the P-wave velocity model and average P-wave velocities are transferred to densities according to Barton (1986). Numbers inside the model indicate densities in $\mathrm{kg\,m^{-3}}$. d): Final density model.**

70

The average difference between the calculated gravity of the final model (Fig. 5.8 d) and the observed free-air gravity values is 7.2 mGal, in contrast to 40.5 mGal for the starting model. The greatest mismatches between modelled and observed gravity occur at model distances of 0 - 65 km and of 110 - 150 km. These regions are in the vicinity of strong positive anomalies off the profile (Fig. 5.1 b) and we therefore interpret these as the influence of 3-D effects.

To obtain residual magnetic anomaly values, the appropriate IGRF reference field values (IGRF-10) were removed from the measured magnetic total intensity. It was necessary to add 100 nT to the anomaly curve to meet the mean level of two published magnetic maps (Verhoef et al., 1996; Maus et al., 2009). The magnetic anomalies (Fig. 5.8 a) vary between positive and negative values of -1146 nT (at a model distance of 32 km) and 1015 nT (47 km). In general, magnetic anomalies have small amplitudes and long wavelengths at the locations of sedimentary basins (at model distances of 68 - 100 km and east of 135 km) and high amplitudes with small wavelengths where the basement is near the surface.

## 5.7  Plate kinematics

We use GPlates (www.gplates.org) to visualize the tectonic evolution of the Davis Strait area. For the relative motion of the Greenland plate to the North American craton, we use the set of rotation poles by Oakey (2005). This recent reconstruction complements the previous reconstruction from Roest & Srivastava (1989). The most relevant time steps in the tectonic evolution of the Davis Strait, as illustrated in Fig. 5.9, are:

90 Ma: Greenland separates from Canada in an eastwards direction; rifting is active, but sea-floor spreading has not started in the Labrador Sea (Roest & Srivastava, 1989; Chalmers & Laursen, 1995).

57 Ma: Greenland and Canada are at a maximum east-west distance in the Davis Strait; the motion of Greenland changes from an eastward to a northeastward direction (Srivastava, 1978); sea-floor spreading is active in the Labrador Sea (Srivastava, 1978; Chalmers & Laursen, 1995).

33 Ma: Sea-floor spreading ceases in the Labrador Sea (Srivastava, 1978); Greenland and Canada are placed at their modern configuration.

Between 57 and 33 Ma, Greenland moved northwards by 310 km relative to the North American craton. This resulted in a narrowing of the central Davis Strait. If we use the location of the Hudson Fracture Zone as shown in Chalmers & Pulvertaft (2001) for the plate boundary, pure strike slip motion occurs along this fault (Fig. 5.9 e). If we use the location of the Ungava Fault Complex instead, a crustal overlap of 70 km width must be compensated. The area of this overlap coincides with the positive free-air gravity anomalies that are associated with the Ungava Fault Complex. This is the area, where transpressional forces were compensated.

71
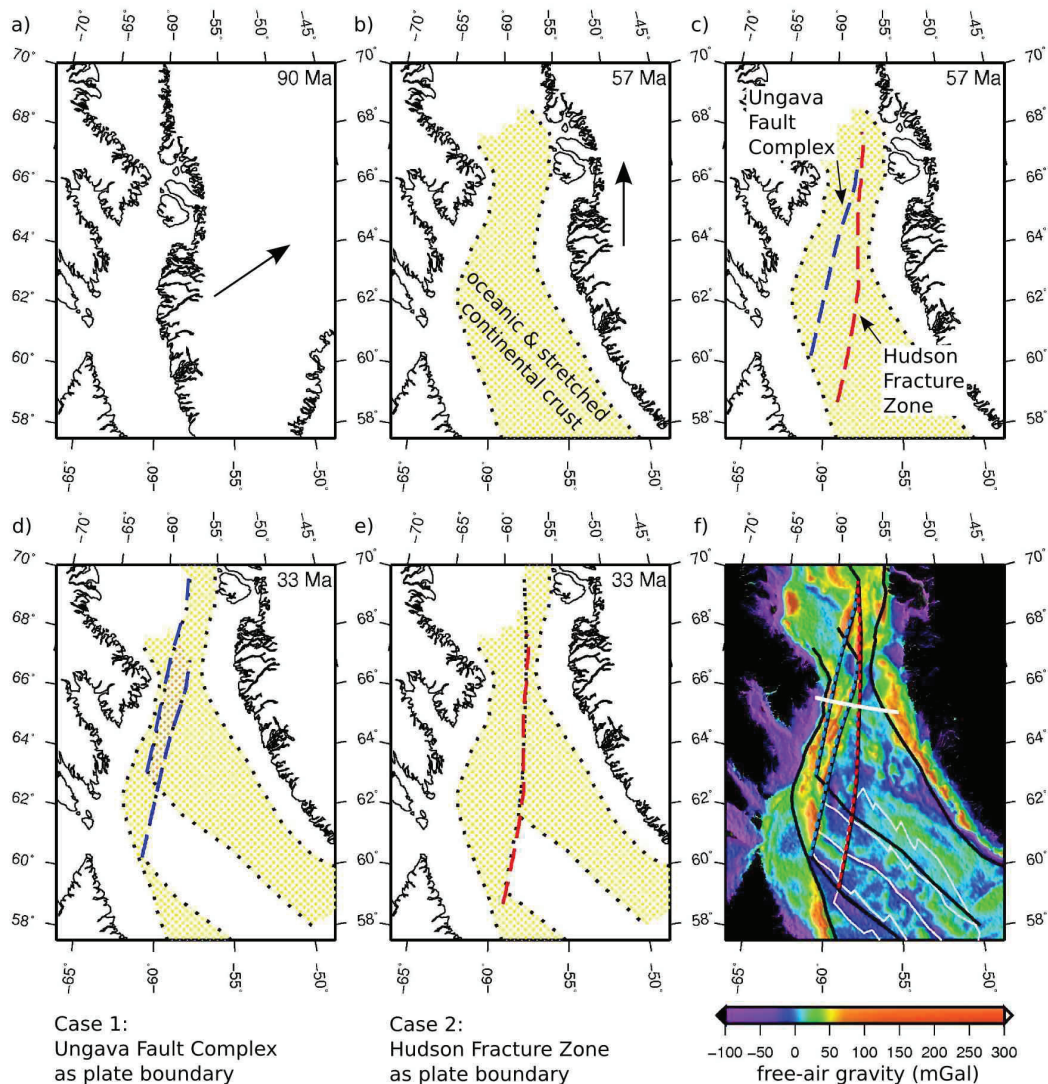
**Figure 5.9: Tectonic evolution of the Davis Strait with poles of rotation from Oakey (2005). a): Configuration at 90 Ma. b) and c): The maximum east-west separation of the North American craton and Greenland is reached at 57 Ma. The area of additional crust relative to 90 Ma (stretched continental and oceanic crust) is shaded in yellow; the location of the Ungava Fault Complex and the Hudson Fracture Zone are marked. Lower row: Relative motion between Greenland and Canada terminates at 33 Ma; the plates are at their present day configuration. d): Case 1: The Ungava Fault Complex is used as plate boundary; due to the northward motion of Greenland an overlap of crust needs to be compensated (shaded in orange). e): Case 2: The Hudson Fracture Zone is used as plate boundary; only strike slip motion is active without thickening or thinning of the crust. f): Free-air gravity anomalies (Sandwell & Smith, 2009), version 18.1, with the outline of overlapping crust, the Ungava Fault Complex in blue, the Hudson Fracture Zone in red, and oceanic crust in the Labrador Sea as outlined by Chalmers & Pulvertaft (2001) in white; line AWI-20080700/BGR08-301 in the Davis Strait as thick white line.**

72
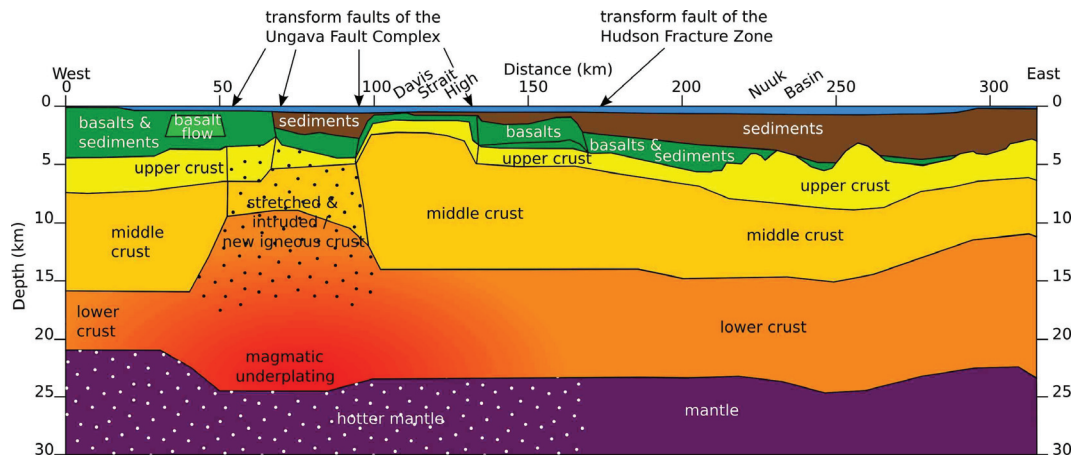
**Figure 5.10: Geological structure of line AWI-20080700/BGR08-301 compiled from the MCS data (Fig. 5.2), the P-wave velocity and the density models (Figs 5.3 and 5.8).**

## 5.8 Discussion

### 5.8.1 Basalts and sediments

Below the sediment packages **sc** and **sd** we modelled a layer **se** (Fig. 5.3). This layer with P-wave velocities of 4.1 - 5.1 km s$^{-1}$ is similar to a layer with P-wave velocities of 4.3 - 5.3 km s$^{-1}$, observed on NUGGET-1 (Funck et al., 2007). This layer was drilled at the Hekja O-71 and the Gjoa G-37 wells (Fig. 5.1 a) and consists of basalts intercalated with sediments (Klose et al., 1982). Due to the similarity of the P-wave velocity character and the proximity to NUGGET-1, we follow this interpretation for line AWI-20080700/BGR08-301.

At a model distance of 55 - 68 km, dipping reflectors in the MCS data confirm this interpretation (basalt flows in closeup A in Fig. 5.2). High amplitudes and frequencies of the magnetic anomaly data also support the interpretation of volcanics near the surface (Fig. 5.8 a).

The only indication of the separately modelled body **bas** with P-wave-velocities of 5.4 km s$^{-1}$ in the MCS data is an undulation of the basement at a modal distance of 38 km (Fig. 5.2). It is confirmed by the density model, where it is modelled with the same density as the upper crust (model distance 35 - 50 km). Due to this high density, we interpret this feature as a separate basalt unit, which is not intercalated with sediments. Model distances 0 - 50 km are underlain by a LVZ, which we interpret as sediments that were covered by the basalt unit (Fig. 5.10).

From a model distance of 95 - 130 km the layer **se** is much thinner than modelled to the west (0.5 km instead of 2 km). High amplitudes and frequencies of the magnetic anomaly data indicate that volcanics are near the surface (Fig. 5.8 a). From the available
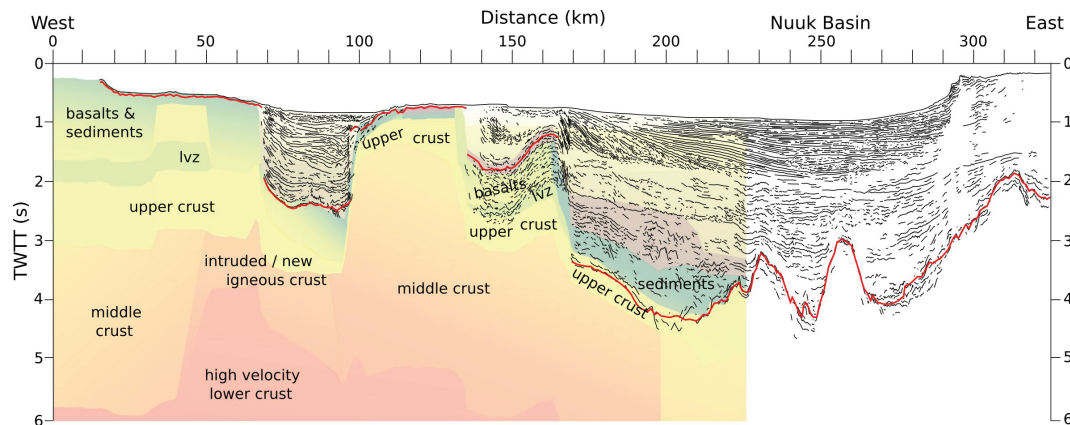
**Figure 5.11: Linedrawing of the MCS data of line BGR08-301 overlain with the time-converted P-wave velocity model from Fig. 5.3.**

data, it is not clear whether this sequence was deposited on this basement high with only 0.5 km thickness, or if it was deposited before an uplift of the basement with 2 km thickness like in the west. In the later case, 1.5 km of it were eroded due to uplift and exposure at the sea-floor. P-wave velocities of 4.8 km s$^{-1}$ from a model distance of 95 - 117 km support this interpretation as do dipping reflectors in the MCS data (Figs 5.2 and 5.11). A graben structure of the interpreted basement separates this section from lower P-wave velocities (4.1 km s$^{-1}$) and densities (2450 - 2200 kg m$^{-3}$) from a model distance of 117 - 130 km (Fig. 5.11). As P-wave velocities of basalts can range between 3.5 to 6.5 km s$^{-1}$ due to varying composition and deposition (Christie et al., 2006) we here also interpret layer **se** as basalts intercalated with sediments.

From a model distance of 130 - 165 km, high-amplitude reflections of low frequency line up in the MCS data (Fig. 5.2 with closeup B). The reflection pattern is similar to drilled volcanics in the vicinity of the Gjoa G-37 well (fig. 9 in Klose et al. (1982)). The P-wave velocity of 5.0 km s$^{-1}$ is also within the range for basalts (Christie et al., 2006). This section is underlain by a LVZ, which represents old sediments that were covered by the basalt flows.

East of a model distance of 165 km, in the Nuuk Basin (Fig. 5.1 b), P-wave velocities of layer **se** are only 4.6 km s$^{-1}$ (Fig. 5.3). This is the only part of the profile, where we interpreted the lower boundary of this layer as basement instead of the upper boundary. The top of layer **se** causes a high-amplitude continuous reflection in the MCS data from a model distance of 165 - 190 km (Fig. 5.2). This is similar to reflections of the top of basalts from a model distance of 140 - 165 km. From 165 - 230 km the upper boundary of layer **se** is characterized by diffuse reflections, which can indicate a broken surface (Fig. 5.2). Although P-wave velocities of layer **se** are lower in the Nuuk Basin than

74

along the rest of the model, we here also interpret basalt flows, due to the high-amplitude reflections in the MCS data (Fig. 5.10).

### 5.8.2 Crustal structure

The P-wave velocity and density model consist of a three-layered crust: the upper, middle, and lower crust. While the P-wave velocity and density structure of the upper crust is uniform along the profile, the middle crust is characterized by higher P-wave velocities and densities from a model distance of 50 - 95 km, like the lower crust between 40 to 170 km. A lateral change was also modelled in the mantle with smaller densities west of a model distance of 170 km.

**Stretched and highly intruded / igneous crust, model distance: 50 - 95 km**

The higher P-wave velocities and densities of the middle and lower crust at a model distance of 40 - 100 km show an increased content of mafic material. This can be in the form of mafic intrusions in a stretched and fractured continental crust, or in the form of newly formed oceanic crust. The following paragraphs discuss both options.

The average thickness of normal oceanic crust is 7.1±0.8 km and of plume affected oceanic crust is 10.3±1.7 km (White et al., 1992). This is only half of the crustal thickness of our model. From the top of layer **c1** to the base of layer **c3** we measure 20 km thickness. Oceanic crust of a similar thickness is reported at oceanic plateaus as parts of large igneous provinces. Gohl & Uenzelmann-Neben (2001) report a 17-km-thick high-velocity lower crust (P-wave velocities of 7.0 - 7.5 km s$^{-1}$) overlain by a 3-km-thick layer of P-wave velocities of 6.5 - 6.8 km s$^{-1}$ at the Agulhas Plateau. This crustal structure is similar to the model of line AWI-20080700 with P-wave velocities of 6.9 - 7.3 km s$^{-1}$ in a 15-km-thick lower crust and 6.3 - 6.9 km s$^{-1}$ in a 3.5-km-thick middle crust. Therefore, an interpretation of new igneous crust from the P-wave velocities is possible.

Other locations of thick oceanic crust are the volcanic continental margins of East Greenland (Holbrook et al., 2001; Hopper et al., 2003) (more than 30 km thickness to 18.3 km thickness depending on the distance to the Iceland hotspot track) and the Vøring Plateau (Mjelde et al., 2005) (23.5 - 9 km thickness). Like the Davis Strait area, both locations were influenced by the Iceland mantle plume, with production of thick basalt flows during the breakup process (Storey et al., 1998; Holbrook et al., 2001; Hopper et al., 2003; Mjelde et al., 2005). Basalt flows are also present along AWI-20080700/BGR08-301 with varying thickness. The basalts from a model distance of 0 - 68 km are part of the sea-ward dipping reflectors at the Baffin Island margin reported by Skaarup et al. (2006).

A difference to the East Greenland margin and the Vøring Plateau are the moderate P-wave velocities in the middle and lower crust. Along AWI-20080700 the middle crust

is 3.5 km thick with an average P-wave velocity of 6.6 km s$^{-1}$ and the lower crust is 14 km thick with an average P-wave velocity of 7.1 km s$^{-1}$. Hopper et al. (2003) model a crust with 6.6 km s$^{-1}$ at the top and 7.5 km s$^{-1}$ at the base. P-wave velocity models of the East Greenland margin shown in Holbrook et al. (2001) exceed 7.5 km s$^{-1}$ in the lower crust. Mjelde et al. (2005) model a layer of 6.8 km s$^{-1}$, of 7.1 km s$^{-1}$ and of 7.3 km s$^{-1}$. It is therefore likely that the crust along AWI-20080700 does not consist completely of new igneous material, but of highly intruded continental crust. According to Rudnick & Fountain (1995) the middle crust of rifted margins is 7.5±5.6 km thick with an average P-wave velocity of 6.4±0.3 km s$^{-1}$; the lower crust is 8.6±5.1 km thick with a P-wave velocity of 7.0±0.3 km s$^{-1}$. Although rifted margins vary greatly, these global averages fit well to the layers of our model (see above). This interpretation requires that the basalt flows along the model are not products of the breakup, but that they are related to volcanism along fractures of the Ungava Fault Complex.

Other methods that are used to identify oceanic crust are magnetic spreading anomalies and the basement morphology. Because of the small scales (45 km of crust), no magnetic sea-floor spreading anomalies can be expected. The basement morphology is only visible below the sedimentary basin from a model distance of 68 - 95 km in the MCS data. But it can not distinguished between a basalt covered continental crust and newly formed oceanic crust.

As we can not rule out either interpretation, we refer to the crust between a model distance of 50 - 95 km as stretched and intruded / igneous crust in the following (Fig. 5.10).

We compare the crustal model along line AWI-20080700/BGR08-301 to that of NUGGET-1 (Funck et al., 2007). Along both profiles, the continental crust of Baffin Island and Greenland is separated by thin crust with a high content of mafic material. On NUGGET-1 (Funck et al., 2007) modelled a 140-km-long section of oceanic layer 2 (5.4 - 6.2 km s$^{-1}$) and 3 (6.7 - 7.0 km s$^{-1}$) underlain by a thick magmatic underplating of P-wave velocities of 7.4 km s$^{-1}$. On NUGGET-1 and AWI-20080700/BGR08-301 this crust is divided into a western and an eastern section. On line AWI-20080700/BGR08-301, at a model distance of 68 km, the upper crust thins by 1.5 km and rises. The western part, from a model distance of 50 - 68 km, is covered by a thick succession of basalts intercalated with sediments. The eastern part, from 68 - 100 km, is also covered by basalts and by a sedimentary basin. On NUGGET-1, a graben structure filled with basalts divides the western and eastern section. We interpret the sharp boundary between the eastern and western segment of intruded / igneous crust as a transform fault of the Ungava Fault Complex.

Funck et al. (2007) propose that the western part of the oceanic crust is related to the volcanic type margin of Baffin Island and Labrador. We expand this interpretation to line AWI-20080700/BGR08-301, as we also imaged basalt flows at the western end of our profile in the models, the MCS and the magnetic anomaly data (Figs 5.2, 5.3,

5.8). These volcanics, southeast of Cape Dyer, are partly exposed at the sea-floor and are mapped by Skaarup et al. (2006) from seismic reflection lines and potential field data.

Funck et al. (2007) further describe the evolution of oceanic crust at the eastern segment as an upwelling of magma in areas of transtensional movement along the Ungava Fault Complex. From the plate kinematic reconstruction (Fig. 5.9) we know that in the period between 57 - 33 Ma strike slip motion and compression were active in the Davis Strait. The stretched crust must therefore have evolved prior to 57 Ma when the strait was opening. The intruded / igneous crust along line AWI-20080700/BGR08-301 and the oceanic crust along NUGGET-1 (Funck et al., 2007) are both in line with gravity anomalies of the Ungava Fault Complex. We therefore propose that stretched and intruded crust / oceanic crust is present between both lines along the Ungava Fault Complex. The location of the Ungava Fault Complex therefore marks the plate boundary between Baffin Island and Greenland prior to 57 Ma.

**High-velocity lower crust**

P-wave velocities of the lower crust higher than $7.0\,\mathrm{km\,s^{-1}}$ are often interpreted as magmatic underplating (Furlong & Fountain, 1986; Marillier & Reid, 1990). Underplating has also been reported on the nearby lines GR89-WA (Gohl & Smithson, 1993) and the NUGGET-1 and -2 (Funck et al., 2007; Gerlings et al., 2009), Fig. 5.1. P-wave velocities of these magmatic underplatings are higher than the velocities we have modelled on line AWI-20080700 (in the range of $7.4 - 7.7\,\mathrm{km\,s^{-1}}$ instead of $6.9 - 7.4\,\mathrm{km\,s^{-1}}$). As there is no boundary detected between lower crust and an underplated body, we interpret a gradual increase of mafic material from the sides to the centre of the model. The thickening of the lower crust from a model distance of 30 - 100 km, shows that mafic material was added to the lower crust. This is similar to the interpretation of a magmatic underplating along other profiles (GR89-WA (Gohl & Smithson, 1993), NUGGET-1 (Funck et al., 2007), and NUGGET-2 (Gerlings et al., 2009)).

Lower mantle densities in the free-air gravity model indicate that the high velocity lower crust is underlain by a hotter mantle than the eastern part of line AWI-20080700/BGR08-301. The high content of mafic material in the centre of the models can be the result of decompressional mantle melts during extension of the lithosphere (McKenzie & Bickle, 1988) and / or due to the influence of a mantle plume (White & McKenzie, 1989).

Funck et al. (2007) relate the magmatic underplating along NUGGET line 1 to the Greenland-Iceland mantle plume. Volcanics of Disco Island are dated to 61 Ma and have been related to the Iceland plume (Storey et al., 1998). Funck et al. (2007) suggest that, according to the hypothesis of Sleep (1997), buoyant plume material flowed southwards along thin lithosphere in the central Davis Strait. Although we can not confirm the origin of the mafic material along line AWI-20080700/BGR08-301, it supports the hypothesis

of Funck et al. (2007) that material of the Iceland plume was channeled southwards along thinned lithosphere in the Davis Strait.

**Continental crust, model distance: 0 - 50, 95 - 315 km**

We interpret the crust, west of a model distance of 40 km and east of a model distance of 100 km, as rifted continental crust according to the P-wave velocity compilation from Rudnick & Fountain (1995) and the thickness of up to 19 km.

The section from a model distance of 95 - 135 km is the Davis Strait High, which crops out farther north. Although the Davis Strait area was a rifting system prior to 57 Ma (see section 5.7), the Davis Strait High is elevated to sea-floor level instead of having subsided. As Chalmers & Pulvertaft (2001) have proposed, this indicates that compressional forces within the Ungava Fault Complex caused an uplift of continental crust. We suggest that the presence of buoyant plume material has supported this uplift.

Steps in the basement morphology indicate faults at a model distance of 68, 95, 135 and 165 km (Fig. 5.2). From the P-wave velocity and density model we introduced an additional fault at the western border of continental to intruded / igneous crust at a model distance of 50 km. The faults from a model distance of 50 - 135 km are within the transform fault system of the Ungava Fault Complex (Sørensen, 2006) and we therefore interpret them as transform faults with a normal component (Fig. 5.10). The fault at 165 km lies at the location of the Hudson Fracture Zone (Chalmers & Pulvertaft, 2001), which is also a transform fault with a normal component. The continental crust is broken into several segments, that have been uplifted relative to one another and were transported along transform faults of the Ungava Fault Complex and the Hudson Fracture Zone.

**model distance 0 - 50 km:** stretched continental crust of 6 - 16 km thickness, divided into upper, middle, and lower crust, covered by basalts intercalated with sediments
**model distance 50 - 95 km:** stretched and intruded crust or new igneous crust with a high-velocity mafic lower crust, covered by basalts intercalated with sediments and partly by a sediment basin
**model distance 95 - 226 km:** stretched continental crust of 12 - 19 km thickness, with a high-velocity lower crust merging into less intruded lower crust from west to east, covered by sediments and partly by basalt flows

## 5.8.3   Ungava Fault Complex and Hudson Fracture Zone

Transform faults of the Ungava Fault Complex are derived by Sørensen (2006) from Bouguer gravity data. Our new models and data offer new constraints on the location of these faults. We use regional magnetic anomaly and satellite derived gravity data to extend the faults perpendicular to our profile (Fig. 5.12).
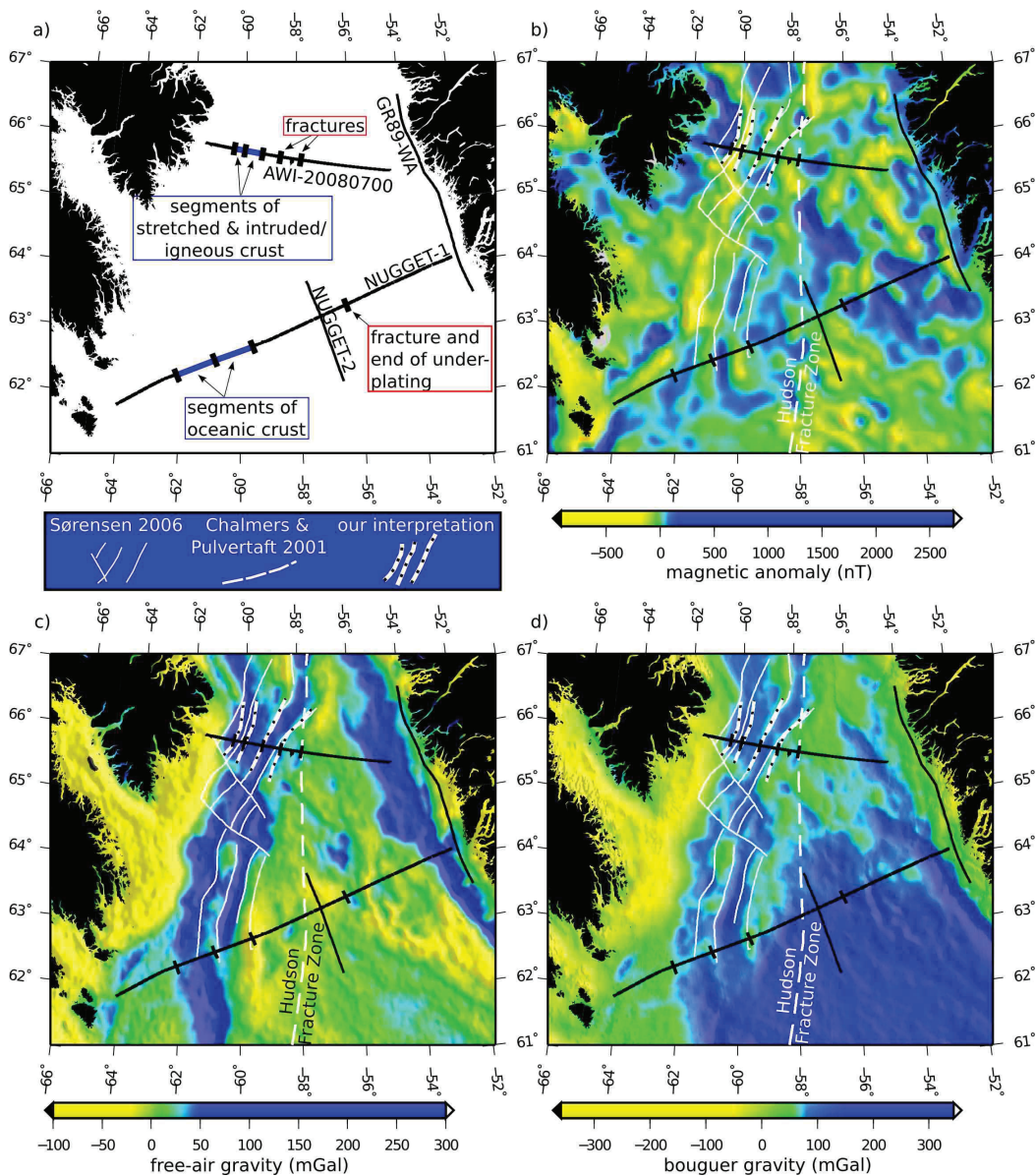
**Figure 5.12: a): Locations of seismic refraction lines (AWI-20080700, GR89-WA (Gohl & Smithson, 1993), NUGGET-1 (Funck et al., 2007), NUGGET-2 (Gerlings et al., 2009)). On the profiles fractures and interpretations are marked. b): Magnetic anomaly data (EMAG2 V2, Maus et al. (2009)) overlain with the same data as in the upper left panel. Locations of faults of the Ungava Fault Complex after Sørensen (2006), the location of the Hudson Fracture Zone after Chalmers & Pulvertaft (2001), and our interpretation are marked. c): Satellite derived free-air gravity anomalies (Sandwell & Smith (2009), version 18.1) overlain with the same information as in the upper right panel. d): Bouguer gravity anomalies reduced to sea-level (DNSC08 free-air gravity data (Andersen et al., 2008) and Smith & Sandwell (1997) topography, version 13.1, used with code from Fullea et al. (2008)) overlain with the same information as in the upper right panel.**

79

The fault at a model distance of 95 km separates intruded / igneous crust from the Davis Strait High and matches exactly the location that Sørensen (2006) proposes (Fig. 5.12). On our line, the eastern border of the Davis Strait High lies 14 km east of the location from Sørensen (2006). We also propose a more north-south striking trend from the gravity data. The fault that bounds the crust of the Nuuk Basin to the west (at a model distance of 170 km) is not mapped by Sørensen (2006). It lies on the Hudson Fracture Zone, which is a north-south striking fault (Srivastava, 1978; Chalmers & Pulvertaft, 2001), that is not clearly imaged by the regional potential field data. While the eastern boundary of the intruded / igneous crust coincides well with the existing fault map, the western boundary needs to be shifted eastwards by 40 km. The north-south extent of this fault is well indicated by a polarity change in the magnetic anomaly data (our interpretation in Fig. 5.12 b). Furthermore, the fault within the intruded / igneous crust is well marked by a polarity change. On our profile this fault had to be shifted 14 km eastwards relative to the Sørensen (2006) interpretation.

To determine the role of the Ungava Fault Complex and the Hudson Fracture Zone in the time between 57 - 33 Ma, we develop two plate tectonic end-member models:

In the first case, we use the Ungava Fault Complex as plate boundary and neglect the Hudson Fracture Zone: Although transform forces dominate the Ungava Fault Complex, compressional forces also occur and must compensate overlapping crust of 70 km width (Fig. 5.9 d). Evidence for compression is the varying thickness of the crust along our line. The middle crust of the Davis Strait High is, for example, 2.5 km thicker than that of the adjacent eastern crust (at a model distance of 140 - 170 km). This can be due to compression. However, these units may have been transported to their present position along the Greenland margin via transform faults of the Ungava Fault Complex, and thus the crustal thickness does not need to be equal. If a deformation in the scale of 70 km has occurred this should also affect the pre-Eocene sediments that directly overly the basement. Deformed sediments are present at a model distance of 140 to 170 km (east the Davis Strait High, closeup B in Fig. 5.2). Balancing the bulged sediments only leads to a lateral extension of 0.5 km, which is far from the expected value of 70 km. On the Davis Strait High, there is no sediment cover detected which could verify deformations. We conclude that our models image transform faults of the Ungava Fault Complex dividing the crust, but compression can only have occurred in a scale of a few kilometers.

In the second case, we use the Hudson Fracture Zone as a plate boundary and neglect the Ungava Fault Complex: No compressional forces occur in the Davis Strait area, only strike slip motion along the Hudson Fracture Zone connects the opening of the Labrador Sea and the Baffin Bay (Fig. 5.9 e). Although this model fits the plate kinematics and the sediment record, some motion must have occurred along the Ungava Fault Complex which is clearly imaged by the data we here present and by the regional potential field data.

Given that the poles of rotation from Oakey (2005) are correct, the Ungava Fault Complex and the Hudson Fracture Zone must have been active in the Davis Strait area. We propose that a change took place from transpression along the Ungava Fault Complex to strike slip motion along the Hudson Fracture zone. Prior to 57 Ma, Davis Strait was opening and highly stretched and intruded continental crust (line AWI-20080700/BGR08-301) or oceanic-type crust (NUGGET-1, Funck et al. (2007)) evolved within the location of the Ungava Fault Complex, which marks the plate boundary at that time. When the Greenland motion relative to the North American craton changed to a more northward direction at 57 Ma, transpression along the Ungava Fault Complex was active as a result of its relative weak lithosphere. As the northward motion of Greenland continued, the stress was no longer compensated by the deformation of crust within the Ungava Fault Complex, but the Hudson Fracture Zone evolved with pure strike slip motion. Although the Hudson Fracture Zone is not well imaged by the regional gravity data and has thus often been neglected in the literature, it likely compensated most of the relative motion between the North American craton and Greenland. As the crust along the Hudson Fracture Zone was not deformed with respect to its thickness, it is not indicated by the regional gravity data.

## 5.9 Conclusions

To determine the nature of the central Davis Strait crust we developed a P-wave velocity and a density model, and interpret these with additional seismic reflection and magnetic anomaly data (Figs. 5.2, 5.3, 5.8). The profile is dominated by continental crust, that is separated by a 45-km-long section of stretched and intruded / new igneous crust (Fig. 5.10). It is similar in the P-wave velocity and density structure to oceanic crust along NUGGET-1 in the northern Labrador Sea, Fig. 5.1 (Funck et al., 2007). On both profiles, this section is divided into an eastern and a western segment by a transform fault of the Ungava Fault Complex. We suggest that oceanic crust / stretched and intruded crust is also present between both lines and follows the gravity anomalies that mark the Ungava Fault Complex (Fig. 5.12 c, d). Beneath the intruded / igneous crust lies a thick high-velocity lower crust (Fig. 5.10) that can be related to the Iceland plume which influenced the Davis Strait region in the Paleocene (Lawver & Müller, 1994; Storey et al., 1998). We infer that buoyant plume material was channeled southwards along thinned lithosphere in the Davis Strait and formed a zone of magmatic underplating in the northern Labrador Sea. Resulting volcanic activity along the Baffin Island margin is also indicated by basalts flows along our profile (Fig. 5.2).

The Davis Strait is dominated by the transform fault system of the Ungava Fault Complex and the Hudson Fracture Zone. We analyzed the role of both fault systems for the Davis Strait area with plate kinematic modelling (Fig. 5.9). While the Davis Strait was opening prior to 57 Ma, stretched and intruded crust evolved along the location

of the Ungava Fault Complex, which was the plate boundary at that time. When the Greenland motion changed to a more northward component, transpressional motion had to be compensated and the Ungava Fault Complex evolved. Crust was deformed and transported along transform faults. At some point compressional deformation of the crust caused more stress than could be compensated and the Hudson Fracture Zone with pure strike slip motion evolved. As this transform fault is not accompanied by crustal thickening or thinning it is not well represented by the regional potential field data and has thus not been recognized to the same extent as the Ungava Fault Complex has. As we only find evidence of minor compression along our profile, most of the motion between the North American plate and Greenland at 57 - 33 Ma must have taken place along the Hudson Fracture Zone.

## 5.10    Acknowledgments

# Chapter 6

# Palaeobathymetric reconstruction of the Davis Strait area - a polar gateway between Canada and Greenland

Sonja K. Suckro[1], Karsten Gohl [1], Volkmar Damm[2]

[1] Alfred Wegener Institute for Polar and Marine Research (AWI), Am Alten Hafen 26, 27568 Bremerhaven, Germany

[2] Federal Institute for Geosciences and Natural Resources (BGR), Stilleweg 2, 30655 Hanover, Germany

83

# 6.1 Abstract

The Davis Strait is a bathymetric high between the Labrador Sea and the Baffin Bay. It acts as a barrier for ocean circulation between the Atlantic and the Arctic Ocean. As a polar gateway, Davis Strait plays a key role for palaeocean circulation models. In order to estimate at what time a water mass transport was possible via Davis Strait and what role the Labrador Sea basin played for the North Atlantic currents, we calculate palaeobathymetry grids. We compile published and new seismic data with information from drill sites. We calculate the effects of flexual unloading, of sediment decompaction, of global sea-level changes, and of thermal subsidence. Palaeolocations of the profiles and the age structure of the crust are derived from our recent plate kinematic model. Although the grids are characterized by great uncertainties, we can conclude that the Davis Strait separated the Labrador Sea from the Baffin Bay from Eocene to Cretaceous times. We propose that, similar to today, an early West Greenland Current formed a cyclonic circulation in the early Labrador Sea basin since the Paleocene.

Keywords: bathymetry, backstripping, plate tectonics, ocean circulation
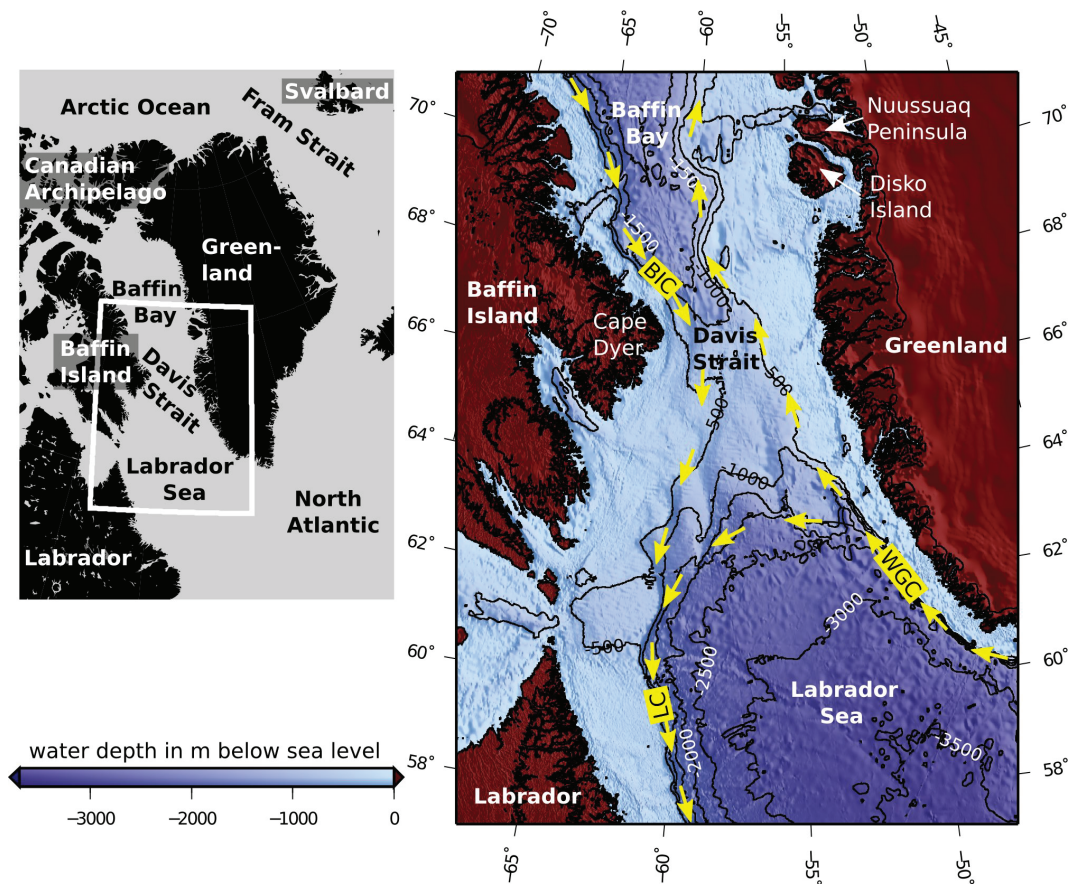
**Figure 6.1:** Left: overview map with names used in the text. Right: Bathymetry of the Davis Strait area (GEBCO_08 Grid, Version 20090202, www.gebco.net) with location names and oceanic currents as sketched in Lazier & Wright (1992); LC = Labrador Current; BIC = Baffin Island Current; WGC = West Greenland Current. The size of the yellow arrows does not scale to velocity or water mass transport.

## 6.2 Introduction

The evolution of oceanic currents as heat transport mechanisms plays an important role in the climate system. Especially polar gateways, that limit the heat transfer between southern latitudes and the Arctic are an important feature. Palaeobathymetric reconstructions of oceanic gateways are a key prerequisite for simulations of palaeocurrent and palaeoclimate scenarios. Here, we focus on Davis Strait, which is a bathymetric high separating the Labrador Sea in the south from Baffin Bay in the north (Fig. 6.1). The Labrador Sea is a northwestward continuation of the Atlantic; Baffin Bay is a polar ocean, connected to the Arctic Ocean via Nares Strait and the Canadian Archipelago. With water depths of less than 700 m, Davis Strait acts as a barrier for regional water

circulation.

The modern surface circulation of the Labrador Sea consists of the West Greenland Current, the Baffin Island Current, and the Labrador Current (Clarke & Gascard, 1983). These surface currents and a deep current form a cyclonic circulation (Clarke & Gascard, 1983). Cold waters of the East Greenland Current form the West Greenland Current, which transports fresh cold waters into the Labrador Sea (e.g. Lazier & Wright, 1992; Cuny et al., 2001). Part of the West Greenland Current continues northward into Baffin Bay, while the major branch bends westward, south of Davis Strait. Combined with cold fresh waters of Baffin Bay from the Baffin Island Current, this branch forms the southward flowing Labrador Current (e.g. Cuny et al., 2001).

We here provide an estimate of the palaeobathymetry of the Davis Strait area to analyze the role of this gateway since the Cretaceous.

We use new and published seismic data with information from drilling sites to backstrip sediment layers and to calculate thermal subsidence. The backstripped segments are rotated in a plate tectonic reconstruction model to their palaeolocations. We construct palaeobathymetric grids for the late Eocene and the end of Cretaceous and compare these with information of drill sites and onshore outcrops.

## 6.3  Database

To reconstruct the palaeobathymetry in the Davis Strait area, we interpreted new seismic lines and collected published interpretations of seismic data (tables 6.1 to 6.3). The sediment stratigraphy of the Davis Strait area is well documented from outcrops, drillings, and seismic data (e.g. Dam & Sønderholm, 1994; Bojesen-Koefoed et al., 2001; Rolle, 1985; Gregersen & Bidstrup, 2008). We use a simplified stratigraphy, based on Chalmers & Pulvertaft (2001); Sørensen (2006); Døssing (2011); Chalmers et al. (1993), Fig. 6.2. New seismic data were collected during the cruise MSM09/3 in 2008 (Gohl et al., 2009; Funck et al., 2012; Suckro et al., 2012), Fig. 6.3. The interpretation of these lines is summarized in C.1.

Sediment thickness maps of the Kenamu (Bell & Moir, 1989b), Cartwright (Bell & Moir, 1989a), and Markland Formation (Bell & Moir, 1989c) and the depth of the acoustic basement (Balkwill et al., 1988) are available at geogratis.gc.ca/api/en/nrcan-rncan/ess-sst. We digitized these data to construct artificial profiles named path 1- 3 along the Labrador margin (Fig. 6.3). To obtain the depth of each formation from the thickness maps, we used GEBCO bathymetry (GEBCO_08 Grid, Version 20090202, www.gebco.net) and the base of the Mokami Formation from dill sites (Wielens & Williams (2009); Jauer et al. (2009); Canada-Newfoundland and Labrador Offshore Petroleum Board, 2008: www.cnlopb.nl.ca/well_alpha.shtml). We constructed a grid of the Mokami depth and added the thickness of the Kenamu, Cartwright, and Markland formation. Path 1- 3 are cuts through these grids.
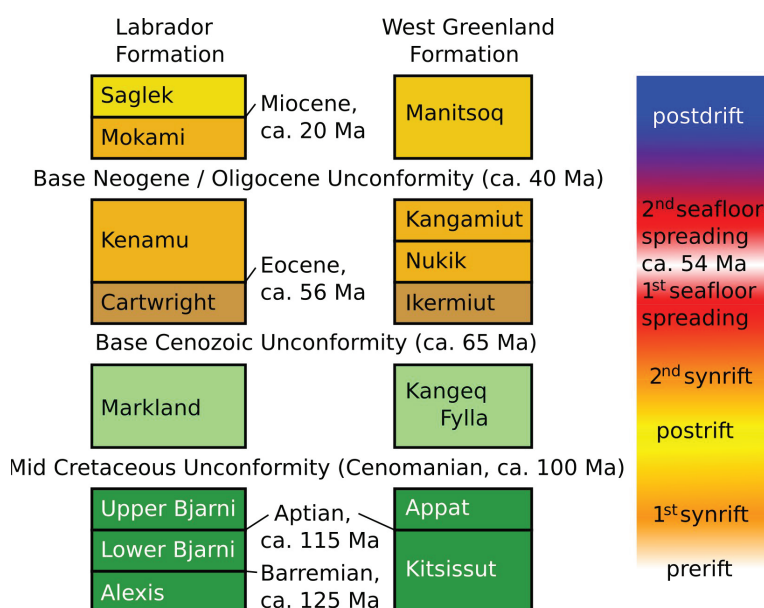
**Figure 6.2: Simplified sediment stratigraphy of the Labrador Sea at the Labrador and West Greenland margin, based on Chalmers & Pulvertaft (2001); Sørensen (2006); Døssing (2011); Chalmers et al. (1993). Box sizes are not to scale with regard to formation thickness and deposition time.**

**Table 6.1: Listing of seismic data used in this study for Late Eocene, drifting - postdrift, 40 Ma; line names and interpreted horizons are named as in the cited publications.**

| Seismic line name | Interpreted formations | References |
| --- | --- | --- |
| BGR77-06, -12, -17, -21 | Tertiary post drift | Chalmers et al. (1993) |
| BUR BG-18 | Tertiary post rift | Chalmers et al. (1993) |
| Fig. 4a, 13 | Mokami | Chalmers & Pulvertaft (2001) |
| Hekja D-D' | Upper Eocene | Klose et al. (1982) |
| path 1, 2, 3 | Mokami | www.GeoGratis.gc.ca |
| connect e-w, n-s | Mokami, Manitsoq, Miocene to Eocene unconformity | BASIN database |
| BGR08-301, -304, -319 | Manitsoq, postdrift | C.1 |

87
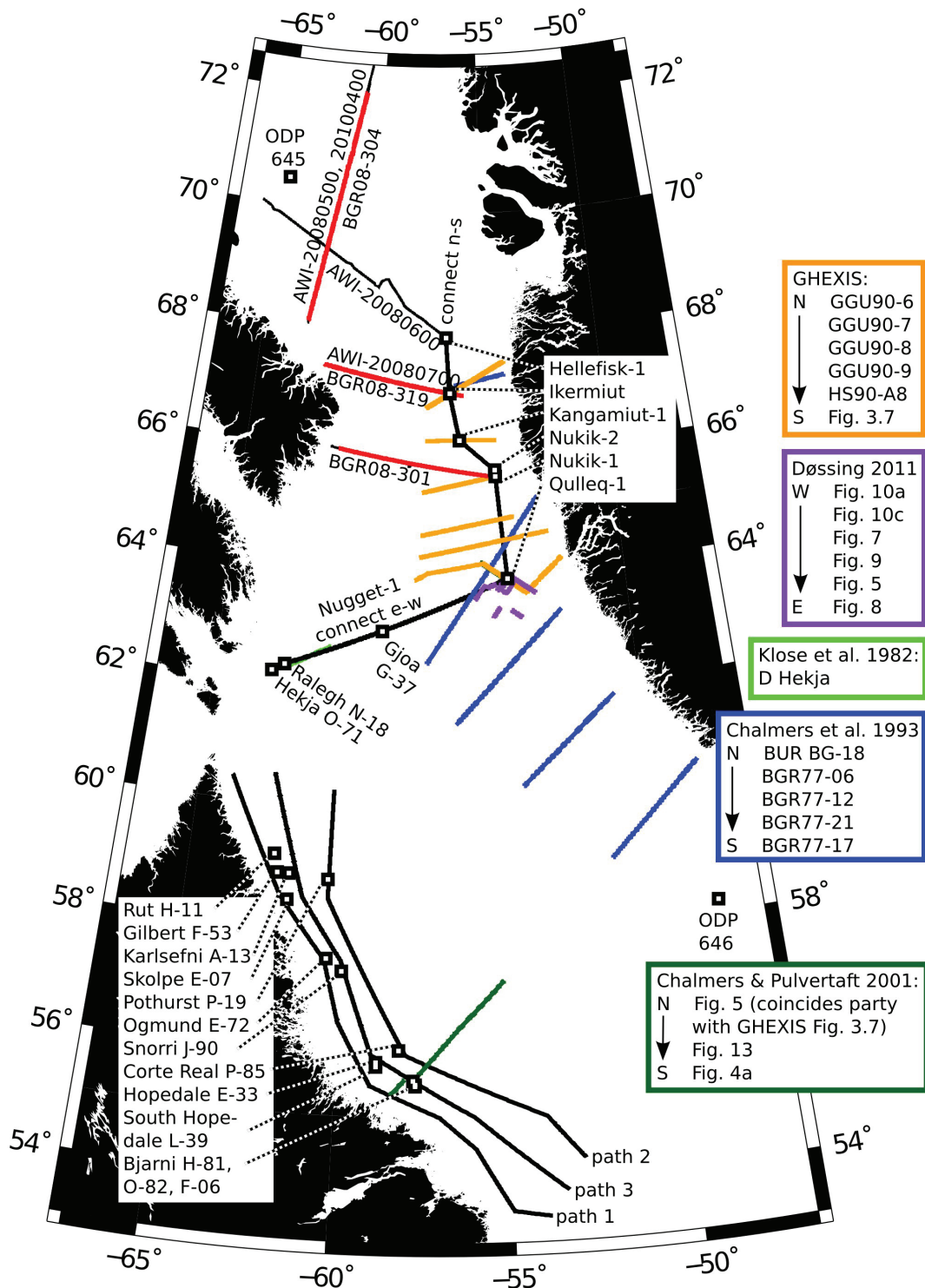
**Figure 6.3: Locations of seismic lines and drill sites used for backstripping.**

**Table 6.2: Listing of seismic data used in this study for Cretaceous/Paleocene, rifting - drifting, 65 Ma; line names and interpreted horizons are named as in the cited publications.**

| Seismic line name | Interpreted formations | References |
|---|---|---|
| BGR77-06, -17 | Tertiary syn drift | Chalmers et al. (1993) |
| BGR77-12 | Tertiary volcanics | Chalmers et al. (1993) |
| BGR77-21 | Tertiary | Chalmers et al. (1993) |
| BUR BG-18 | Tertiary syn rift | Chalmers et al. (1993) |
| Fig. 4a | Cartwright | Chalmers & Pulvertaft (2001) |
| Fig. 5 | Nukik | Chalmers & Pulvertaft (2001) |
| Fig. 13 | basalts below Cartwright | Chalmers & Pulvertaft (2001) |
| Fig. 5, 7, 8, 9, 10a, 10c | Paleocene | Døssing (2011) |
| GGU 90-6 | Paleocene | GHEXIS (www.geus.dk/ghexis/) |
| GGU 90-7, -8, -9, HS_90A-8, Fig. 3.7 | Paleocene basalts | GHEXIS (www.geus.dk/ghexis/) |
| path 1, 2, 3 | Cartwright | www.GeoGratis.gc.ca |
| connect e-w, n-s | basalts below Cartwright, Ikermiut, Hellefisk, top Campanian | BASIN database, Funck et al. (2007) |
| BGR08-301, -319 | Ikermiut, postrift | C.1 |
| BGR08-304 | basalts below syn drift | C.1 |

**Table 6.3: Listing of seismic data used in this study for Mid Cretaceous, prerift - rifting, 100 Ma; line names and interpreted horizons are named as in the cited publications.**

| Seismic line name | Interpreted formations | References |
|---|---|---|
| BGR77-06 | Pretertiary post rift | Chalmers et al. (1993) |
| Fig. 4a | Freydis | Chalmers & Pulvertaft (2001) |
| GGU 90-6, -7, -8, -9, Fig. 3.7 | Kangeq | GHEXIS (www.geus.dk/ghexis/) |
| path 1, 2, 3 | Markland | www.GeoGratis.gc.ca |
| BGR08-319 | Kangeq, synrift | C.1 |

a) original setting        b) flexually unloaded        c) decompacted
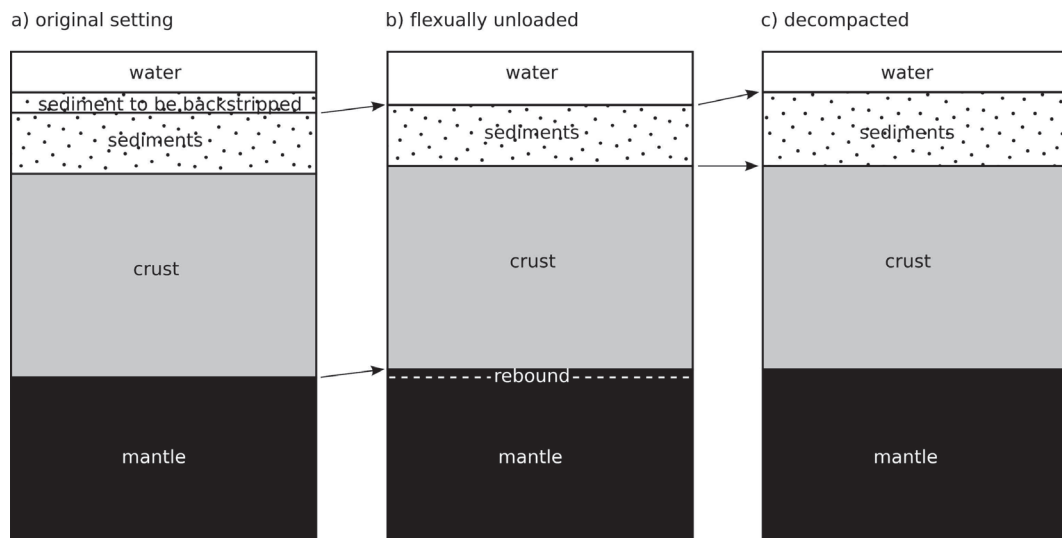
**Figure 6.4: Sketch of backstripping process.**

We also developed artificial profiles from drilling sites in the Davis Strait area (basin.gdr.nrcan.gc.ca/wells/index_e.php). We use the depth of formations from Hekja O-71, Ralegh N-18, Gjoa G-37 (Wielens & Williams, 2009; Jauer et al., 2009), and Qulleq-1 (GEUS well data summary sheets at geuskort. geus.dk/GeusMap/info_samba.jsp?iWellName=list_all&iSector=GREENLAND) which lie on the seismic refraction line Nugget-1 (Funck et al., 2007). With the basement depth and basalt thickness from the P-wave velocity model (Funck et al., 2007) we construct the profile "connect e-w". For the profile "connect n-s" we only interpolated between the formations from drill sites Hellefisk-1, Ikermiut, Kangamiut-1, Nukik-2, Nukik-1 (Rolle, 1985), and Qulleq-1 (GEUS well data summary sheets).

Data coverage of the time slices varies in the cited publications and depends on the data quality and drilling depth. Most authors document the Base Neogene/Oligocene Unconformity (ca. 40 Ma), the Base Cenozoic Unconformity (ca. 65 Ma), and the Mid Cretaceous Unconformity (ca. 100 Ma).

## 6.4 Method

In a first step, seismic two-way traveltimes (TWTT) of sediment horizons and basement are converted to depth. The depth-converted profiles are then backstripped, which includes flexual unloading, decompaction of sediments (Fig. 6.4), and adjustment to palaeo-sea-level. In some cases, levels were adjusted manually to account for local tectonics. To determine the locations of profiles during the tectonic evolution of the Davis Strait area, we rotate the profiles in a plate-kinematic model based on rotation poles by
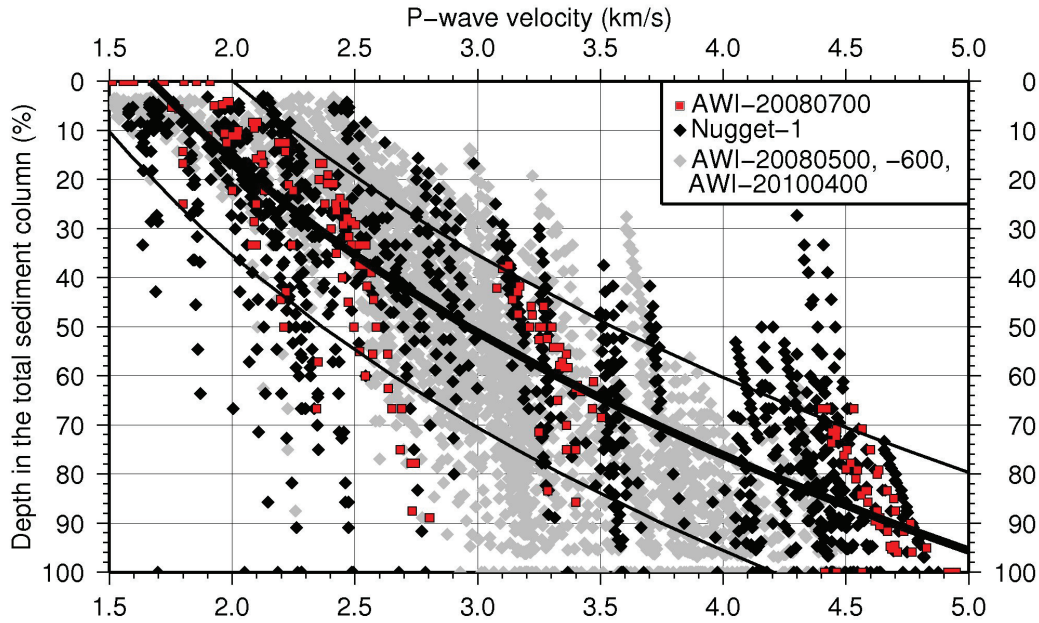
**Figure 6.5: Sediment P-wave velocities of seismic refraction lines in the Davis Strait area (Nugget-1, Funck et al. (2007); AWI-20080700, Suckro et al. (2013)) and in southern Baffin Bay (AWI-20080600, Funck et al. (2012); AWI-20080500 & AWI-20100400, Suckro et al. (2012)). An exponential fit to the Davis Strait data with a corridor of ±20% is plotted in black.**

Oakey (2005) and Oakey & Chalmers (2012). The data are then gridded and corrected for thermal subsidence of the lithosphere. Each step of the palaeobathymetry calculation is described in detail in the following paragraphs.

## 6.4.1   Depth conversion of seismic data

For depth conversion of TWTT we use P-wave velocity models from seismic refraction data in the Davis Strait area: line Nugget-1 (Funck et al., 2007) and AWI-20080700 (Suckro et al., 2013), Fig. 6.3. P-wave velocity models in southern Baffin Bay are also included in Fig. 6.5 for comparison. We extracted velocity-depth profiles for the sediment cover every 10 km along these models. To compare the velocities despite the varying thickness of the sediment cover, we refer to depth as percentage of the total sediment cover at each location. P-wave velocity $vp$ with depth $d_{perc}$ is best estimated by the following fit:

$$vp = 1.667 \exp(0.0116\, d_{perc}) \ , \ \text{rms error} = 0.45 \qquad (6.1)$$

We transfer eq. 6.1 into a TWTT dependent equation (Fig. 6.6). To calculate depth
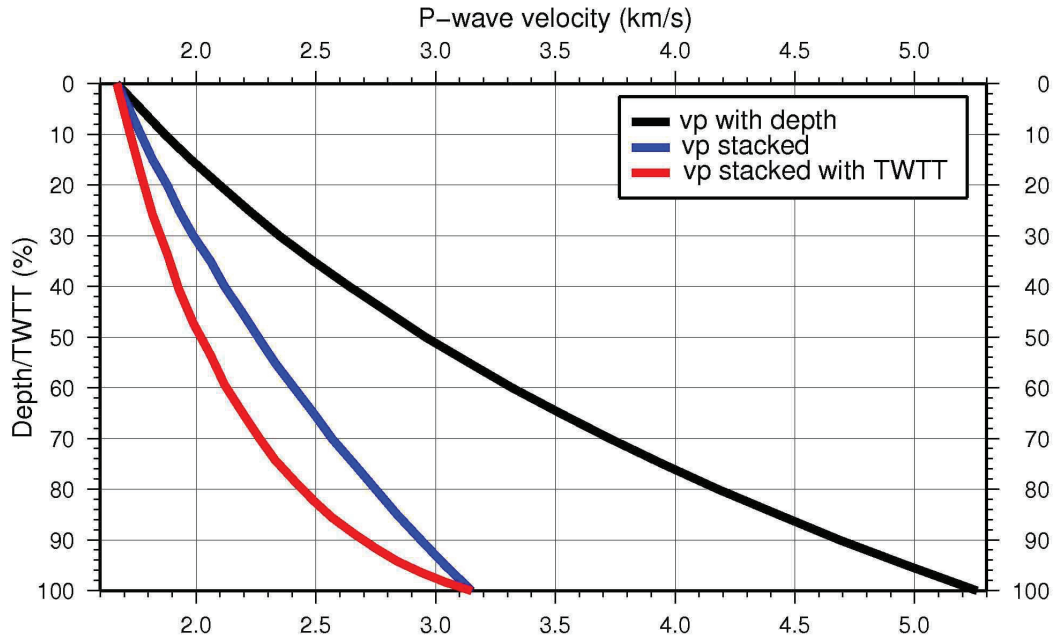
**Figure 6.6:** **Average depth-velocity profile for the Davis Strait area (black); stacked velocities (blue), stacked and converted to two-way traveltimes for depth conversion (red).**

from any TWTT in the sediment column, rms velocities $vp_{rms}$ are needed. The best fit is a fourth order polynom:

$$vp_{rms} = 5.14E^{-8}\ TWTT^4 - 8.63E^{-6}\ TWTT^3 + 5.6E^{-4}\ TWTT^2 \\ -7.3E^{-3}\ TWTT + 1.75 \tag{6.2}$$

$TWTT$ is again given in percent of the whole sediment column. We assume that the P-wave velocity within each sediment layer is constant. Eq. 6.2 is applied to a representative location of each profile to assign rms velocities to each horizon.

### 6.4.2 Flexual unloading

For flexual unloading, we calculate the Airy isostasy at every datapoint along a profile. We use the relationship given by Watts (2001) for an elastic beam as a mathematical loading function to account for the rigidity of the lithosphere. A detailed explanation of this process is given in the Appendix C.2.1.

**Table 6.4: Density of the upper sediment layers.**

| data source | sediment density | reference |
|---|---|---|
| Upper 500 meters, ODP site 645, central Baffin Bay, bulk density | 1600 - 2300 kg/m$^3$ | Shipboard Scientific Party (1987a) |
| Upper 500 meters, ODP site 646, eastern Labrador Sea, bulk density | 1300 - 2100 kg/m$^3$ | Shipboard Scientific Party (1987b) |
| Upper 500 meters, Nugget-1, southern Davis Strait, density model | 1680 - 1950 kg/m$^3$ | Funck et al. (2007) |
| Upper 4 kilometers, AWI-20080500/AWI-20100400, southern Baffin Bay, density model | 2100 - 2250 kg/m$^3$ | Suckro et al. (2012) |
| Upper 3 kilometers, AWI-20080700, central Davis Strait, density model | 2200 kg/m$^3$ | Suckro et al. (2013) |

**Table 6.5: Upper mantle density from gravity models.**

| line name and location | mantle density | reference |
|---|---|---|
| R2, Greenland margin, Labrador Sea | 3300 kg/m$^3$ | Chian & Louden (1994) |
| Line 5, northern Labrador | 3220 - 3315 kg/m$^3$ | Funck & Louden (1999) |
| Nugget-1, southern Davis Strait | 3300 - 3330 kg/m$^3$ | Funck et al. (2007) |
| AWI-20080500/AWI-20100400, southern Baffin Bay | 3200 kg/m$^3$ | Suckro et al. (2012) |
| AWI-20080700, central Davis Strait | 3200 - 3300 kg/m$^3$ | Suckro et al. (2013) |

Necessary input parameters are the densities of sea water ($\rho_w$), the backstripped sediment layer ($\rho_1$), and the upper mantle ($\rho_m$). Also the flexual length parameter $\lambda$ is needed; the crust is no longer affected by a load in the distance of $\pm 2\lambda$. We use:

- $\rho_w = 1030\,kg/m^3$, unpublished CTD measurements during cruise MSM09/3 (Gohl et al., 2009) and ARK-XXV/3 (Damm, 2010)

- $\rho_1 = 1800\,kg/m^3$, see table 6.4; we use a very low density value mainly founded on data from ODP site 646, because we also use the porosity-depth function from this location.

- $\rho_{mantle} = 3300\,kg/m^3$, see table 6.5

- $\lambda = 150\,km$, several examples in Watts (2001) show, that the crust is no longer affected by a load in a distance of 300 km.

### 6.4.3 Decompaction

According to Sclater & Christie (1980) the porosity $f(d)$ of sediments decreases with increasing depth ($d$) by an exponential law:

$$f(d) = f_0 \, exp(-c \cdot d) \qquad (6.3)$$

$f_0$ is the porosity at the top of the sediment column; $c$ is a constant.

After backstripping the top sediment layer, the relative depth of each remaining sediment horizon decreases. Therefore the depth-dependent porosity changes. The calculation of the decompacted depth of horizons is given in the C.2.2. Necessary input parameters are the top porosity $f_0$ and the depth dependent constant $c$. Porosity values with depth are available at ODP site 645 in southern Baffin Bay and 646 in the eastern Labrador Sea (Shipboard Scientific Party, 1987a,b), Fig. 6.7. Due to a material change at 335 m depth at ODP site 645, this site cannot be described with one set of $f_0$ and $c$ values. Because porosities from the lower part of ODP site 645 are similar to the values from site 646 we use only these to obtain an average $f_0$ and $c$. We use: $f_0 = 0.69$, $c = 0.0007$.

### 6.4.4 Palaeosea-level

A change in sea-level ($sl$) has the same isostatic effect as the unloading of sediment has (section 6.4.2). Similar to eq. C.1 the rebound thickness $d_{sl}$ due to sea-level changes is calculated by:

$$d_{sl} = \frac{\rho_{water}}{\rho_{mantle} - \rho_{water}} \cdot (-sl) \qquad (6.4)$$

We use the global sea-level curves presented in Miller (2005) from Vail et al. (1977); Haq et al. (1987); Haq & Al-Qahtani (2005). Sea-level was estimated to be 140 m higher than today at 40 Ma and 200 m higher at 65 and 100 Ma.

### 6.4.5 Plate tectonic reconstruction

We use the most recent plate-kinematic reconstruction of the opening of the Labrador Sea and Baffin Bay which is described in detail in Suckro et al. (2013) and is based on rotation poles from Oakey (2005); Oakey & Chalmers (2012). Rotation was performed using the software GPlates (www.GPlates.org). Fig. 6.8 summarizes the evolution of the Davis Strait area and shows the projected palaeolocations of the seismic data that we use.
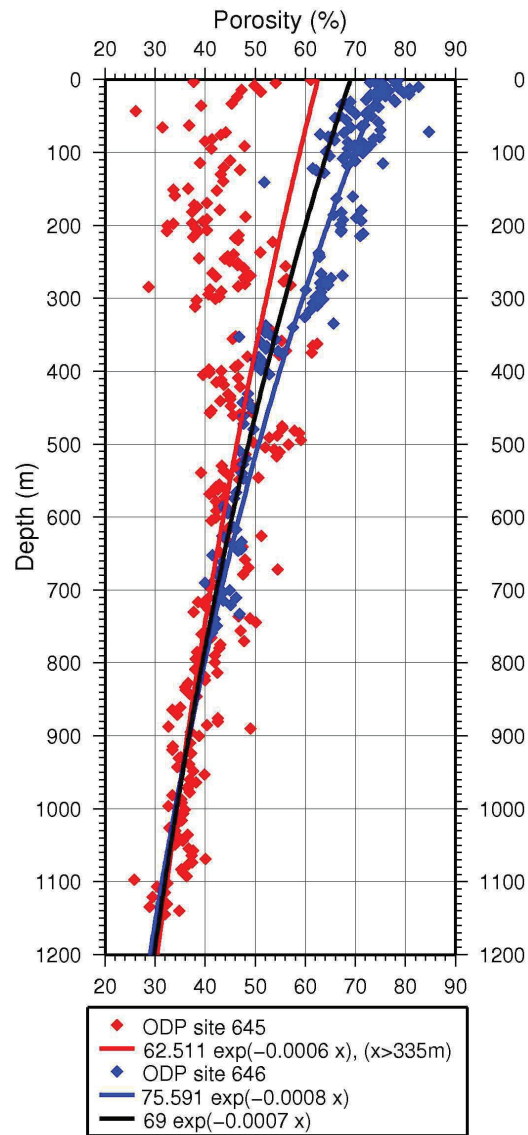
**Figure 6.7: Porosity-depth profiles of ODP sites 645 and 646 with exponential functions.**

- 90 Ma: Greenland separates from the North American craton in a northeast-ward direction. Rifting is active in the Labrador Sea (Roest & Srivastava, 1989; Chalmers & Laursen, 1995). We use the 90 Ma-reconstruction for the 100 Ma grid, because this is oldest reliable time step given in Oakey (2005).

- 65 Ma: Seafloor spreading is active in the Labrador Sea and southern Baffin Bay (Roest & Srivastava, 1989; Chalmers & Laursen, 1995; Suckro et al., 2012).

- 57 Ma: The Davis Strait had opened to the widest extent. The Greenland motion changes from the former northeastward direction to a more northward direction (Srivastava, 1978). The Ungava Fault Complex evolves (Suckro et al., 2013).

- 54 Ma: The convergence within the Ungava Fault Complex can no longer be com-pensated and the Hudson Fracture Zone evolves with strike-slip motion (Srivas-tava, 1978; Suckro et al., 2013).

- 40 Ma: The second phase of seafloor spreading is active in the Labrador Sea and southern Baffin Bay (Oakey & Chalmers, 2012).

- 33 Ma: Seafloor spreading ceases in the Labrador Sea; Greenland and the North American craton move as a single plate from this time on (Srivastava, 1978; Chalmers & Pulvertaft, 2001).

A detailed overview of the Labrador Sea and Baffin Bay evolution is given in Chalmers & Pulvertaft (2001); detailed tectonic models of the southern Baffin Bay and Davis Strait evolution are given in Suckro et al. (2012) and Suckro et al. (2013).

## 6.4.6   Thermal subsidence

After rifting and seafloor spreading, the lithosphere subsides due to cooling. The sub-sidence of oceanic lithosphere is proportional to the square root of its age (Parsons & Sclater, 1977). Subsidence of rifted continental lithosphere can be calculated by an ex-ponential age-relationship (McKenzie, 1978). In addition to fixed parameters, listed in table C.3, the lithospheric extension factor is needed. As crustal models in the Davis Strait and Labrador Sea area are available, we use the thinning of crust as equivalent to the extension of the lithosphere. We take 40-km-thickness as original crustal thickness according to the crustal thickness of northern Labrador (Funck & Louden, 1999) and di-vide this value by the thickness of rifted crust (26 - 5 km, Chalmers et al. (1999); Chian & Louden (1994)). A comparison of the different subsidence calculations is shown in Fig. 6.9. To assign an age to the crust we use the tectonic model described in section 6.4.5 and map segments of the same age (Fig. 6.10). The equations for the calculation of thermal subsidence are given in C.2.3.
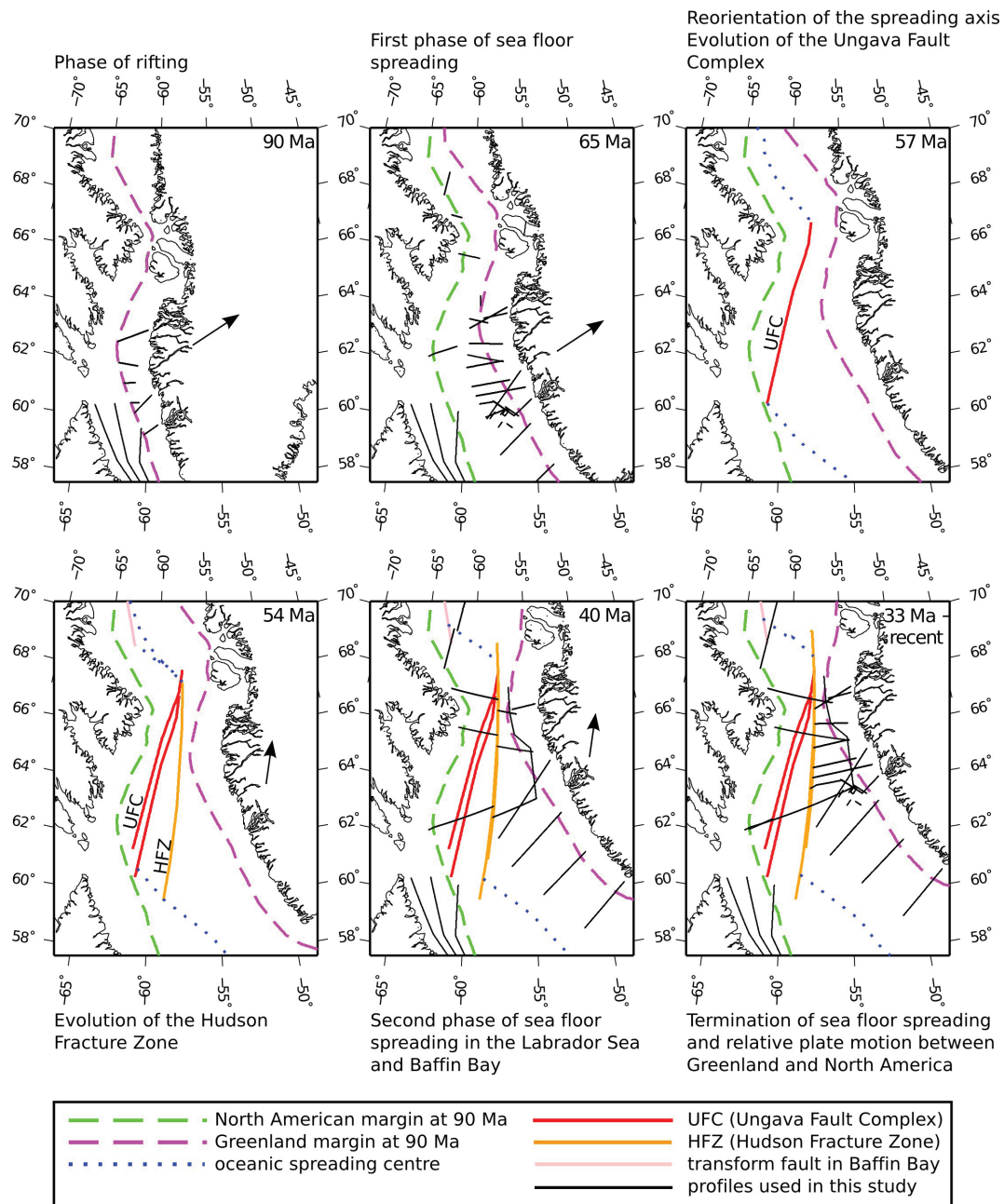
**Figure 6.8: Plate-tectonic evolution of the Davis Strait area, modified from Suckro et al. (2013).**
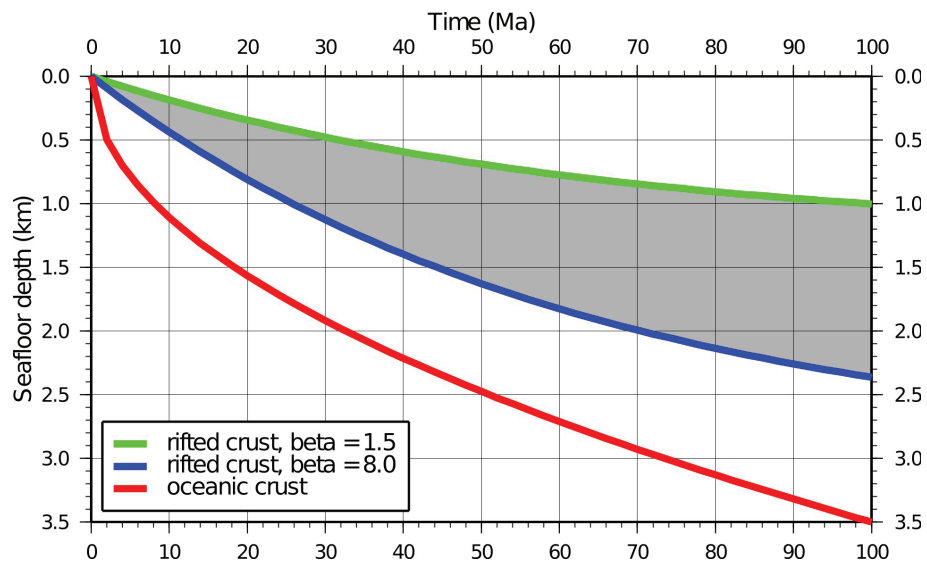
**Figure 6.9: Thermal subsidence of rifted continental lithosphere (equation C.7, McKenzie (1978)) within the range of expected thinning factors; thermal subsidence of oceanic crust (equation C.6, Parsons & Sclater (1977)).**

As thermal subsidence changes the depth of seafloor and thus the water depth, isostatic rebound has to be recalculated with equation 6.4.

### 6.4.7   Gridding

We produce palaeobathymetry grids with the "blockmean" and "surface" modules in GMT (gmt.soest.hawaii.edu/). The gridding increment is 0.2°W and 0.1°N; tension factor 0.2. To obtain a more natural looking bathymetry, we keep points along the Greenland, Labrador, and Baffin Island coast fixed to 0 m palaeosea-level.

## 6.5   Results

Fig. 6.11 displays compilations of the thicknesses of postdrift, syndrift, and synrift sediments. We treat basalts that are intercalated with sediments like other sediments, thus these layers also add to the thickness maps. The sedimentation rates and patterns changed during the tectonic evolution of the Davis Strait area. Postdrift sediments reach 2 km thickness in the southern Baffin Bay and the eastern Labrador Sea. This corresponds to an average sedimentation rate of $0.05 \, \mathrm{m \, ka^{-1}}$. At the Labrador shelf, less than 1.5 km were deposited. This was different during the phase of seafloor spreading in the Paleocene to Eocene. At that time sedimentation rates were highest at the Labrador shelf with a deposition of up to 5 km thickness ($0.2 \, \mathrm{m \, ka^{-1}}$). At the Greenland shelf less
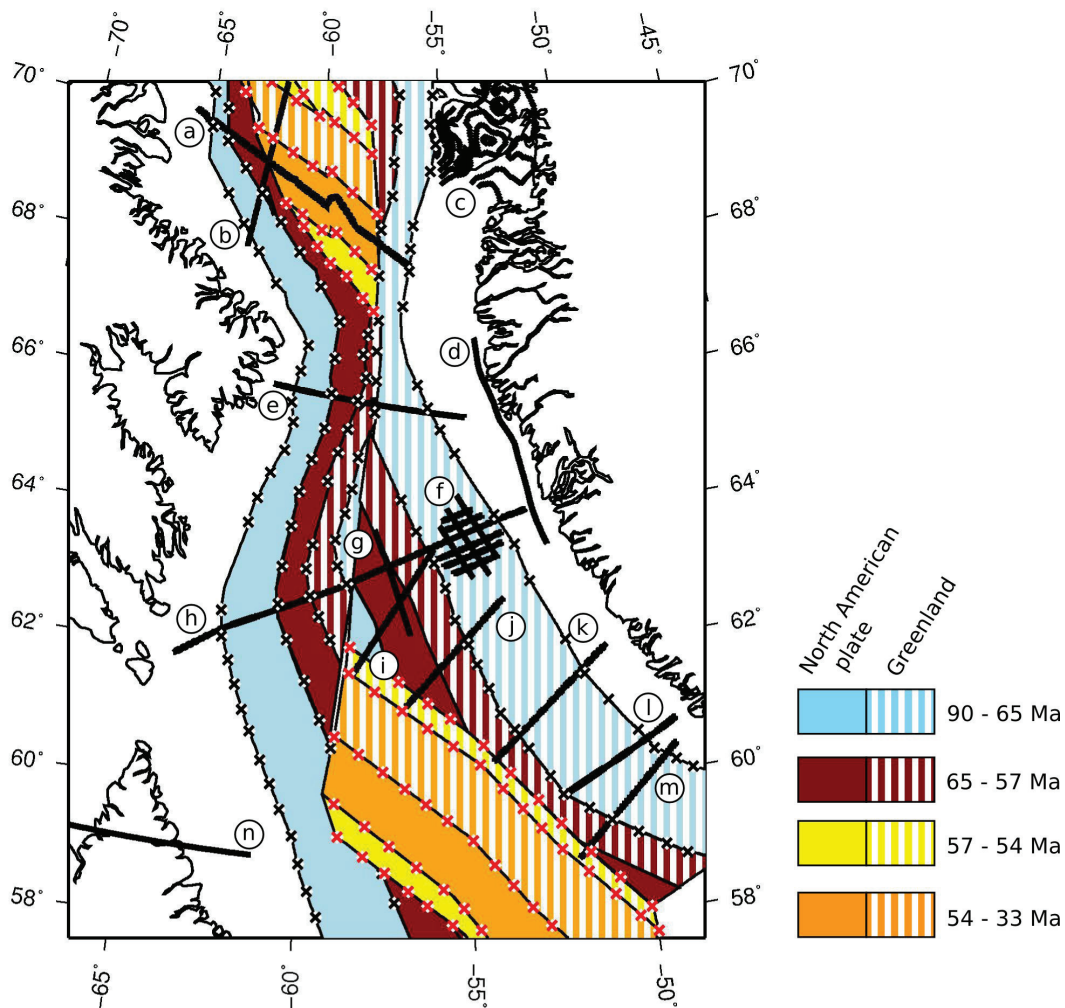
**Figure 6.10: Crustal age as determined from the tectonic model (section 6.4.5). White diamonds with black crosses mark locations where we calculate thermal subsidence of rifted crust; white diamonds with red crosses mark locations where we calculate subsidence of oceanic crust; locations of crustal models are marked in black: seismic refraction lines a) AWI-20080600 (Funck et al., 2012), b) AWI-20080500 & AWI-20100400 (Suckro et al., 2012), d) GR89-WA (Gohl & Smithson, 1993), e) AWI-20080700 (Suckro et al., 2013), g) NUGGET-2 (Gerlings et al., 2009), h) NUGGET-1 (Funck et al., 2007), l) R2 (Chian & Louden, 1994), n) line 5 (Funck & Louden, 1999); seismic reflection lines i) BGR77-06, j) BGR77-12, k) BGR77-21, m) BGR77-17 (Chalmers, 1997); gravity modelling c) (Chalmers et al., 1999), f) (Døssing, 2011).**

**Figure 6.11: Thicknesses of the sediment cover in the Davis Strait area, compiled from seismic reflection data and drill sites in Fig. 6.3.**

than 1 km of sediment was deposited. The indicated change of the deposition pattern can be the product of a change in the ocean currents or in the erosional system on land.
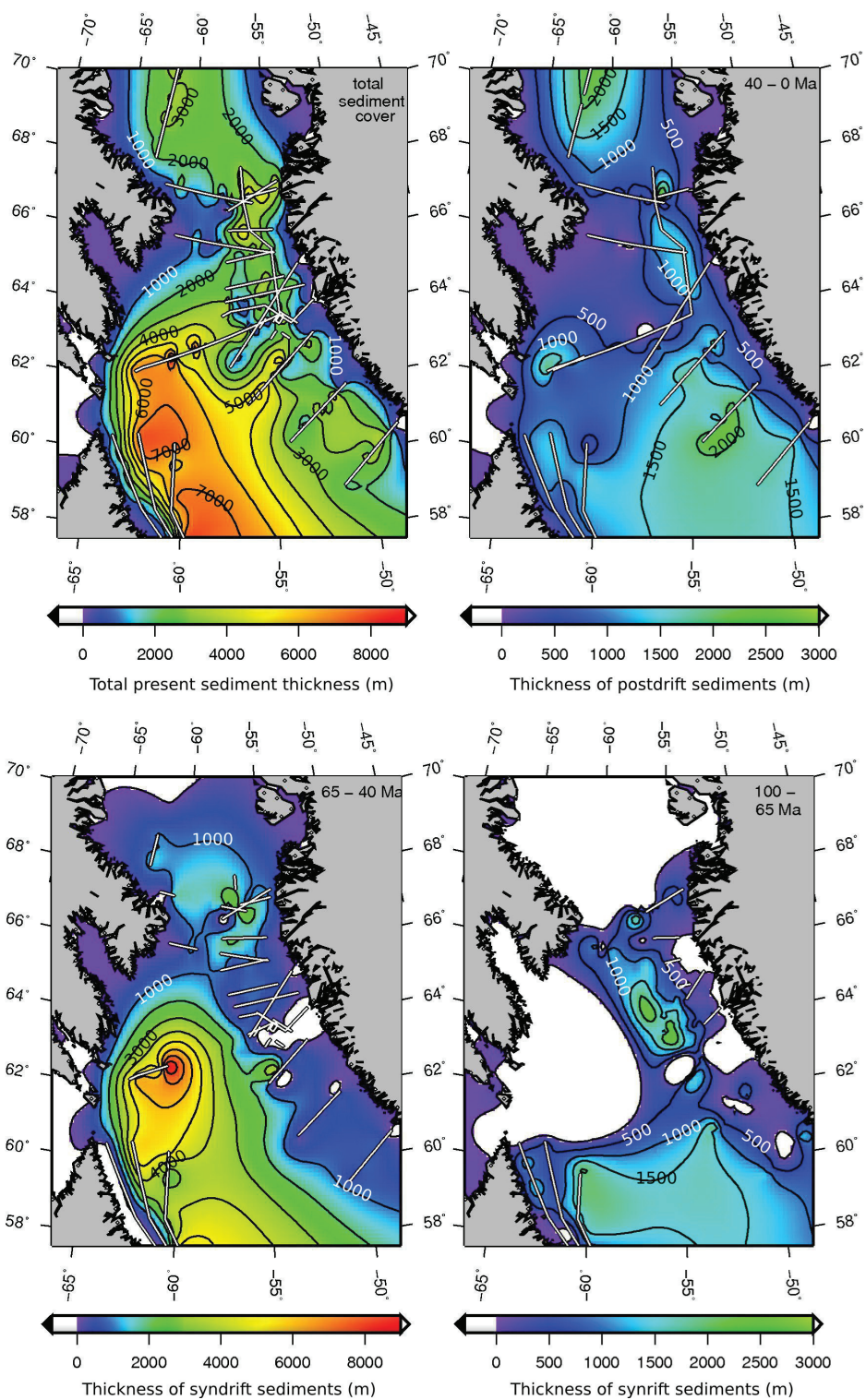
With the backstripping routine and thermal subsidence calculation described in chapter 6.4, we obtain the palaeobathymetry grids in Fig. 6.12. At the end of the drifting phase (ca. 40 Ma) water depths of the Labrador Sea were similar to today (3000 m compared to 3500 m today). The main basin was located in the eastern half of the Labrador Sea, near the Greenland coast. The setting of the Davis Strait and the southern Baffin Bay differed from today with large areas above sea-level. At the beginning of sea-floor spreading (ca. 65 Ma), the main basin of the Labrador Sea was located near southern Baffin Island and northern Labrador. The Davis Strait was above sea-level, as were vast areas off West Greenland. During early rifting, at ca. 90 Ma, a small oceanic basin can only be expected in the northern Labrador Sea.

## 6.6 Discussion

We first discuss the accuracy of the palaeobathymetry calculations. Due to the choice of input parameters the relative errors are high. We compare our grids with drilling information and outcrops onshore. This gives an indication of the accuracy of our grids and of the amplitude of regional tectonics.

### 6.6.1 Accuracy of the palaeobathymetry

**Depth conversion**

Fig. 6.5 shows that sediment P-wave velocities vary $\pm 1$ km/s for different locations. It is reasonable to assume a relative error of $\pm 20\%$, as indicated in Fig. 6.5.

**Flexual unloading**

Errors of flexual unloading result from the set of chosen density values. The density of sea water is well known with a relative error of $\pm 1\%$ (unpublished CTD measurements during cruise MSM09/3 (Gohl et al., 2009) and ARK-XXV/3 (Damm, 2010)). The density of the backstripped sediment layer varies between 1300 and 2300 kg/m$^3$ (table 6.4). This is a relative error of $\pm 28\%$ to 1800 kg/m$^3$. Upper mantle density is better known with values between 3200 to 3330 kg/m$^3$, and a relative error of -3% / +1% to 3300 kg/m$^3$. The choice of $\lambda$ does not influence the amount of uplift due to backstripping, but the shape of the bathymetry. Errors are made especially along small profiles where we extrapolate the edges to calculate a flexual unloading within $\pm 2\lambda$ for all data points.
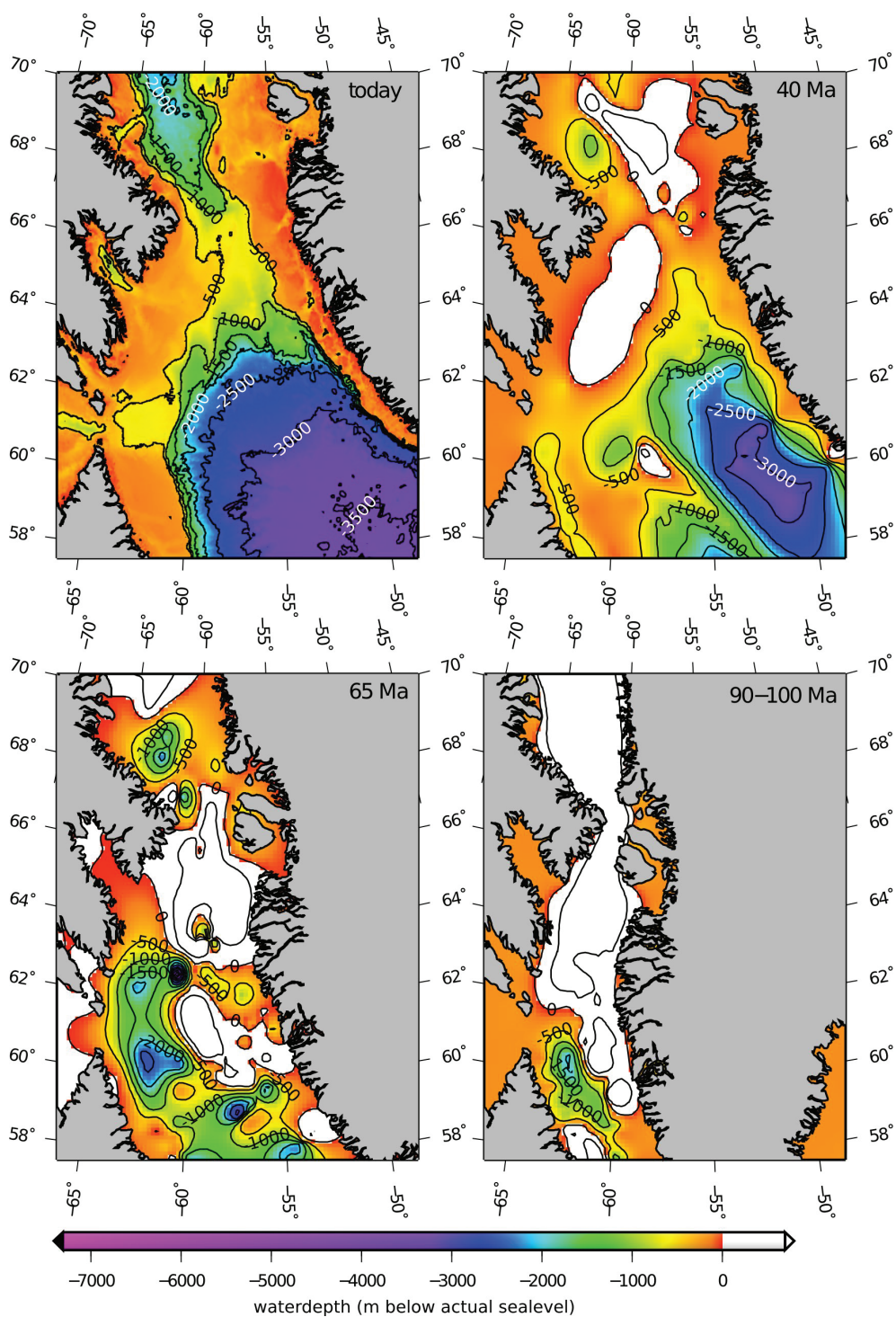
**Figure 6.12: Bathymetry in m below present and palaeosea-level. Today's bathymetry is from the GEBCO_08 Grid, Version 20090202, www.gebco.net. Palaeobathymetry at 40, 65, 90 Ma is calculated as discribed in chapter 6.4.**

102

**Decompaction**

We have chosen the porosity parameter $f_0$ and $c$ according to ODP site 646 and the lower section of site 645 (Shipboard Scientific Party, 1987a,b). To compare these values with other porosity-depth profiles, we plot ODP data from the East Greenland margin in Fig. 6.13. $f_0$ can be chosen between 50 and 80% and $c$ between 0.0005 and 0.0007. This leads to relative errors of -28% / +16% for $f_0$ (69%) and -29% for $c$ (0.0007).

**Palaeosea-level**

Despite the large spread in the reconstructed sea-level in the literature, we here again use the parameters $\rho_w$ and $\rho_m$ from flexual unloading. Both are assigned with relative errors of $\pm 1\%$ and -3% to +1%, respectively.

**Thermal subsidence**

Errors in the calculation of thermal subsidence can originate from errors of the input parameters and from the validity of the empirical equations used.

Thermal subsidence is calculated from the crustal age. We use a simplified tectonic model which is based on rotation poles of Oakey & Chalmers (2012) and is described in Suckro et al. (2013). The actual setting is most likely more complicated than the model in Fig. 6.10 illustrates, with more small scale fracture zones and thus smaller sectors of equally aged crust. If we assume an error of $\pm 3$ Ma in the age determination, this results in a relative error of $\pm 9\%$ on average for the time interval analyzed here. But for the early cooling times, the relative error can be as high as $\pm 100\%$.

The choice of a lithospheric extension factor depends on the accuracy of the crustal models in the Davis Strait region. We assume that the crustal thickness is determined to $\pm 2$ km. For values around 7-km-thickness the relative error is 3.0%, while in locations of thick crust (24 km) the error is 13.5%. At 65 Ma, we only use the equations for rifted crust, although first oceanic crust evolved during this time (Chalmers & Pulvertaft, 2001). The difference between subsidence of rifted and of oceanic crust at 65 Ma is 1 km.

Accuracy of other parameters used in the calculation add up to $\pm 66\%$ (C.2.3).

The subsidence equations used are designed for Atlantic type "normal" oceanic and rifted crust. But there are indications that Greenland and the Davis Strait area were affected by the early Iceland mantle plume (Chalmers et al., 1993; Storey et al., 1998; Funck et al., 2007). The crust therefore underwent a different thermal evolution. Regional tectonics in West Greenland cause uplift with an amplitude of 1 to 2 km (Bonow et al., 2006, 2007; Japsen et al., 2011). Thus, uncertainties of this magnitude are possible in the elevation calculations.
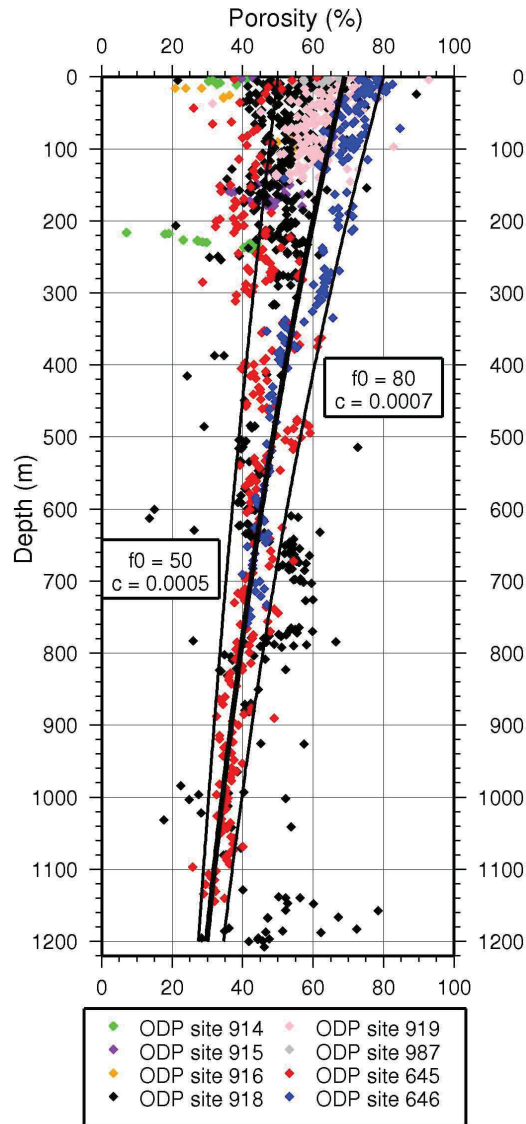
**Figure 6.13: Porosity-depth profiles of ODP sites 914 to 987 on the East Greenland margin (Shipboard Scientific Party, 1994a,b,c,d,e, 1996), of site 645 in Baffin Bay and of 646 in the Labrador Sea (Shipboard Scientific Party, 1987a,b); the thick black line is the porosity depth relation in eq. 6.3 that we use with $f_0 = 69\%$ and $c = 0.0007$ (section 6.4.3); thin black lines display alternative parameters.**

Relative errors due to the choice of parameters for the palaeobathymetry calculation add up to -197% and +152% at most. Although these values are high, it is unlikely that all parameters are chosen in a way that the grid is affected by these maximum errors. The maximum errors are most likely smaller because we choose the density $\rho_1$ in accordance with the porosity $f_0$. This means that for smaller porosity values one also has to choose a higher density. Another large error source is the calculation of thermal subsidence with the parameters listed in Table C.3. But we decided that it is better to include this important step than omitting it.

### 6.6.2 Deposition hiatuses

The stratigraphy in the Davis Strait area is characterized by several depositional hiatuses, especially in the Oligocene to Eocene and the Maastrichtian to Campanian (Sørensen, 2006; Døssing, 2011). As no information is available on the amount of eroded sediment during this time, the palaeobathymetry that we calculate is always a maximum depth estimate.

### 6.6.3 Comparison with wells and onshore information

We compare the palaeowater-depth of our grids with biostratigraphic information of the drill sites Hekja O-71, Ralegh N-18, Gjoa G-37, and Qulleq-1 (Fig. 6.3, Table 6.6). While depths of the two eastern drill sites coincide with our calculations, there is a discrepancy of 450 m and -100 m at the two eastern sites. We therefore exclude a systematic error in our calculations. Although the drilling locations are not representable for the whole grid area, we can assume that the grid is accurate to -100/+450 m.

According to Dam & Sønderholm (1994), the central Nuussuaq Peninsula represents the palaeoshore-line in latest Campanian to earliest Maastrichtian. Our grid at 65 Ma yields values between -39 to -68 m depth at this location. Tertiary basalts of the Cape Dyer area were extruded at approximately 70 m waterdepth according to Clarke & Upton (1971). We also compare these information with the 65 Ma grid, because the basalts can represent volcanics related to the onset of the drifting phase. Our palaeobathymetry has values between -159 to -281 m depth at this location. Although Nuussuaq Peninsula and Cape Dyer are at the edge of our grids, we conclude that it is possibly 50 - 200 m too low. In Fig. 6.14 we show a minimum and maximum palaeobathymetry with a range of $\pm 500$ m for each time step. We also included the possible direction of palaeocean currents. The currents are oriented along contour lines, as we think that they are mainly effected topographic steering.

In Cretaceous times (Fig. 6.14, 90-100 Ma), the Labrador Sea was a small rift basin. Due to its small size we do not draw any conclusions on ocean currents at that time.
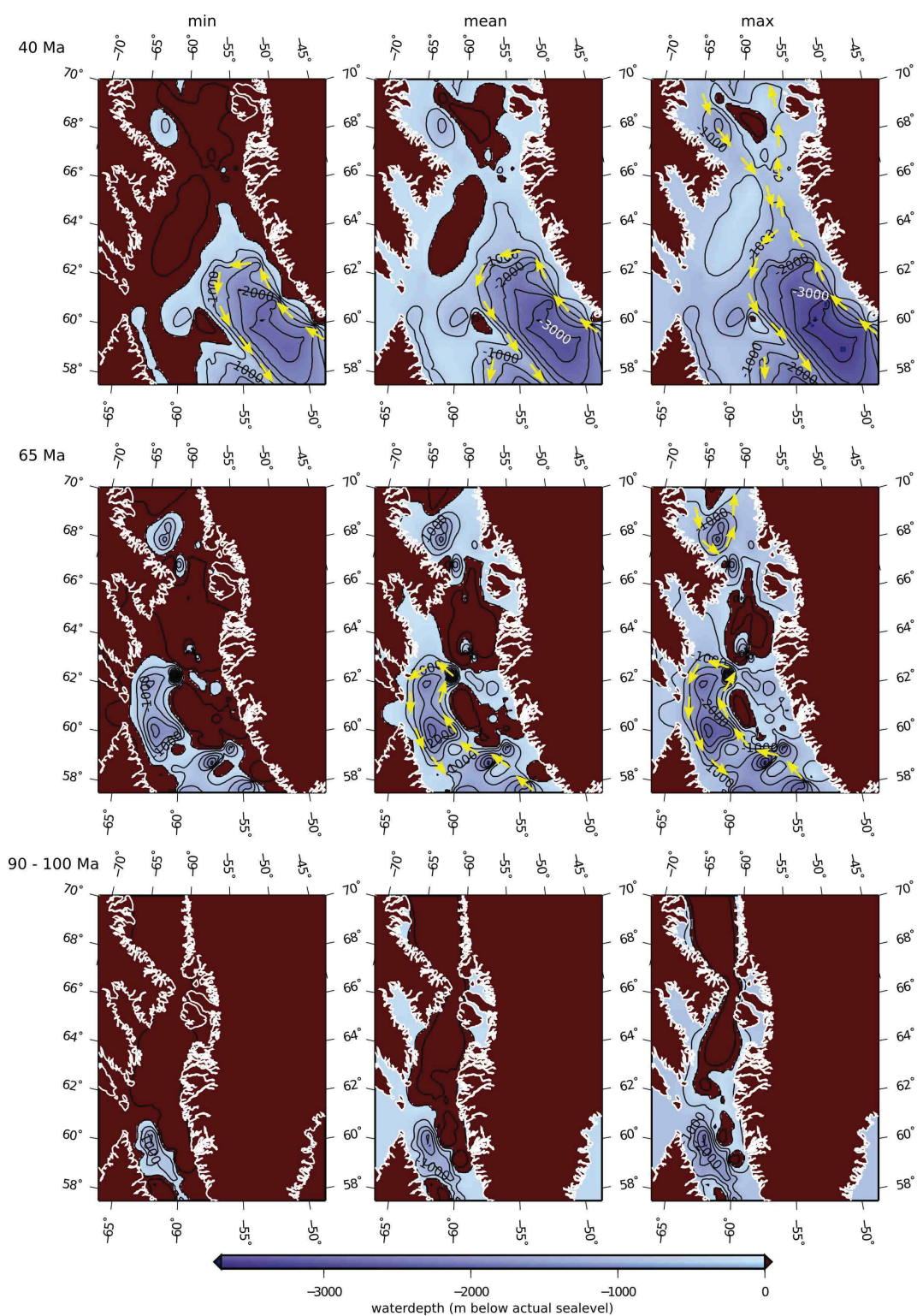
**Figure 6.14: Bathymetry in m below palaeosea-level. Centre column as shown in Fig. 6.12; left column lifted by 500 m; right column lowered by 500 m. Yellow arrows indicate likely directions of palaeocean currents.**

106

**Table 6.6: Comparison of palaeowater-depth and biostratigraphic information from dill site information at 40 Ma. Drill site locations are marked in Fig. 6.3.**

| Drill site | Palaeo-bathymetry | Palynology | Depth | Difference |
|---|---|---|---|---|
| Hekja O-71 | -477 m | non-marine to coastal-marginal marine (Williams, 2007a) | ~ 0 m | 450 m |
| Ralegh N-18 | 87 m | marginal marine to inner shelf: with shallow tidal channels and/or bars, intertidal? (Miller & D'Eon, 1987) | <100 m | -100 m |
| Gjoa G-37 | -209 m | outer neritic (Williams, 2007b) | 100 - 200 m | 10 m |
| Qulleq-1 | -1003 m | open marine to oceanic (Piasecki, 2003) | >200 m | 0 m |

At the end of the rifting and beginning of the drifting phase (Fig. 6.14, 65 Ma), the Labrador Sea probably did have a cyclonic, anti-clockwise current, similar to today. If we apply the maximum depth-calculation, it is also likely that a cyclonic current was present in the early Baffin Bay. For a minimum depth calculation we doubt that a cyclonic current evolved in the Labrador Sea at all, because the region consists of isolated basins.

At the end of seafloor-spreading (Fig. 6.14, 40 Ma), the Labrador Sea basin is well developed and a cyclonic current similar to today must have existed. Although the maximum depth calculation suggests a water transfer via Davis Strait, we think that it is unlikely because the normal and minimum calculation oppose this scenario. That a water transfer was not possible is confirmed by data of the Davis Strait Drift Complex: According to Nielsen et al. (2011) a present-day oceanographic setting with an Arctic-Atlantic connection was not established prior to Middle Miocene.

# 6.7 Conclusions

We use seismic data and drill site information for a backstripping process and thermal subsidence calculation in combination with a plate kinematic model to derive a palaeo-bathymetric model in the Davis Strait area from Eocene to Cretaceous.

By compiling thickness maps of sediment formations, we showed that syndrift sediments mainly accumulated at the Labrador shelf, causing the asymmetric shelf widths of the Labrador Sea. The cause of this accumulation pattern can be the transport of suspended material with ocean currents or the evolution of a depositional system on land.

The palaeobathymetry grids demonstrate that a transfer of water masses via the polar gateway Davis Strait established in post-Eocene times. This supports the interpretations of Nielsen et al. (2011) of the Davis Strait Drift Complex.

A cyclonic current, similar to the West Greenland and Labrador Current of today, probably existed already at the end of Cretaceous. Combined with palaeobathymetric models from the North Atlantic (Wold, 1995; Ehlers & Jokat, 2013), our grids can be used for palaeoclimate studies in palaeocean circulation simulations.

Although our palaeobathymetry still suffers from large uncertainties, it is currently the best possible estimate from present day data and the first study of the Davis Strait gateway that provides a regional picture for further palaeo-modelling.

## 6.8 Acknowledgements

# Chapter 7

# Conclusions and Outlook

Most of the research questions in chapter 1.3 could be answered with the analysis of the new geophysical data from cruise leg MSM09/3 and ARK XXV/3.

The crustal model in chapter 4 confirms that **southern Baffin Bay is underlain by oceanic crust**. The thickness and velocity structure is similar to the world average, presented by White et al. (1992). The extend of oceanic crust matches the map of Chalmers & Oakey (2007) well. Like in the Davis Strait, also **the breakup of southern Baffin Bay was accompanied by volcanism**. This is indicated by basalt flows, visible in the seismic reflection data of the Greenland margin. While large volcanic sequences of the breakup were reported previously offshore Baffin Island, this is the first mapping of breakup volcanics at the conjugate margin.

**The crust in central Davis Strait consists of sections of stretched continental crust, separated by a 45-km-wide unit. This can be interpreted as oceanic crust or as highly intruded, stretched, continental crust** (chapter 5). This is similar to a crustal model in southern Davis Strait (NUGGET-1, Funck et al. (2007)). Interestingly, the crust within the area of the Ungava Fault Complex did not subside - the Davis Strait High is a basement high that crops out at the sea floor. The Nuuk Basin, adjacent to the east, subsided like most rift basins. We think that **compressional tectonics and the influence of the early North Atlantic mantle plume caused an uplift of the western Davis Strait area**.

Although the interpretations are based on models, which are always ambiguous, the summarized results are distinct enough to remain. Even though, new data or a reanalysis of the presented data may lead to different P-wave velocity and density distributions.

For southern Baffin Bay and the Davis Strait area we developed a plate kinematic model. This is based on the newest set of rotation poles by Oakey (2005); Oakey & Chalmers (2012). **In southern Baffin Bay, the plate kinematic modelling confirmed the general location and extend of Paleocene and Eocene oceanic crust as outlined by Chalmers & Oakey (2007)**. We suggest, that magnetic spreading anomalies were not clearly imaged because small scaled crustal fragments, that are divided by fractures,

are rotated and shifted to each other. This results in small scaled fragments. Additionally, a thick sediment cover damps the signal. We propose to locate the fracture zone, that connects the northern and southern Eocene spreading centre in the Baffin Bay along a magnetic anomaly. Chalmers & Oakey (2007) in contrast locate the fracture zone along a gravity anomaly. Both anomalies differ by an azimuth of only 6°.

Kinematic modelling in the Davis Strait area shows that it is not possible to compensate compressional forces that result from the reorientation of the Greenland plate in the Late Paleocene by the Ungava Fault Complex alone. **It is essential to introduce a zone of pure strike slip motion in the Davis Strait. The Hudson Fracture Zone**, which is found in the literature of the 1970ies exactly fits this location. All published sets of rotation poles lead to this conclusion (Roest & Srivastava, 1989; Oakey, 2005; Müller et al., 2008). We therefore think, that the existence of the Hudson Fracture Zone has to be reconsidered.

The compilation of seismic stratigraphy data in chapter 6 shows that **syndrift sediments accumulated mainly at the Labrador shelf** and not at the Greenland shelf. We suggest, that the asymmetric deposition results from the transportation pattern of suspended material in the water or from a depositional system onland. Both possibilities should be further investigated.

We continue to use the plate kinematic model from chapters 4 and 5 for the palaeobathymetric reconstruction of the Davis Strait area in chaper 6. Although uncertainties of the calculations depending on the choice of input parameters are great, we can confirm results of previous studies. It is likely that **a water transport via Davis Strait developed in post Eocene times. A cyclonic current, similar to today, probably existed in the Labrador Sea since the Paleocene**. A study that combines the palaeobathymetric grids of the North Atlantic and the Norwegian-Greenland Sea (Wold, 1995; Ehlers, 2009; Ehlers & Jokat, 2013) with our grids will be of great value for palaeocean modellers.

The plate kinematic model played a big role in all subtopics. It is based on the rotation poles from Oakey (2005); Oakey & Chalmers (2012). Although the poles were carefully developed and the accuracy is stated to be high, the study of the Baffin Bay - Labrador Sea system would have been more complete with a re-analysis of rotation poles. To accomplish this, magnetic spreading anomalies of the Labrador Sea, the North Atlantic, and the Norwegian-Greenland Sea have to be reanalyzed. New data, e.g. north of Greenland (Lehmann, 2012) should be extended and incorporated.

Seismic refraction lines and other geophysical data, acquired in central and northern Baffin Bay during ARK XXV/3, are currently analyzed at the AWI by Tabea Altenbernd. Her crustal models will complement the studies presented here.

# Bibliography

Altenbernd, T., 2010. *Seismistratigraphie und tektonische Entwicklung der Davistraße*, Master's thesis, Leibniz Universität Hannover.

Andersen, O., Knudsen, P., Berry, P., & Kenyon, S., 2008. The DNSC08 ocean wide altimetry derived gravity anomaly field, talk, EGU-2008, Vienna, Austria.

Balkwill, H., Cridland, R., Crous, C., Hunter, D., Laving, G., Petyhyrycz, B., G.Sullivan, Kyle, R., Pape, J., Moir, P., Bell, J., Kyle, R., Barss, M., Jenkins, W., Utting, J., Sherrington, P., & Kruger Enterprises, 1988. Structure iii, Labrador Sea, Subcrop Surface at Seismic Basement and Basement Structure, 1:2,000,000.

Barton, P., 1986. The relationship between seismic velocity and density in continental crust - a useful constraint?, *Geophysical Journal of the Royal Astronomical Society*, **87**, 195–208.

Bell, J. & Moir, P., 1989a. Isopach/net sandstone III, Labrador Sea, Gudrid/Cartwright Formations (Early Paleocene to Early Eocene), 1:2,000,000.

Bell, J. & Moir, P., 1989b. Isopach/net sandstone IV, Labrador Sea, Kenamu Formation (Early to Late Eocene), 1:2,000,000.

Bell, J. & Moir, P., 1989c. Isopach/net sandstone II, Labrador Sea, Markland Formation (Late Cretaceous to Early Paleocene), 1:2,000,000.

Block, M., Damm, V., Ehrhardt, A., Berglar, K., Schnabel, M., & Altenbernd, T., 2012. Characteristics of the West Greenland margin in the southern Baffin Bay, in press.

Bojesen-Koefoed, J., Dam, G., Nytoft, H., Pedersen, G., & Petersen, H., 2001. Drowning of a nearshore peat-formation environment, Atane Formation (Cretaceous) at Asuk, West Greenland: sedimentology, organic petrography and geochemistry, *Organic Geochemistry*, **32**, 967–980.

Bonow, J., Japsen, P., Lidmar-Bergström, K., Chalmers, J., & Pedersen, A., 2006. Cenozoic uplift of Nuussuaq and Disko, West Greenland - elevated erosion surfaces as uplift markers of a passive margin, *Geomorphology*, **80**, 325–337.

Bonow, J., Lidmar-Bergström, K., Japsen, P., Chalmers, J., & Green, P., 2007. Elevated erosion surfaces in central West Greenland and southern Norway: their significance in integrated studies of passive margin development, *Norwegian Journal of Geology*, **87**, 197–206.

Boyden, J., Müller, R., Gurnis, M., Torsvik, T., Clark, J., Turner, M., Ivey-Law, H., Watson, R., & Cannon, J., 2011. Next-generation plate-tectonic reconstructions using GPlates, in *Geoinformatics: Cyberinfrastructure for the Solid Earth Sciences*, pp. 95–116, eds Keller, G. & Baru, C., Cambridge University Press.

Bullock, A. & Minshull, T., 2005. From continental extension to seafloor spreading: crustal structure of the Goban Spur rifted margin, southwest of the UK, *Geophysical Journal International*, **163**, 527–546.

Castagna, J., Batzle, M., & Eastwood, R., 1985. Relationships between compressional-wave and shear-wave velocities in clastic silicate rocks, *Geophysics*, **50**(4), 571–581.

Chalmers, J., 1997. The continental margin off southern Greenland: along-strike transition from an amagmatic to a volcanic margin, *Journal of the Geological Society, London*, **154**, 571–576.

Chalmers, J. & Laursen, K., 1995. Labrador Sea: the extent of continental and oceanic crust and the timing of the onset of seafloor spreading, *Marine and Petroleum Geology*, **12**, 205–217.

Chalmers, J. & Oakey, G., 2007. Cretaceous-Paleogene development of Labrador Sea and Davis Strait, Presentation at the Annual Assembly of the European Geoscience Union, Vienna, Geophysical Research Abstracts, 9, 01638.

Chalmers, J. & Pulvertaft, T., 2001. Development of continental margins of the Labrador Sea: a review, in *Non-Volcanic Rifting of Continental Margins: A Comparison of Evidence from Land and Sea*, vol. 187, pp. 77–105, eds Wilson, R., Whitmarsh, R., Taylor, B., & Froitzheim, N., Geologic Society of London.

Chalmers, J., Pulvertaft, T., Christiansen, F., Larsen, H., Larsen, K., & Ottesen, T., 1993. The southern West Greenland continental margin: rifting history, basin development, and petroleum potential, in *Petroleum Geology of Northwest Europe: Proceedings of the 4th Conference*, pp. 915–931, ed. Parker, J., The Geological Society, London.

Chalmers, J., Pulvertaft, T., Marcussen, C., & Pedersen, A., 1999. New insight into the structure of the Nuussuaq Basin, central West Greenland, *Marine and Petroleum Geology*, **16**, 197–224.

112

Chian, D. & Louden, K., 1994. The continent-ocean crustal transition across the southwest Greenland margin, *Journal of Geophysical Research*, **99**(B5), 9117–9135.

Chian, D., Keen, C., Reid, I., & Louden, K., 1995. Evolution of nonvolcanic rifted margins: New results from the conjugate margins of Labrador Sea, *Geology*, **23**, 589–592.

Chian, D., Reid, I., & Jackson, H., 2001. Crustal structure beneath Orphan Basin and implications for nonvolcanic continental rifting, *Journal of Geophysical Research*, **106**(B6), 10923 – 10940.

Christensen, N. & Mooney, W., 1995. Seismic velocity structure and composition of the continental crust: A global review, *Journal of Geophysical Research*, **100**(B7), 9761–9788.

Christie, P., Gollifer, I., & Cowper, D., 2006. Borehole seismic studies of volcanic succession from the Lopra-1/1a borehole in the Faroe Islands, northern North Atlantic, *Geological Survey of Denmark and Greenland Bulletin*, **9**, 23–40.

Clarke, D. & Upton, B., 1971. Tertiary Basalts of Baffin Island: Field Relations and Tectonic Setting, *Canadian Journal of Earth Sciences*, **8**(248), 248–258.

Clarke, R. & Gascard, J.-C., 1983. The Formation of Labrador Sea Water. Part I: Large-Scale Processes, *Journal of Physical Oceanography*, **13**, 17641778.

Cuny, J., Rhines, P., Niiler, P., & Bacon, S., 2001. Labrador Sea Boundary Currents and the Fate of the Irminger Sea Water, *Journal of Physical Oceanography*, **32**, 627–647.

Dalhoff, F., Larsen, L., Ineson, J., Stouge, S., Bojesen-Koefoed, J., Lassen, S., Kuijpers, A., Rasmussen, J., & Nøhr-Hansen, H., 2006. Continental crust in the Davis Strait: new evidence from seabed sampling, *Geological Survey of Denmark and Greenland Bulletin*, **10**, 33–36.

Dam, G. & Sønderholm, M., 1994. Lowstand slope channels of the Itilli succession (Maastrichtian - Lower Paleocene), Nuussuaq, West Greenland, *Sedimentary Geology*, **94**, 49–71.

Damm, V., 2010. The Expedition of the Research Vessel "Polarstern" to the Arctic in 2010 (ARK-XXV/3), in *Berichte zur Polar- und Meeresforschung (Reports on Polar and Marine Research)*, vol. 621, p. 234, ed. Damm, V., Alfred Wegener Institute for Polar and Marine Research, Bremerhaven, ISSN: 1866-3192.

Dickie, K., Keen, C., Williams, G., & Dehler, S., 2011. Tectonostratigraphic evolution of the Labrador margin, Atlantic Canada, *Marine and Petroleum Geology*, **28**, 1663–1675.

Døssing, A., 2011. Fylla Bank: structure and evolution of a normal-to-shear rifted margin in the northern Labrador Sea, *Geophysical Journal International*, **187**(2), 655–676.

Ehlers, B. & Jokat, W., 2013. Paleo-bathymetry of the northern North Atlantic and consequences for the opening of the Fram Strait, *Marine Geophysical Research*, accepted.

Ehlers, B.-M., 2009. *A geodynamic model of the northern North Atlantic*, Ph.D. thesis, Jacobs University Bremen.

Engen, O., Faleide, J., & Dyreng, T., 2008. Opening of the Fram Strait gateway: A review of plate tectonic constraints, *Tectonophysics*, **450**, 51–69.

Fox, P., Schreiber, E., & Peterson, J., 1973. The Geology of the Oceanic Crust: Compressional Wave Velocities of Oceanic Rocks, *Journal of Geophysical Research*, **78**(23), 5155–5172.

Fullea, J., Fernández, M., & Zeyen, H., 2008. FA2BOUG-A FORTRAN 90 code to compute Bouguer gravity anomalies from gridded free-air anomalies: Application to the Atlantic-Mediterranean transition zone, *Computers and Geosciences*, **34**(12), 1665–1681.

Funck, T. & Louden, K., 1999. Wide-angle seismic transect across the Torngat Orogen, northern Labrador: Evidence for a Proterozoic crustal root, *Journal of Geophysical Research*, **104**(B4), 7463–7480.

Funck, T., Jackson, H., Dehler, S., & Reid, I., 2006. A Refraction Seismic Transect from Greenland to Ellesmere Island, Canada: The Crustal Structure in Southern Nares Strait, *Polarforschung*, **74**(1-3), 97–112.

Funck, T., Jackson, H., Louden, K., & Klingelhöfer, F., 2007. Seismic study of the transform-rifted margin in Davis Strait between Baffin Island (Canada) and Greenland: What happens when a plume meets a transform, *Journal of Geophysical Research*, **112**(B04402), doi:10.1029/2006JB004308.

Funck, T., Gohl, K., Damm, V., & Heyde, I., 2012. Tectonic evolution of southern Baffin Bay and Davis Strait: Results from a seismic refraction transect between Canada and Greenland, *Journal of Geophysical Research*, **117**(B04107), doi:10.1029/2011JB009110.

Furlong, K. & Fountain, D., 1986. Continental Crustal Underplating: Thermal Considerations And Seismic-Petrologic Consequences, *Journal of Geophysical Research*, **91**(B8), 8285–8294.

114

Geoffroy, L., Callot, J.-P., Scaillet, S., Skuce, A., Gélard, J., Ravilly, M., Angelier, J., Bonin, B., Cayet, C., Perrot, K., & Lepvrier, C., 2001. Southeast Baffin volcanic margin and North American-Greenland plate separation, *Tectonics*, **20**(4), 566–584.

Gerlings, J., Funck, T., Jackson, H., Louden, K., & Klingelhöfer, F., 2009. Seismic evidence for plume-derived volcanism during formation of the continental margin in southern Davis Strait and northern Labrador Sea, *Geophysical Journal International*, **176**, 980–994.

Gilbert, L. & Salisbury, M., 2011. Oceanic crustal velocities from laboratory and logging measurements of Integrated Ocean Drilling Program Hole 1256D, *Geochemistry Geophysics Geosystems*, **12**(9), doi:10.1029/2011GC003750.

Gohl, K. & Smithson, S., 1993. Structure of Archean Crust and Passive Margin of Southwest Greenland From Seismic Wide-Angle Data, *Journal of Geophysical Research*, **98**(B4), 6623–6638.

Gohl, K. & Uenzelmann-Neben, G., 2001. The crustal role of the Agulhas Plateau, southwest Indian Ocean: evidence from seismic profiling, *Geophysical Journal International*, **144**(3), 632–646.

Gohl, K., Schreckenberger, B., & Funck, T., 2009. The Expedition of the Research Vessel "Maria S. Merian" to the Davis Strait and Baffin Bay in 2008 (MSM09/3), in *Berichte zur Polar- und Meeresforschung (Reports on Polar and Marine Research)*, vol. 587, p. 104, eds Gohl, K., Schreckenberger, B., & Funck, T., Alfred Wegener Institute for Polar and Marine Research, Bremerhaven, ISSN: 1866-3192.

Gradstein, F., Ogg, J., & Smith, A., 2004. *A Geological Time Scale 2004*, Cambridge University Press.

Gregersen, U. & Bidstrup, T., 2008. Structures and hydrocarbon prospectivity in the northern Davis Strait area, offshore West Greenland, *Petroleum Geoscience*, **14**, 151–166.

Gregersen, U. & Skaarup, N., 2007. A mid-Cretaceous prograding sedimentary complex in the Sisimiut Basin, offshore West Greenland - stratigraphy and hydrocarbon potential, *Marine and Petroleum Geology*, **24**, 15–28.

Haq, B. & Al-Qahtani, A., 2005. Phanerozoic cycles of sea-level change on the Arabian Platform, *GeoArabia*, **10**(2), 127–160.

Haq, B., Hardenbol, J., & Vail, P., 1987. Chronology of Fluctuating Sea Levels Since the Triassic, *Science*, **235**, 1156–1167.

115

Harrison, J., St-Onge, M., Petrov, O., Strelnikov, S., Lopatin, B., Wilson, F., Tella, S., Paul, D., Lynds, T., Shokalsky, S., Hults, C., Bergmann, S., Jepsen, H., & Solli, A., 2008. *Geological map of the Arctic*, https://apps1.grd.nrcan.gc.ca/mirage/full_result_e.php?id=225705, August 2011, Geological Survey of Canada, Open File, map number 5816.

Hinz, K., Mutter, J., Zehnder, C., Alsop, J., Buhl, P., Meyer, H., Roeser, H., & Olaffson, I., 1987. Symmetric conjugation of continent-ocean boundary structures along the Norwegian and East Greenland Margins, *Marine and Petroleum Geology*, **4**, 166–187.

Holbrook, W., Larsen, H., Korenaga, J., Dahl-Jensen, T., Reid, I., Kelemen, P., Hopper, J., Kent, G., Lizarralde, D., Bernstein, S., & Detrick, R., 2001. Mantle thermal structure and active upwelling during continental breakup in the North Atlantic, *Earth and Planetary Science Letters*, **190**, 251–266.

Hopper, J., Dahl-Jensen, T., Holbrook, W., Larsen, H., Lizarralde, D., Korenaga, J., Kent, G., & Kelemen, P., 2003. Structure of the SE Greenland margin from seismic reflection and refraction data: Implications for nascent spreading center subsidence and asymmetric crustal accretion during North Atlantic opening, *Journal of Geophysical Research*, **108**(B5, 2269), doi:10.1029/2002JB001996.

Jackson, H. & Reid, I., 1994. Crustal thickness variations between the Greenland and Ellesmere Island margins determined from seismic refraction, *Canadian Journal of Earth Sciences*, **31**, 1407–1418.

Jackson, H., Keen, C., & Falconer, R., 1979. New geophysical evidence for sea-floor spreading in central Baffin Bay, *Canadian Journal of Earth Sciences*, **16**, 2122–2135.

Jackson, H., Dickie, K., & Marillier, F., 1992. A seismic reflection study of northern Baffin Bay: implication for tectonic evolution, *Canadian Journal of Earth sciences*, **29**, 2353–2369.

Japsen, P., Chalmers, J., Green, P., & Bonow, J., 2011. Elevated, passive continental margins: Not rift shoulders, but expressions of episodic, post-rift burial and exhumation, *Global and Planetary Change*, **90-91**, 73–86.

Jauer, C., Wielens, H., & Williams, G., 2009. Hydrocarbon prospectivity of Davis Strait and Labrador Shelf: seismic setting and stratigraphy for Gjoa G-37, Hekja O-71, Rut H-11, Gilbert F-53, Karlsefni A-13, and Skolp E-07, Geological Survey of Canda, Open File 5910.

Jokat, W. & Schmidt-Aursch, M., 2007. Geophysical characteristics of the ultraslow spreading Gakkel Ridge, Arctic Ocean, *Geophysical Journal International*, **168**, 983–998.

Keen, C. & Barrett, D., 1972. Seismic Refraction Studies in Baffin Bay: An Example of a Developing Ocean Basin, *Geophysical Journal of the Royal Astronomical Society*, **30**, 253–271.

Klose, G., Malterre, E., McMillan, N., & Zinkan, C., 1982. Petroleum Exploration Offshore Southern Baffin Island, Northern Labrador Sea, Canada, in *Arctic Geology and Geophysics: Proceedings of the Third International Symposium on Arctic Geology*, pp. 233–244, eds Embry, A. & Balkwill, H., Canadian Society of Petroleum Geologists, Calgary, Alberta.

Larsen, L., Rex, D., Watt, W., & Guise, P., 1999. $^{40}$Ar-$^{39}$Ar dating of alkali basaltic dykes along the southwest coast of Greenland: Cretaceous and Tertiary igneous activity along the eastern margin of the Labrador Sea, *Geology of Greenland Survey Bulletin*, **184**, 19–29.

Larsen, L., Heaman, L., Creaser, R., Duncan, R., Frei, R., & Hutchison, M., 2009. Tectonomagmatic events during stretching and basin formation in the Labrador Sea and Davis Strait: evidence from age and composition of mesozoic tp palaeogene dyke swarms in West Greenland, *Journal of the Geological Society, London*, **166**, 999–1012.

Lau, K., Louden, K., Funck, T., Tucholke, B., Holbrook, W., Hopper, J., & Larsen, H., 2006. Crustal structure across the Grand Banks - Newfoundland Basin Continental Margin - I. Results from a seismic refraction profile, *Geophysical Journal International*, **167**, 127–156.

Lawver, L. & Müller, R., 1994. Iceland hotspot track, *Geology*, **22**, 311–314.

Lazier, J. & Wright, D., 1992. Annual Velocity Variations in the Labrador Current, *Journal of Physical Oceanography*, **23**, 659–678.

Lehmann, P., 2012. *Geophysikalische Messungen vor Nordgrönland*, Master's thesis, Institut für Geowissenschaften, Friedrich-Schiller-Universität Jena.

Livermore, R., Hillenbrand, C.-D., Meredith, M., & Eagles, G., 2007. Drake Passage and Cenozoic climate: An open and shut case?, *Geochemistry, Geophysics, Geosystems*, **8**(Q01005), doi:10.1029/2005GC001224.

Lutter, W. & Nowack, R., 1990. Inversion for Crustal Structure Using Reflections From the PASSCAL Ouachita Experiment, *Journal of Geophysical Research*, **95**(B4), 4633–4646.

117

Mackenzie, G., Thybo, H., & Maguire, P., 2005. Crustal velocity structure across the Main Ethiopian Rift: results from two-dimensional wide-angle seismic modelling, *Geophysical Journal International*, **162**(3), 994–1006.

MacLean, B., Falconer, R., & Clarke, D., 1978. Tertiary basalts of western Davis Strait: bedrock core samples and geophysical data, *Canadian Journal of Earth Sciences*, **15**, 773–780.

Marillier, F. & Reid, I., 1990. Crustal underplating beneath the carboniferous Magdalen basin (Eastern Canada): evidence from seismic reflection and refraction, in *The Potential of Deep Seismic Profiling for Hydrocarbon Exploration*, pp. 209–218, eds Pinet, B. & Bois, C., Editions Technip, Paris.

Marincovich Jr., L., Brouwers, E., Hopkins, D., & McKenna, M., 1990. Late Mesozoic Cenozoic paleogeographic and paleoclimatic history of the Arctic Ocean Basin, based on shallow-water marine faunas and terrestrial vertebrates, in *The Geology of North America: The Arctic Ocean region*, vol. L, chap. 23, pp. 403–423, eds Grantz, A., Johnson, L., & Sweeney, J., Geological Society of America.

Maus, S., Barckhausen, U., Berkenbosch, H., Bournas, N., Brozena, J., Childers, V., Dostaler, F., Fairhead, J., Finn, C., von Frese, R., Gaina, C., Golynsky, S., Kucks, R., Lühr, H., Milligan, P., Mogren, S., Mueller, R., Olesen, O., Pilkington, M., Saltus, R., Schreckenberger, B., Thébault, E., & Tontini, F., 2009. EMAG2: A 2-arc min resolution Earth Magnetic Anomaly Grid compiled from satellite, airborne, and marine magnetic measurements, *Geochemistry, Geophysics, Geosystems*, **10**(Q08005), doi:10.1029/2009GC002471.

McKenzie, D., 1978. Some Remarks on the Development of Sedimentary Basins, *Earth and Planetary Science Letters*, **40**, 25–32.

McKenzie, D. & Bickle, J., 1988. The Volume and Composition of Melt Generated by Extension of the Lithosphere, *Journal of Petrology*, **29**(3), 625–679.

Miller, K., 2005. The Phanerozoic Record of Global Sea-Level Change, *Science*, **310**, doi: 10.1126/science.1116412.

Miller, P. & D'Eon, G., 1987. Labrador Shelf - Paleoenvironments, Geological Survey of Canada Open File Report 1722.

Minshull, T., 2009. Geophysical characterisation of ocean-continent transitoin at magma-poor rifted margins, *C. R. Geoscience*, **341**, 382–393.

Mjelde, R., Raum, T., Myhren, B., Shimamura, H., Murai, Y., Takanami, T., Karpuz, R., & Næss, U., 2005. Continent-ocean transition on the Vøring Plateau, NE Atlantic, derived from densely sampled ocean bottom seismometer data, *Journal of Geophysical Research*, **110**(B05101), doi:10.1029/2004JB003026.

Müller, R., Sdrolias, M., Gaina, C., & Roest, W., 2008. Age, spreading rates, and spreading asymmetry of the world's ocean crust, *Geochemistry Geophysics Geosystems*, **9**(4), Q04006, doi:10.1029/2007GC001743.

Nielsen, T., Andersen, C., Knutz, P., & Kuijpers, A., 2011. The Middle Miocene to Recent Davis Strait Drift Complex: implications for Arctic-Atlantic water exchange, *Geo-Marine Letters*, **31**(5-6), 419–426.

Oakey, G., 2005. *Cenozoic evolution and lithosphere dynamics of the Baffin Bay-Nares Strait region of Arctic Canada and Greenland*, Ph.D. thesis, Vrije Universiteit, Amsterdam.

Oakey, G. & Chalmers, J., 2012. A new model for the Paleogene motion of Greenland relative to North America: Plate reconstructions of the Davis Strait and Nares Strait regions between Canada and Greenland, *Journal of Geophysical Research*, **117**(B10401), doi:10.1029/2011JB008942.

Olesen, O., Ebbing, J., Lundin, E., Mauring, E., Skilbrei, J., Torsvik, T., Hansen, E., Henningsen, T., Midboe, P., & Sand, M., 2007. An improved tectonic model for the Eocene opening of the Norwegian-Greenland Sea: Use of modern magnetic data, *Marine and Petroleum Geology*, **24**, 56–66.

Parsons, B. & Sclater, J., 1977. An Analysis of the Variation of Ocean Floor Bathymetry and Heat Flow with Age, *Journal of Geophysical Research*, **82**(5), 803–827.

Pedersen, A., Larsen, L., Pedersen, G., & Dueholm, K., 2006. Five slices through the Nuussuaq Basin, West Greenland, *Geological Survey of Denmark Bulletin*, **10**, 53–56.

Piasecki, S., 2003. Neogene dinoflagellate cysts from Davis Strait, offshore West Greenland, *Marine and Petroleum Geology*, **20**(9), 1075–1088.

Reid, I. & Jackson, H., 1997. A review of three transform margins off eastern Canada, *Geo-Marine Letters*, **17**, 87–93.

Rekacewicz, P., 2005. Ocean currents and sea ice extent, Barentswatch Atlas, UNEP/GRID-Arendal.

119

Rice, P. & Shade, B., 1982. Reflection seismic interpretation and seafloor spreading history of Baffin Bay, in *Arctic Geology and Geophysics: Proceedings of the Third International Symposium on Arctic Geology*, pp. 245–265, eds Embry, A. & Balkwill, H., Canadian Society of Petroleum Geologists, Calgary, Alberta.

Rintoul, S., Hughes, C., & Olbers, D., 2001. The Antarctic Circumpolar Current System, in *Ocean Circulation and Climate*, chap. 4.6, pp. 271–302, eds Siedler, G., Church, J., & Gould, J., Academic Press.

Roeser, H., Steiner, C., Schreckenberger, B., & Block, M., 2002. Structural development of the Jurassic Magnetic Quiet Zone off Morocco and identification of Middle Jurassic magnetic lineations, *Journal of Geophysical Research*, **107**(B10), doi:10.1029/2000JB000094.

Roest, W. & Srivastava, S., 1989. Sea-floor spreading in the Labrador Sea: A new reconstruction, *Geology*, **17**, 1000–1003.

Rolle, F., 1985. Late Cretaceous-Tertiary sediments offshore central West Greenland: lithostratigraphy, sedimentary evolution, and petroleum potential, *Canadian Journal of Earth Sciences*, **22**(7), 1001–1019.

Rudnick, R. & Fountain, D., 1995. Nature and composition of the continental crust: a lower crustal perspective, *Reviews of Geophysics*, **33**(3), 267–309.

Sandwell, D. & Smith, W., 2009. Global marine gravity from retracked Geosat and ERS-1 altimetry: Ridge segmentation versus spreading rate, *Journal of Geophysical Research*, **114**(B01411), doi:10.1029/2008JB006008.

Sclater, J. & Christie, P., 1980. Continental Stretching: an Explanation of the Post-Mid-Cretaceous Subsidence of the Central North Sea Basin, *Journal of Geophysical Research*, **85**(B7), 3711–3739.

Shipboard Scientific Party, 1987a. SITE 645, in *Baffin Bay and Labrador Sea sites 645 - 647*, vol. 105 of **Proceedings of the Ocean Drilling Program, Initial Reports**, chap. 4, eds Srivastava, S., Arthur, M., Clement, B., & et al., Ocean Drilling Program, Texas A and M University.

Shipboard Scientific Party, 1987b. SITE 646, in *Baffin Bay and Labrador Sea sites 645 - 647*, vol. 105 of **Proceedings of the Ocean Drilling Program, Initial Reports**, chap. 5, eds Srivastava, S., Arthur, M., Clement, B., & et al., Ocean Drilling Program, Texas A and M University.

Shipboard Scientific Party, 1994a. SITE 914, in *East Greenland Margin sites 914-919*, vol. 152 of **Proceedings of the Ocean Drilling Program, Initial Reports**, chap. 6,

eds Larsen, H., Saunders, A., Clift, P., & et al., Ocean Drilling Program, Texas A and M University.

Shipboard Scientific Party, 1994b. SITE 915, in *East Greenland Margin sites 914-919*, vol. 152 of **Proceedings of the Ocean Drilling Program, Initial Reports**, chap. 7, eds Larsen, H., Saunders, A., Clift, P., & et al., Ocean Drilling Program, Texas A and M University.

Shipboard Scientific Party, 1994c. SITE 916, in *East Greenland Margin sites 914-919*, vol. 152 of **Proceedings of the Ocean Drilling Program, Initial Reports**, chap. 8, eds Larsen, H., Saunders, A., Clift, P., & et al., Ocean Drilling Program, Texas A and M University.

Shipboard Scientific Party, 1994d. SITE 918, in *East Greenland Margin sites 914-919*, vol. 152 of **Proceedings of the Ocean Drilling Program, Initial Reports**, chap. 11, eds Larsen, H., Saunders, A., Clift, P., & et al., Ocean Drilling Program, Texas A and M University.

Shipboard Scientific Party, 1994e. SITE 919, in *East Greenland Margin sites 914-919*, vol. 152 of **Proceedings of the Ocean Drilling Program, Initial Reports**, chap. 12, eds Larsen, H., Saunders, A., Clift, P., & et al., Ocean Drilling Program, Texas A and M University.

Shipboard Scientific Party, 1996. SITE 987, in *North Atlantic - Arctic Gateways II sites 980 - 987*, vol. 162 of **Proceedings of the Ocean Drilling Program, Initial Reports**, chap. 10, eds Jansen, E., Raymo, M., Blum, P., & et al., Ocean Drilling Program, Texas A and M University.

Skaarup, N., Jackson, H., & Oakey, G., 2006. Margin segmentation of Baffin Bay/Davis Strait, eastern Canada based on seismic reflection and potential field data, *Marine and Petroleum Geology*, **23**, 127–144.

Sleep, N., 1997. Lateral flow and ponding of starting plume material, *Journal of Geophysical Research*, **102**(B5), 10001–10012.

Smith, W. & Sandwell, D., 1997. Global seafloor topography from satellite altimetry and ship depth soundings, *Science*, **277**, 1957–1962.

Sørensen, A., 2006. Stratigraphy, structure and petroleum potential of the Lady Franklin and Maniitsoq Basins, offshore southern West Greenland, *Petroleum Geoscience*, **12**, 221–234.

Srivastava, S., 1978. Evolution of the Labrador Sea and its bearing on the early evolution of the North Atlantic, *Geophysical Journal of the Royal Astronomical Society*, **52**, 313–357.

Srivastava, S., MacLean, B., Macnab, R., & Jackson, H., 1982. Davis Strait: Structure and Evolution as Obtained from a Systematic Geophysical Survey, in *Arctic Geology and Geophysics: Proceedings of the Third International Symposium on Arctic Geology*, pp. 267–278, eds Embry, A. & Balkwill, H., Canadian Society of Petroleum Geologists, Calgary, Alberta.

Stickley, C., Brinkhuis, H., Schellenberg, S., Sluijs, A., Röhl, U., Fuller, M., Grauert, M., Huber, M., Warnaar, J., & Williams, G., 2004. Timing and nature of the deepening of the Tasman Gateway, *Paleoceanography*, **19**(PA4027), doi:10.1029/2004PA001022.

Storey, M., Duncan, R., Larsen, A., & Larsen, H., 1998. $^{40}$Ar/$^{39}$Ar geochronoly of the West Greenland Tertiary volcanic province, *Earth and Planetary Science Letters*, **160**, 569–586.

Suckro, S., Gohl, K., Funck, T., Heyde, I., Ehrhardt, A., Schreckenberger, B., Gerlings, J., Damm, V., & Jokat, W., 2012. The crustal structure of southern Baffin Bay: implications from a seismic refraction experiment, *Geophysical Journal International*, **190**(1), 37–58.

Suckro, S., Gohl, K., Funck, T., Heyde, I., Schreckenberger, B., Gerlings, J., & Damm, V., 2013. The Davis Strait crust - a transform margin between two oceanic basins, *Geophysical Journal International*, **193**(1), 78–97.

Talwani, M. & Eldholm, O., 1977. Evolution of the Norwegian-Greenland Sea, *Geological Society of America Bulletin*, **88**, 969–999.

Tessensohn, F. & Piepjohn, K., 2000. Eocene Compressive Deformation in Arctic Canada, North Greenland and Svalbard and Its Plate Tectonic Causes, *Polarforschung*, **68**, 121–124.

Vail, P., Mitchum, R., & Thompson, S., 1977. Relative changes of sea-level from coastal onlap (part3) and Global cycles of relative changes of sea-level (part4), in *Seismic Stratigraphy - Applications to Hydrocarbon exploration*, vol. 26, pp. 63–97, ed. Payton, C., Mem. Am. Assoc. Pet. Geol.

Verhoef, J., Roest, W., Macnab, R., & Arkani-Hamed, J., 1996. Magnetic Anomalies of the Arctic and North Atlantic oceans and adjacent land areas, in *Open File Report 3125A*, Geological Survey of Canada, Calgary, Canada.

Voss, M. & Jokat, W., 2007. Continent-ocean transition and voluminous magmatic underplating derived from P-wave velocity modelling of the East Greenland continental margin, *Geophysical Journal International*, **170**(2), 580–604.

Voss, M., Schmitd-Aursch, M., & Jokat, W., 2009. Variations in magmatic processes along the East Greenland volcanic margin, *Geophysical Journal International*, **117**, 755–782.

Watt, W., 1969. The coast-parallel dike swarm of southwest Greenland in relation to the opening of the Labrador Sea, *Canadian Journal of Earth Sciences*, **6**(5), 1320–1321.

Watts, A., 2001. *Isostasy and Flexure of the Lithosphere*, Cambridge University Press.

Watts, A. B. & Fairhead, J. D., 1999. A process-oriented approach to modeling the gravity signature of continental margins, *The Leading Edge*, **18**(2), 258–263.

White, R. & McKenzie, D., 1989. Magmatism at Rift Zones: The Generation of Volcanic Continental Margins and Flood Basalts, *Journal of Geophysical Research*, **94**(B6), 7685–7729.

White, R., McKenzie, D., & R.K.O'Nions, 1992. Oceanic Crustal Thickness From Seismic Measurements and Rare Earth Element Inversion, *Journal of Geophysical Research*, **97**(B13), 19683–19715.

Wielens, H. & Williams, G., 2009. Stratigraphic cross section Gjoa-Snorri, Saglek-Hopedale Basin, in the Labrador Sea, on the east coast of Canada, from North to South, Geological Survey of Canda, Open File 5903.

Williams, G., 2007a. Palynological analysis of Aquitaine et al. Hekja O-71, Saglek Basin, Davis Strait., Geological Survey of Canada Open File Report 5448.

Williams, G., 2007b. Palynological analysis of Esso-H.B. Gjoa G-37, Saglek Basin, Davis Strait., Geological Survey of Canada Open File Report 5449.

Wold, C., 1995. Palaeobathymetric reconstruction on a gridded database: the northern North Atlantic and southern Greenland-Iceland-Norwegian sea, in *The Tectonics, Sedimentation and Palaeoceanography of the North Atlantic Region*, pp. 271–302, eds Scrutton, R., Stoker, M., Shimmield, G., & Tudhope, A., The Geological Society, Special Publications.

Zelt, C., 1994. 3-D velocity structure from simultaneous traveltime inversion of in-line seismic data along intersecting profiles, *Geophysical Journal International*, **118**, 795–801.

Zelt, C. & Smith, R., 1992. Seismic traveltime inversion for 2-D crustal velocity structure, *Geophysical Journal International*, **108**, 16–34.

# A

# Appendix, The crustal structure of southern Baffin Bay
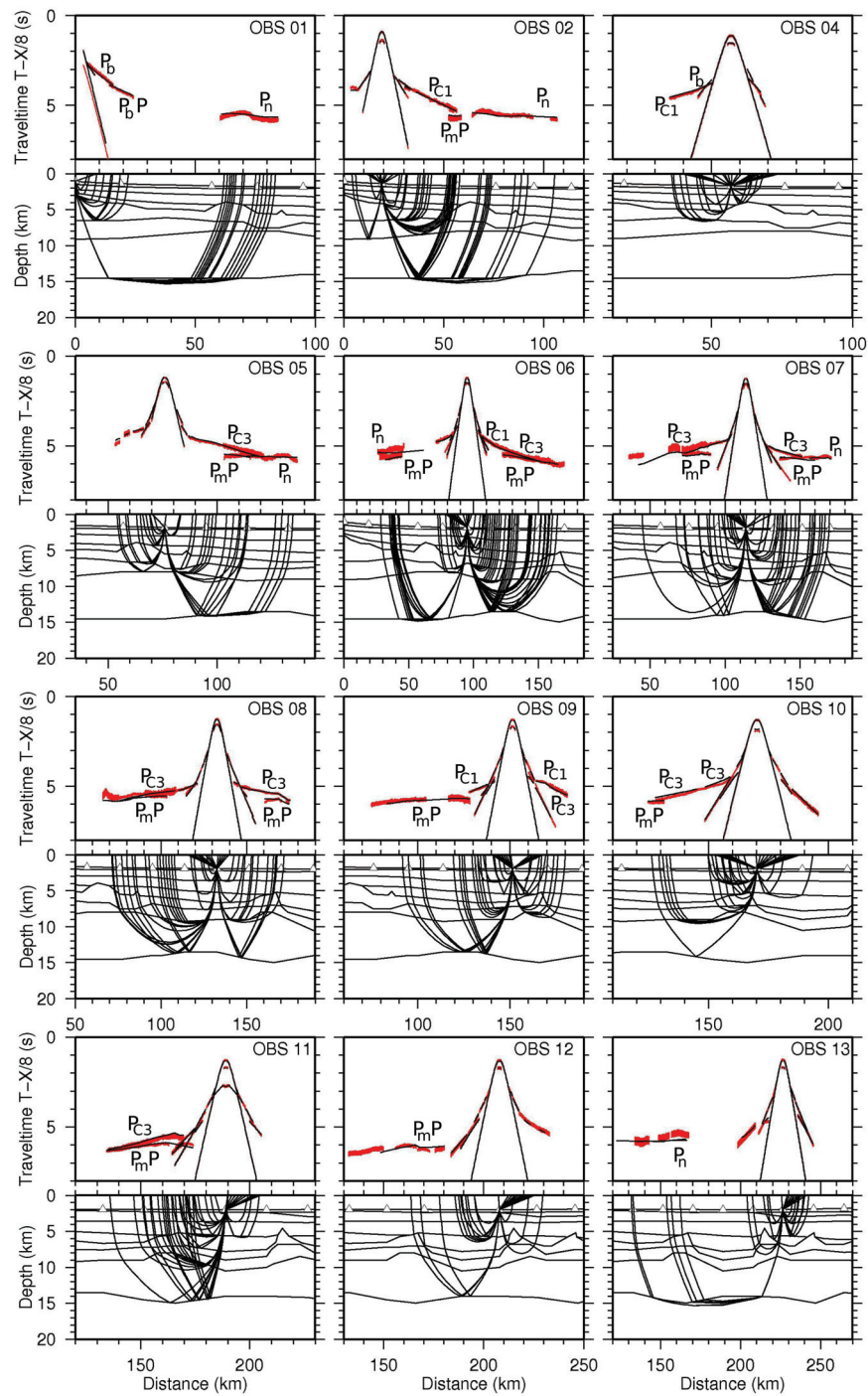
**Figure A.1: Raytracing in the P-wave velocity model for OBS 1 - 13. Top pannels: Picked phases in red, with vertical bar length according to the assigned pick uncertainty, calculated travel times as thin black lines and phase names. A reduction velocity of $8\,\mathrm{km\,s^{-1}}$ is used for plotting. Bottom pannels: Raypaths of the corresponding phases in the model. For clarity, only every 20th ray is plotted.**

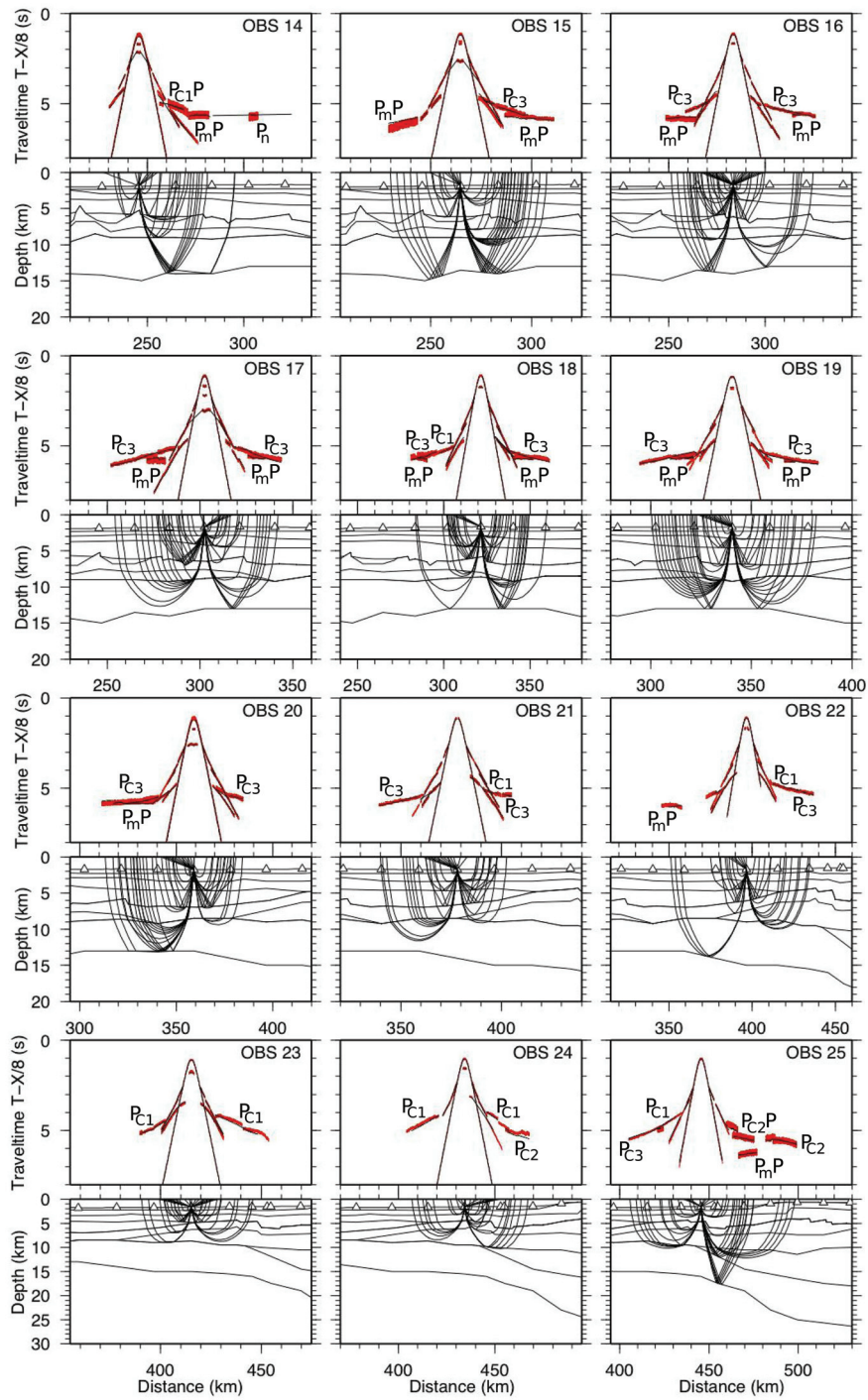126

**Figure A.2: Raytracing in the P-wave velocity model for OBS 14 - 25. For the description of the pannels see Fig. A.1.**
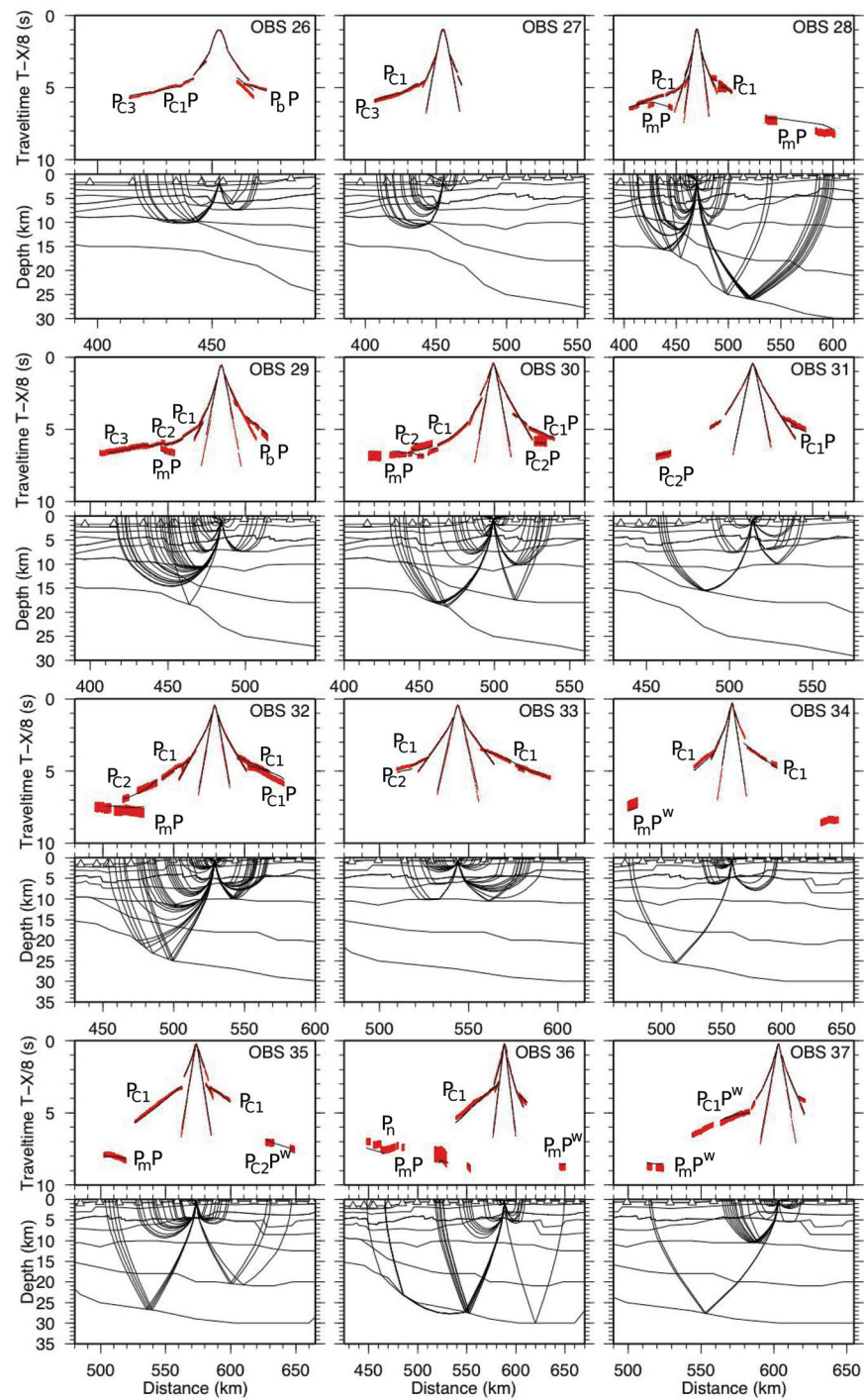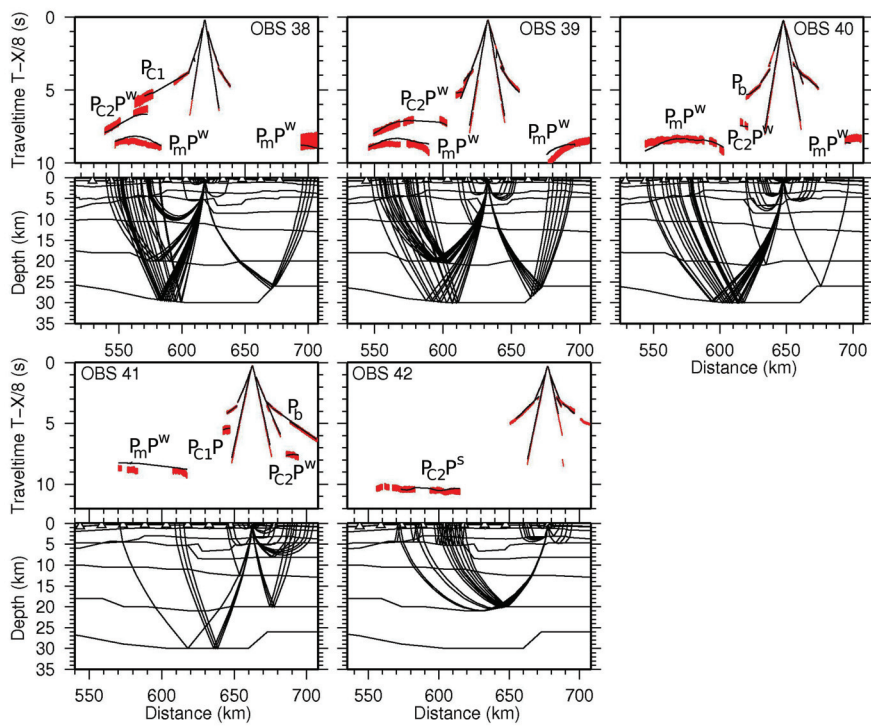
127

**Figure A.3: Raytracing in the P-wave velocity model for OBS 26 - 37. For the description of the pannels see Fig. A.1.**

128

**Figure A.4: Raytracing in the P-wave velocity model for OBS 38 - 42. For the description of the pannels see Fig. A.1.**

# B

# Appendix, The Davis Strait crust
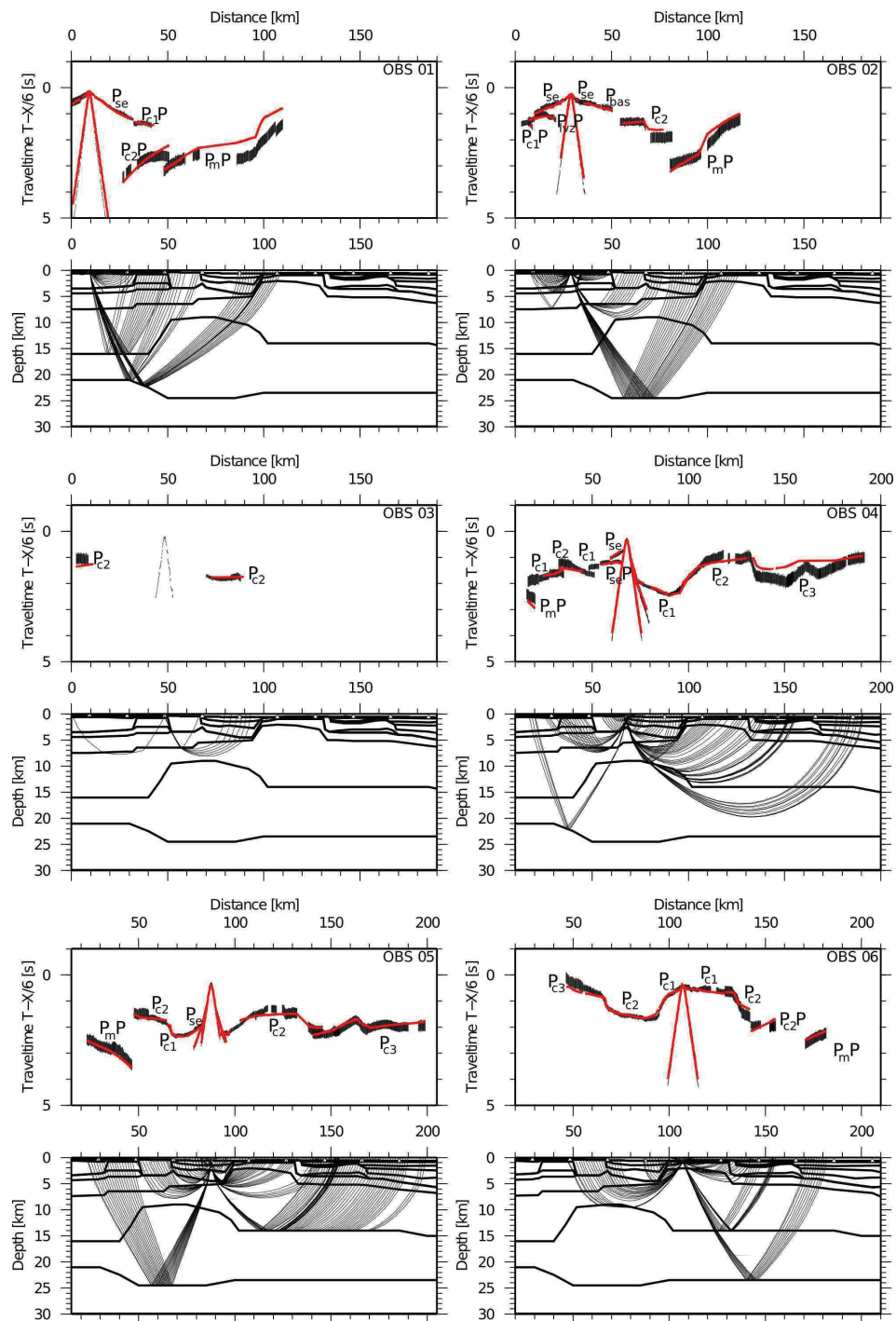
**Figure B.1: Raytracing in the P-wave velocity model for OBS 1 - 6. Top panels: Picked phases in red with vertical bar length according to the assigned pick uncertainty; calculated traveltimes as thin black lines; phase names are annotated; a reduction velocity of $6\,\mathrm{km\,s^{-1}}$ is used. Lower panels: Raypaths of the corresponding phases in the P-wave velocity model. For clarity only every 10th ray is plotted.**

132
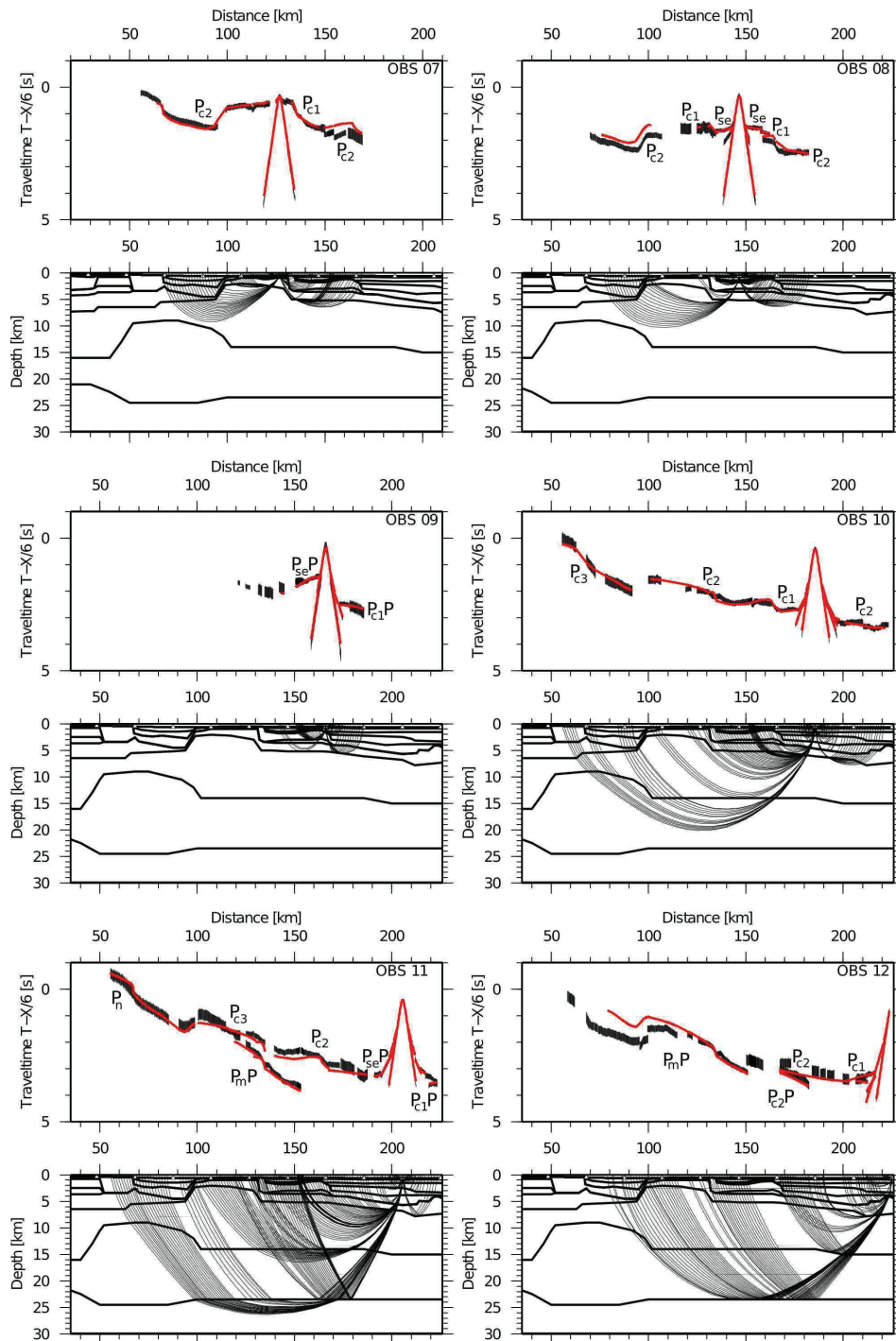
**Figure B.2: Raytracing in the P-wave velocity model for OBS 7 - 12. Top panels: Picked phases in red with vertical bar length according to the assigned pick uncertainty; calculated traveltimes as thin black lines; phase names are annotated; a reduction velocity of $6\,\mathrm{km\,s^{-1}}$ is used. Lower panels: Raypaths of the corresponding phases in the P-wave velocity model. For clarity only every 10th ray is plotted.**

133

# C

# Appendix, Palaeobathymetric reconstruction of the Davis Strait area

## C.1  Interpretation of new seismic lines

During cruise MSM09/3 of RV Maria S. Merian in 2008, multichannel seismic reflection (MCS) data were acquired (Gohl et al., 2009). We here show lines BGR08-301, -304, and -319 (Fig. 6.3). Setup parameters of the survey and processing steps are listed in table C.1 and C.2.

BGR08-301 crosses the Davis Strait with the Ungava Fault Complex and the Hudson Fracture Zone. The profile is also shown in Suckro et al. (2013) and Altenbernd (2010). Drilling Nukik-1 at the eastern termination of the seismic line allows an interpretation of the Manitsoq, Kangamiut and Nukik Formation in the Nuuk Basin (Fig. C.1). We propose that also sediments of the Ikermiut Formation overly the synrift strata. West of the Hudson Fracture Zone a correlation is not possible. Due to similarities in the reflection pattern and thickness, we interpret the Kangamiut Formation ontop of basalts west of the Hudson Fracture Zone (120 to 150 km distance). Because an erosion fan

Table C.1: Setup parameters of the MCS survey during MSM09/3.

| | |
|---|---|
| Streamer length | 3450 m |
| Number of channels | 276 |
| Sampling rate | 2 ms |
| Recording length | 14 s |
| Seismic source | array of 16 G.Guns$^{TM}$ |
| Operation pressure | 100 - 135 bar |
| Total source volume | 50.8 litres, 3100 in$^3$ |
| Shot interval | 18 s |
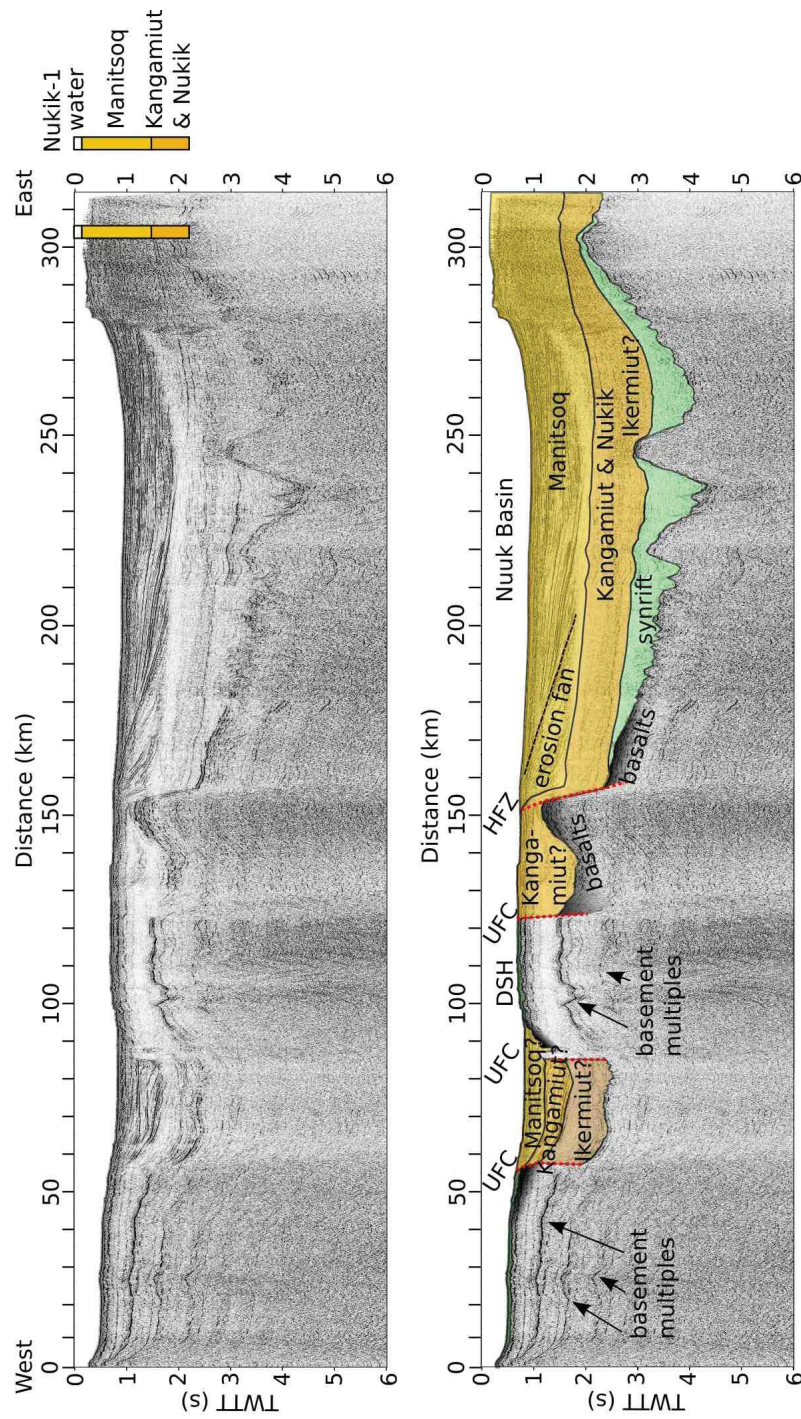
**Figure C.1: MCS data of line BGR08-301. Top: processed seismic data with stratigraphic information from drilling Nukik-1 (Rolle, 1985). Bottom: interpretation of formations and faults. UFC = Ungava Fault Complex, HFZ = Hudson Fracture Zone, DSH = Davis Strait High.**

**Table C.2: Processing of the MCS data from MSM09/3.**

| FOCUS™ processing of line BGR08-304 | ProMAX™ processing of line BGR08-301, -319 |
|---|---|
| - Resampling: 4 ms | - Resampling: 4 ms |
| - Geometry: CMP binning of 6.25 m | - Geometry: CMP binning of 6.25 m |
| - Interactive velocity analysis | - Bandpass filter: 4-8-80-160 Hz |
| - Gain: spherical divergence | - Velocity analysis |
| - Bandpass filter: 2-7-90-120 Hz | - Surface related multiple estimation |
| - Multiple suppression: fk filter "zmult" | - Velocity analysis |
| - Normal move out (NMO) correction | - Predictive deconvolution |
| - Stack | - Normal move out correction |
| - Kirchhoff migration | - Stack |
| - Coherency filter after two-way travel-time of first multiple | - Poststack Kirchhoff migration |

begins from this section and fanns into the Nuuk Basin, we suggest that the section from 120 to 150 km distance has been uplifted prior to the main deposition of the Manitsoq Formation. The tectonic model in Suckro et al. (2013) shows that the sediment basin between 55 to 85 km distance evolved from Late Cretaceous to the end of Paleocene. We therefore propose that it is based by Paleocene sediments of the Ikermiut Formation. We suggest the Kangamiut and Manitsoq Formations for stratigraphic borders at 1.2 and 1.5 s TWTT.

BGR08-319 crosses the northern Davis Strait where the Ungava Fault Complex and the Hudson Fracture Zone merge (Fig. 6.1, 6.3). This line is also presented in Altenbernd (2010). We could trace the Manitsoq, Kangamiut, and Ikermiut Formation between the basement high at CDP number 25000 and the eastern termination of the profile from the Ikermiut drilling (Rolle, 1985), Fig. C.2. A formation of at least Cretaceous age must underly these sediments, so we assign the Kangeq Sequence. The Ungava Fault Complex and Hudson Fracture Zone highly disturb the Cretaceous and Paleocene formations in this part of the profile. The western part of BGR08-319 is underlain by basalt flows (CDP number 47000 to 30000). These volcanics can have formed during the breakup of Greenland and the North American plate in Late Cretaceous. They can then represent new igneous crust which implies a phase of drifting. The basalts can also be products of the influence of the Greenland-Iceland mantle plume in the Early Paleocene (Storey et al., 1998). Instead of representing new igneous crust, the basalts can be extruded from fractures within stretched continental crust. This implies only a phase of rifting. In either case, the postrift or postdrift sediments that overly the basalt flows are of Paleocene to Eocene age.

BGR08-304 crosses the extinct Eocene and Paleocene spreading centers in southern
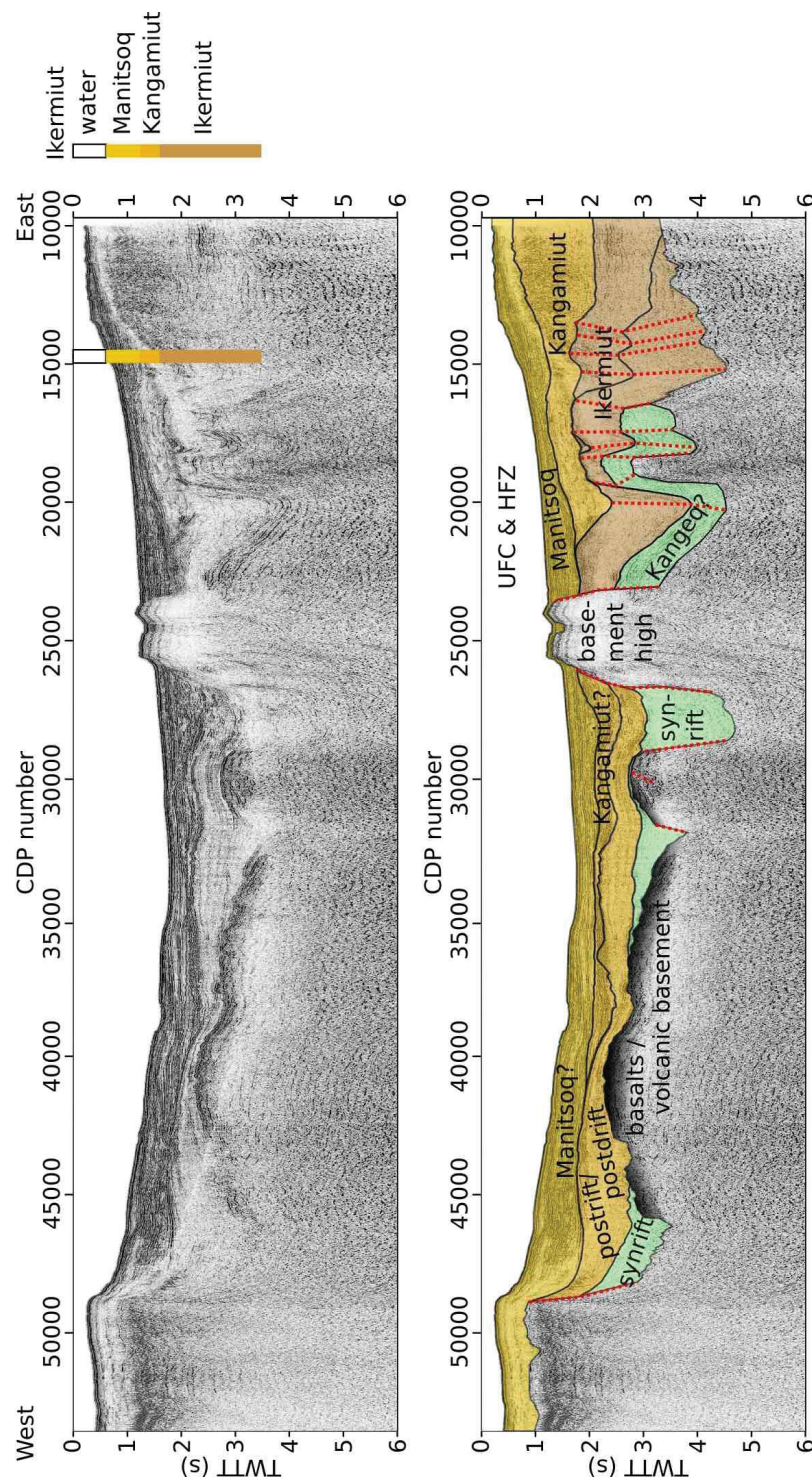
**Figure C.2: MCS data of line BGR08-319. Top: processed seismic data with stratigraphic information from drilling Ikermiut (Rolle, 1985). Bottom: interpretation of formations and faults. UFC = Ungava Fault Complex, HFZ = Hudson Fracture Zone.**
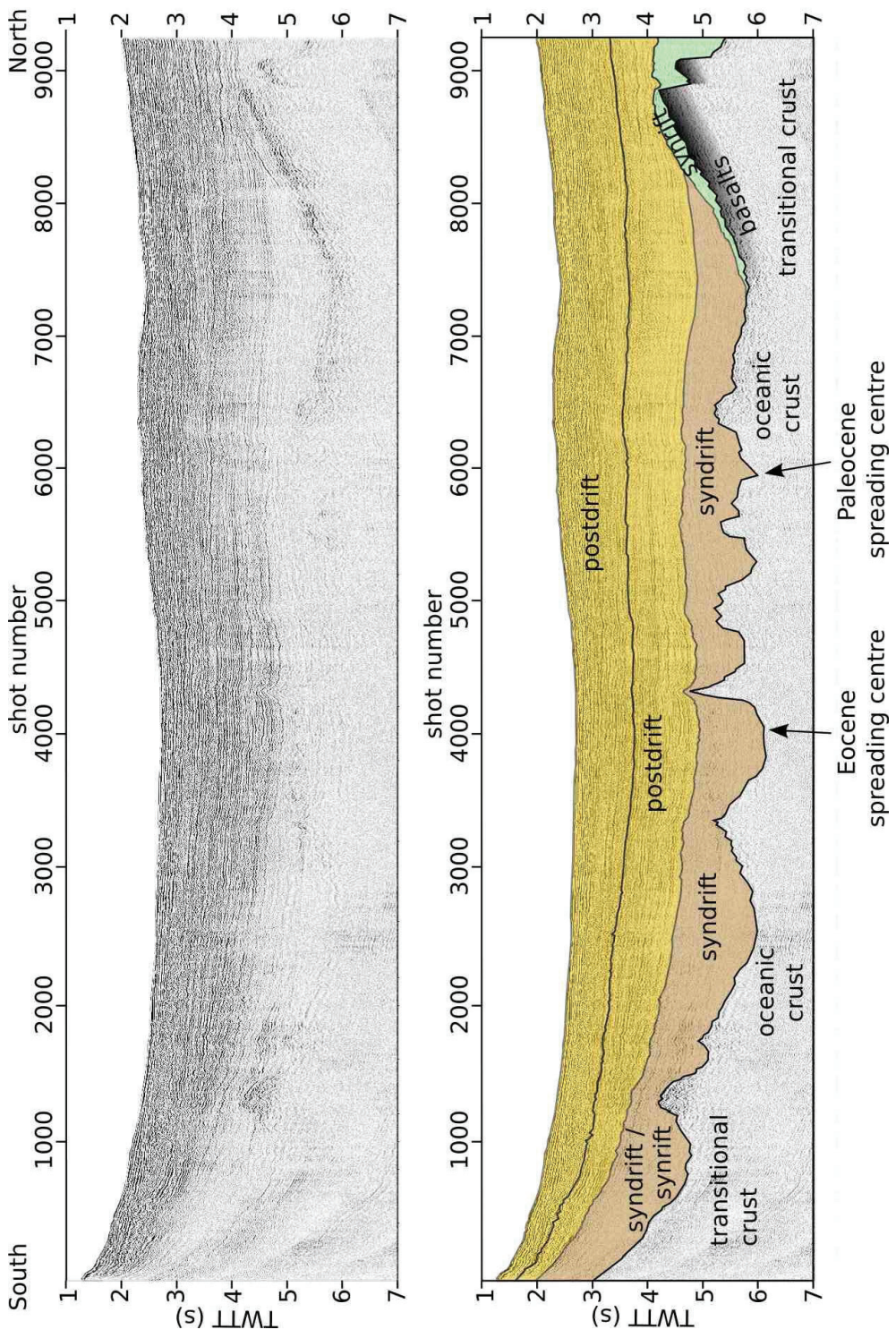
138

**Figure C.3: MCS data of line BGR08-304. Top: processed seismic data. Bottom: interpretation of formations.**

139

Baffin Bay (Chalmers & Oakey (2007); Suckro et al. (2012), Fig. 6.3). This line is also shown in Suckro et al. (2012); Block et al. (2012). From shot point 1600 to 7400, the profile is underlain by oceanic crust (Fig. C.3). At the northern termination of the profile, basalt flows are covered by synrift sediments. According to the tectonic model in Suckro et al. (2012), we propose a Late Cretaceous age. Postdrift sediments make up most of the total sediment cover. The oldest postdrift sediments are according to the stratigraphic chart in Fig. 6.2 of Late Eocene age.

## C.2   Backstripping method

### C.2.1   Flexual unloading

Flexual unloading is a weighted isostatic rebound. The backstripped sediment package is replaced by a volume of water and mantle; thickness of the crust and the remaining sediments are kept constant at this stage. According to Airy's law, isostasy is reached, when:

$$d_{sed1} \cdot \rho_1 = d_{rebound} \cdot \rho_m + (d_{sed1} - d_{rebound}) \cdot \rho_w$$

$d_{sed1}$: thickness of the backstripped sediments
$\rho_1$: density of the backstripped sediments
$d_{rebound}$: amount of rebound
$\rho_m$: density of the mantle
$\rho_w$: density of sea water

$$d_{rebound} = \frac{\rho_1 - \rho_{water}}{\rho_{mantle} - \rho_{water}} d_{sed1} \qquad (C.1)$$

The depth of the remaining sediment layers and the crust are the original depth subtracted by the rebound.

The calculation of Airy isostasy at every datapoint along a profile neglects the rigidity of the crust. Neighboring displacements influence each other. For the flexure of the crust we use the relation given by Watts (2001) for the deformation of a beam. The displacement $y$ at a location $x$ is given by:

$$y = D_0 \, e^{-\lambda x}(cos\lambda x + sin\lambda x) \qquad (C.2)$$

$D_0$ is the resulting displacement of a force acting at $x = 0$. $\lambda$ is a material parameter of flexual length. Depression is transformed to a bulge at $x = \pm 3\pi/4\lambda$. For our estimation, the deformation is small enough to be disregarded for values outside $\pm 2\lambda$. We use eq. C.2 as mathematical loading of the Airy rebound from eq. C.1. Subsequent normalizing leads to the displacement in Fig. C.4
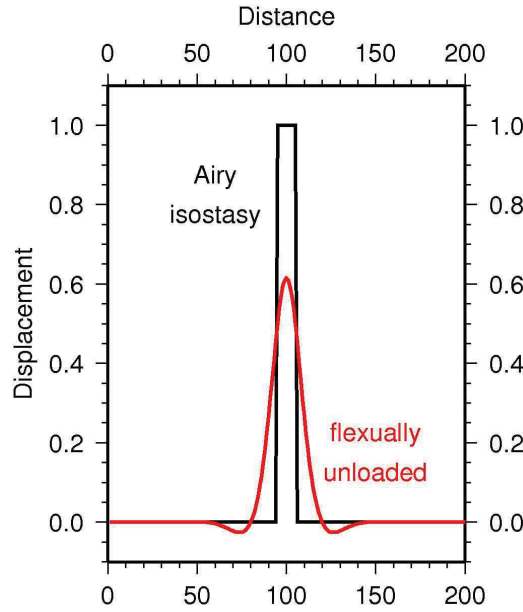
**Figure C.4: Rebound of the crust due to Airy isostasy (displacement = 1.0 for 95 > x < 105) in black and due to flexual unloading ($\lambda = 25$) in red.**

Because every point along the profile is influenced by data in the distance of $\pm 2\lambda$, we need to enlarge each profile by $2\lambda$ at the terminations. We here use $rebound(0)$ for all values smaller than 0 and $rebound(n)$ for all values greater than $n$.

## C.2.2 Decompaction

During decompaction the original porosity is reconstructed below the backstripped layer. While all sediment layers gain in volume, the depth of the basement remains constant as we do not consider porosity changes in the crust. We also assume that no porosity changes occur in basalt layers. Sclater & Christie (1980) show that the thickness of a sediment layer is given by the volume of sediment particles and the volume of water within the pore space. The water content between depth $d1$ and $d2$ follows this exponential law:

$$w(d1, d2) = \int_{d1}^{d2} f_0 exp(-c \cdot d) = \frac{f_0}{c} \Big[ exp(-c \cdot d_1) - exp(-c \cdot d_2) \Big] \qquad (C.3)$$

Because the volume of sediment particles below the backstripped layer stays constant, the following relation is true:

**Table C.3: Parameters that are used for the subsidence calculation of rifted crust.**

| Para-meter | Name | Used value | Reference |
|---|---|---|---|
| $a$ | lithosphere thickness | $125 \pm 10$ km | (Parsons & Sclater, 1977) |
| $\rho_m$ | density of the mantle | $3.30$ g/cm$^3$ | section 6.4.2, Table 6.5 |
| $\rho_w$ | density of sea water | $1.03$ g/cm$^3$ | section 6.4.2 |
| $\alpha$ | thermal expansion coefficient | $(3.1 \pm 1.1) \cdot 10^{-5}$ 1/°C | (Parsons & Sclater, 1977) |
| $T_1$ | asthenosphere temperature | $1365 \pm 276$°T | (Parsons & Sclater, 1977) |
| $\tau$ | thermal time constant | $62.8$ Ma | (Parsons & Sclater, 1977) |

$$(dfu_b - dfu_{s1}) - w(dfu_b, dfu_{s1}) = (dfu_b - decom_{s1}) - w(dfu_b, decom_{s1}) \quad \text{(C.4)}$$

$dfu_b$: depth of basement after flexural unloading
$dfu_{s1}$: top of the remaining sediment column after flexural unloading
$decom_{s1}$: top of the remaining decompacted sediment column / water depth after decompaction

Substitution of eq. C.3 into eq. C.4 leads to:

$$
\begin{aligned}
(dfu_b - dfu_{s1}) &- \frac{f_0}{c}\Big[ exp(-c \cdot (dfu_{s1})) - exp(-c \cdot dfu_b) \Big] \\
&= (dfu_b - decom_{s1}) - \frac{f_0}{c}\Big[ exp(-c \cdot decom_{s1}) - exp(-c \cdot dfu_b) \Big]
\end{aligned}
\quad \text{(C.5)}
$$

We solve equation C.5 iteratively first for the total sediment column below the back-stripped layer and then for each horizon within this column.

## C.2.3 Thermal subsidence

According to Parsons & Sclater (1977), the subsidence $d(t)$ of oceanic crust depends only on the age $t$ of the crust. For $t < 70$ Ma the following empirical relation describes the seafloor depth:

$$d(t) = 2500 + 350\sqrt{t} \quad \text{[m]} \quad \text{(C.6)}$$

The subsidence of rifted crust depends on the time since rifting ($t$) and on the extension of continental lithosphere, $\beta$, (McKenzie, 1978). The first order approximation of the seafloor depth $d(t)$ is given by:

$$d(t) = E_0 r \, exp\left(\frac{-t}{\tau}\right) \quad \text{[m]} \quad \text{(C.7)}$$

with the factors:

$$E_0 = \frac{4a\rho_m\alpha T_1}{\pi^2(\rho_m - \rho_w)} \; , \quad r = \left(\frac{\beta}{\pi}\right)sin\left(\frac{\pi}{\beta}\right)$$

Variable names and values that we use are summarized in Table C.3. If we assume that the volume of crust remains constant during rifting, we can use the crustal thinning factor instead of the lithospheric stretching factor. For published crustal models of the Davis Strait area $\beta$ varies between 8.0 and 1.5 (Fig. 6.9).

We calculate the effect of subsidence $\sigma$ at a given time $T$, e.g. 40 Ma. Therefore we have to calculate the difference between the subsidence of today ($t$) and the given time $T$:

$$\sigma(T) = d(t) - d(t - T) \tag{C.8}$$

143

# Danksagung

Ich danke Herrn Miller und Herrn Villinger, dass sie eingewilligt haben diese Dissertationsschrift zu begutachten und damit den einhergehenden Zeit- und Arbeitsaufwand auf sich nehmen.

Karsten Gohl danke ich für die Betreuung meiner Promotion. Er war stets für Fragen erreichbar und hat mich erfolgreich re-motivieren können, wenn mir der direkte Sinn meiner Arbeit abhanden kam.

Wilfried Jokat danke ich für meine Teilnahme an ARK XXV/3 und dass ich "mein" 2008er Profil dabei verlängern konnte. Außerdem danke ich ihm für das Unterschreiben von 29 Dienstreiseanträgen und daraus resultierenden 115.000 Reisekilometern.

Thomas Funck danke ich für seine Hilfe bei der P-Wellen Modellierung und der Interpretation der Modelle. Seine sorgsamen Korrekturen der einzureichenden Manuskripte haben diese deutlich verbessert.

Gabi danke ich für die Teilnahme an zwei grandiosen Expeditionen mit Maria S. Merian und Sonne, die meine Doktoranden-Zeit sehr viel kurzweiliger gestaltet haben.

Meinen Kollegen und Freunde in der AWI Geophysik danke ich für eine unvergessliche Zeit, auf die ich immer gerne zurücksehen werde. Ich bedauere sehr, dass es vorbei ist und hoffe, dass wir weiter in Kontakt bleiben.

Der Muddi und dem Vater danke ich für ihre vielen e-mails auf's Schiff und für ihre Unterstützung meines Tuns.

Besonders danke ich meinem lieben Jens, der stets bei mir war und an den Wochenenden emsig Bahn-Bonus-Meilen gesammelt hat.

# Curriculum Vitae

**Sonja Katharina Suckro**, * 28th February 1983 in Sigmaringen, Germany

### Occupations and Education

| | |
|---|---|
| Sept. 2009 - April 2013 | Ph.D. at the Alfred Wegener Institute, department of geophysics: evaluation of seismic refraction and reflection data, development of a palaeobathymetry calculation |
| Feb. 2008 - July 2009 | Research assistant at the Institute for Geophysics, University of Münster: assistance in the development of an airborne ground penetrating radar system |
| 2002 - 2008 | Study of geophysics at the University of Münster, Germany; Diploma thesis: Thickness and internal structure of the central part of the King George Island ice cap, Antarctica - results of GPR measurements (grade 1.3) |
| 1989 - 2002 | School, graduation with Abitur (grade 2.0) |

### Expeditions and Field Campaigns

| | |
|---|---|
| Oct. - Nov. 2012 | Cruise SO 224 to the Manihiki Plateau, Pacific, RV Sonne, in the group for seismic reflection data |
| Oct. - Dec. 2011 | Cruise MSM19/3 to the Agulhas Ridge, South Atlantic, RV Maria S. Merian, in the group for seismic reflection data |
| Aug. - Oct. 2010 | Cruise AKR-XXV/3 to the Baffin Bay, Arctic, RV Polarstern, in the group for seismic refraction data with Ocean Bottom Seismometers |
| 2008 - 2009 | Several field campaigns with ground based and air-borne GPR systems in Chile (Atacama desert, salt mine near Iquique, glaciers in Patagonia), Antarctica (Antarctic Peninsula, King George Island), Switzerland (Gorner, Rhone, Aletsch glaciers) |

| | |
|---|---|
| Dec. 2007 - Jan. 2008 | Field campaign on King George Island, Antarctica, acquisition of ground based GPR and DGPS profiles |
| Oct. 2007 | Volunteer at the Dublin Institute for Advanced Studies (DIAS) in the PICASSO project (Program to Investigate the Convective Alboran Sea System Overturn); two-weeks field campaign in Spain to set up magneto telluric stations |
| Jan. - Feb. 2007 | Field campaign on King George Island, Antarctica, acquisition of ground based GPR and DGPS profiles |
| Feb. - Apr. 2006 | Cruise ANT-XXIII/4 to the Pine Island Bay, Antarctica, RV Polarstern, in the group for aero-magnetic data |

## Peer-Reviewed Publications

**The Davis Strait crust - a transform margin between two oceanic basins.** *Geophysical Journal International* **193**, 2013, 78-97. Suckro, S., Gohl, K., Funck, T., Heyde, I., Schreckenberger, B., Gerlings, J., and Damm, V.

**Cold ice in the ablation zone: its relation to glacier hydrology and ice water content.** *Accepted for publication by Journal of Geophysical Research - Earth Surface, 16$^{th}$ Nov. 2012.* Ryser, C., Lüthi, M., Blindow, N., Suckro, S., Funk, M., and Bauder, A.

**The crustal structure of southern Baffin Bay: implications from a seismic refraction experiment.** *Geophysical Journal International* **190**, 2012, 37-58. Suckro, S., Gohl, K., Funck, T., Heyde, I., Ehrhardt, A., Schreckenberger, B., Gerlings, J., Damm, V., and Jokat, W.

**Observed glacial changes on the King George Island ice cap, Antarctica, in the last decade.** *Global and Planetary Change* **79**, 2011, 99-109. Rückamp, M., Braun, M., Suckro, S., and Blindow, N.

**Geometry and thermal regime of the King George Island ice cap, Antarctica, from GPR and GPS.** *Annals of Glaciology* **51**(55), 2010, 103-109. Blindow, N., Suckro, S., Rückamp, M., Braun, M., Schindler, M., Breuer, B., Saurer, H., Simes, J., and Lange, M.

**Dynamics of the ice cap on King George Island, Antarctica: field measurements and numerical simulations.** *Annals of Glaciology* **51**(55), 2010, 80-90. Rückamp, M., Blindow, N., Suckro, S., Braun, M., and Humbert, A.

## Conference Contributions as First Author

**Paleo-bathymetry of the Davis Strait, a polar gateway between Canada and Greenland.** Suckro, S., Gohl, K., and Damm, V. *Talk at the European Geosciences Union General Assembley*, April 2013, Vienna.

**The crust of Davis Strait and southern Baffin Bay - seismic refraction profiles between Canada and Greenland.** Suckro, S., Gohl, K., Funck, T., Hyde, I., Schreckenberger, B., Ehrhardt, A., Damm, V., and Jokat, W. *Talk at the GeoHannover GeoRohstoffe*, Oct. 2012, Hannover.

**The evolution of Davis Strait, a polar gateway - seismic data and tectonic modelling.** Suckro, S., Gohl, K., Funck, T., Hyde, I., Schreckenberger, B., Ehrhardt, A., and Damm, V. *Poster at the European Geosciences Union General Assembley*, April 2012, Vienna.

**The tectonic history of southern Baffin Bay and Davis Strait - seismic refraction experiments and the evolution of oceanic crust.** Suckro, S., Gohl, K., Funck, T., Hyde, I., Schreckenberger, B., Ehrhardt, A., Gerlings, J., Damm, V., and Jokat, W. *Poster at the fall meeting of the American Geophysical Union*, Dec. 2011, San Francisco.

**Tectonic evolution of southern Baffin Bay: implications from a refraction seismic experiment.** Suckro, S., Gohl, K., Funck, T., Ehrhardt, A., Heyde, I., Schreckenberger, B., Damm, V., and Jokat, W. *Poster at the International Conference on Arctic Margins VI*, June 2011, Fairbanks.

**Die Krustenstruktur der südlichen Baffin-Bucht und Davisstrasse abgeleitet aus refraktionsseismischen Messungen. (The crustal structure of southern Baffin Bay and Davis Strait derived from seismic refraction lines)** Suckro, S., Gohl, K., Funck, T., Heyde, I., Schreckenberger, B., Ehrhardt, A., Altenbernd, T., and Damm, V. *Talk at the 71st annual assembly of the German Geophysical Union*, Feb. 2011, Köln.

**Evidence of oceanic crust in the southern Baffin Bay from a seismic refraction experiment.** Suckro, S., Gohl, K., Funck, T., Ehrhardt, A., Heyde, I., Schreckenberger, B., and Damm, V. *Poster at the fall meeting of the American Geophysical Union*, Dec. 2010, San Francisco.

**Tectonic Evolution of Southern Baffin Bay in the Light of New Refraction Seismic Data.** Suckro, S., Gohl, K., Funck, T., Heyde, I., Ehrhardt, A., and Schreckenberger, B. *Poster at the International Polar Year Science Conference*, June 2010, Oslo.

**Tektonische Entwicklung zwischen Kanada und Grönland - erste Ergebnisse der Krustenstruktur in der südlichen Baffin Bay. (Tectonic evolution between**

**Canada and Greenland - first results of the crustal structure in southern Baffin Bay)** Suckro, S., Gohl, K., Funck, T., Heyde, I., Ehrhardt, A., and Schreckenberger, B. *Poster at the 70th annual assembly of the German Geophysical Union*, March 2010, Bochum.

**Ice thickness and internal structure of Patagonian glaciers measured with the University of Münster Airborne Ice Radar.** Suckro, S., Blindow, N., and Rückamp, M. *Talk at the 69th annual assembly of the German Geophysical Union*, March 2009, Kiel.

**Ice thickness, Raymond bumps, watertable, and firn structure of the ice cap of King George Island.** Suckro, S., Blindow, N., Rückamp, M., Braun, M., Moll, A., and Lange, M. *Talk at the 23rd International Polar Conference of the German Society of Polar Research*, March 2008, Münster.

**Geometry and internal structure of the temperate ice cap of King George Island, Antarctica, from GPR and GPS measurements.** Suckro, S., Blindow, N., and Rückamp, M. *Talk at the 68th annual assembly of the German Geophysical Union*, March 2008, Freiberg.

Bremerhaven, 25. April 2013          ------------------------------------

150